

**Effect of Local Stress Ratio Variation on Fatigue Behavior
of Notched Component**

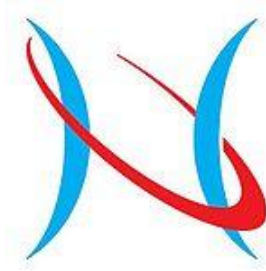
(切欠き材の疲労挙動に及ぼす局所応力比変動の影響)

AYE THANT HTOO

11506983

Supervisor: Associate Professor Yukio Miyashita

A dissertation submitted in partial fulfillment of the requirements for the
degree of Doctor of Engineering in Materials Science



Department of Materials Science and Engineering
Nagaoka University of Technology
Nagaoka, Niigata, Japan
August, 2016

Effect of Local Stress Ratio Variation on Fatigue Behavior of Notched Component

(切欠き材の疲労挙動に及ぼす局所応力比変動の影響)

Approved by:

Dr. Yoshiharu Mutoh
Department of System Safety
Nagaoka University of Technology

Dr. Yukio Miyashita
Department of Mechanical
Engineering
Nagaoka University of Technology

Dr. Yuichi Otsuka
Department of System Safety
Nagaoka University of Technology

Dr. Masakazu Okazaki
Department of Mechanical
Engineering
Nagaoka University of Technology

Dr. Shinji Hashimura
Department of Engineering
Science and Mechanics
Shibaura Institute of Technology

Dr. Shigeo Sakurai
Hitachi Ltd.

ACKNOWLEDGEMENTS

I would like to express my deep sense of gratitude to Professor Yoshiharu Mutoh. I wish to thank him for his constant support, guidance, wonderful comments, suggestion, encouragement, trust and all the fruitful discussions. I wish to thank him for his unique understanding and being such an attainable and likable teacher.

I would also to express my very sincere gratitude to Associate Professor Yukio Miyashita for supervision, guidance, teaching, discussions and supporting me constantly during whole periods to understanding of my research. This thesis would not have been possible without the valuable suggestion and useful advices from him.

I would like to offer my greatest thankful to Associate Professor Yuichi Otsuka for enthusiastic advice, kind guidance, supporting me throughout my study, his helpful comments, discussions and my sincere thanks to him again for providing knowledge and teaching me in numerical analysis and related to my research.

I also wish to express my sincere thank to the doctoral examination committee members Prof. M. Okazaki, Dr. S. Sakurai and Associate Prof. S. Hashimura for their time, valuable comments and useful suggestions on my thesis work. I also wish to express my gratitude to Hitachi Ltd for providing me sufficient specimens to conduct my experimental work.

My heartfelt thanks are extended to Mr. Yosunobu Hosakai, Mr. Hoshino Hideo, Mr. Yoshii Kazuo and Mr. Sato Kenta for necessary technical support in machining work. It is a pleasure to give sincere thanks to people in International Affair Division and Administrative Section of NUT for their support and guideline during my stay in Nagaoka. I had the opportunity to work in a very nice work experiment and I also thankful for all of my friends and lab colleagues.

I recognize that this research would not have been possible without the financial support of MEXT. That's why, the financial support of the Japanese Government (MONBUKAGAKUSHO: MEXT) is gratefully acknowledge.

The last but not the least, I would like to thank every member of my family, especially my DAD, who have always encouraged me to pursue my goals, always succeed, and never admit defeat.

Finally, a very special thanks goes out to Mr. Kyaw Ye Lynn, for giving me kind understanding, moral support, encouragement and self-confidence to achieve this goal.

AYE THANT HTOO

ABSTRACT

In the present study, the effect of local stress ratio variation on fatigue behavior of notched round bar specimens was investigated in the wide range of fatigue from low cycle fatigue to high cycle fatigue regions including the transition region. Fatigue experiments with notched components in Ti-6Al-4V alloy were conducted combining with the finite element analysis under cyclic loading with the positive remote stress ratio (>0). The S-N curve was deflected in the intermediate region between high cycle fatigue and low cycle fatigue regions. In the high cycle fatigue region, the local stress ratio at notch root was not varied and the same as the applied remote stress ratio. However, in the transition region above the critical nominal stress amplitude for the kinking behavior, the local stress ratio was decreasing with increasing applied nominal strain due to further development of local plastic deformation at notch root. Finally, the local stress ratio at notch root reached -1 in the low cycle fatigue region even under the positive remote stress ratio. The region of local stress ratio variation can be defined the transition region between low and high cycle fatigue regions. The variation of local stress ratio at notch root was associated with the constraint due to reversed elastic deformation during unloading is speculated to be the main mechanism to induce the compressive stress and vary the mean stress and local stress ratio.

Since the fatigue life prediction in the transition region has not yet been established, fatigue life of notched specimens in the wide range of fatigue from low cycle fatigue to high cycle fatigue regions including transition region was predicted by taking into account the local stress ratio variation at notch root based on the SWT parameter combined with elastic-plastic finite element analysis under cyclic loading.

The predicted results showed good agreement with the experimental results for all three regions. Therefore, it is suggested that low cycle fatigue life predicted assuming the stress ratio of -1 in transition region would give unsafe life prediction and local mean stress effect should be consider for safe prediction in notch components.

The local stress ratio variation in the transition region and its effect on notch fatigue behavior were also investigated for A2024-T4 alloy with lower yield stress to confirm the effect of material. Based on the results similar transition behavior in S-N curve and the local stress ratio variation have been found Effects of material on kinking behaviour and transition behaviour were more significant in A2024-T4 alloy with lower yield stress. In addition the fatigue life prediction method proposed could be also successfully applied to the A2024-T4 alloy.

Table of Contents

| | |
|---|-------------|
| Acknowledgement | i |
| Abstract | ii |
| Table of Contents | iv |
| List of Figures | viii |
| List of Tables | xv |
| Chapter 1 Introduction | |
| 1.1 Background | 2 |
| 1.1.1 Importance of fatigue and cyclic deformation | 2 |
| 1.1.2 The S-N curve | 4 |
| 1.1.3 High cycle versus low cycle fatigue | 5 |
| 1.1.4 Notch | 6 |
| 1.1.5 Stress concentration at notch root | 6 |
| 1.1.6 Effect of notch on fatigue | 8 |
| 1.1.7 Traditional notch root analysis and fatigue life prediction | 9 |
| 1.1.8 Fatigue notch factor and notch sensitivity | 10 |
| 1.1.9 Strain-life approaches for notch | 10 |
| 1.1.10 Elastic-plastic stress concentration factor | 11 |
| 1.1.11 Influence of mean stress on fatigue behavior | 13 |
| 1.1.12 Models for predicting mean stress effect | 16 |
| 1.1.13 Cyclic stress-strain behavior | 19 |
| 1.2 Current status of research on notch fatigue behavior | 21 |
| 1.2.1 Life prediction of notch specimen | 21 |
| 1.2.2 Effect of mean stress on smooth and notch fatigue behavior | 26 |
| 1.3 Objective of the present study | 29 |

| | | |
|------------------|--|----|
| Chapter 2 | Notch fatigue behavior of Ti-6Al-4V alloy under load-controlled high cycle fatigue tests | |
| 2.1 | Introduction | 39 |
| 2.2 | Experimental and analytical procedures | 41 |
| 2.2.1 | Material and specimens | 41 |
| 2.2.2 | Load-controlled fatigue strength test for high cycle fatigue region | 43 |
| 2.2.3 | Cyclic stress-strain curve | 44 |
| 2.2.4 | Finite element analysis | 45 |
| 2.3 | Results | 48 |
| 2.3.1 | Load-controlled fatigue strength tests of the smooth and notched specimens | 48 |
| 2.3.2 | Fracture surface observation | 49 |
| 2.3.3 | Cyclic stress-strain behavior | 52 |
| 2.3.4 | Elastic-plastic FEA for the notched specimen | 53 |
| 2.3.4.1 | Stress distribution at notch root for R=0.1 | 56 |
| 2.3.4.2 | Stress strain response hysteresis loop at notch root for R=0.1 | 56 |
| 2.3.4.3 | Stress distribution at notch root for R=0.5 | 63 |
| 2.3.4.4 | Stress strain response hysteresis loop at notch root for R=0.5 | 63 |
| 2.4 | Discussion | 70 |
| 2.4.1 | Critical nominal stress amplitude | 70 |
| 2.4.2 | Variation of local stress ratio at notch root | 70 |
| 2.5 | Conclusions | 73 |
| Chapter 3 | Notch fatigue behavior of Ti-6Al-4V alloy under displacement-controlled low cycle fatigue tests | |
| 3.1 | Introduction | 78 |
| 3.2 | Experiments and FEM analysis | 81 |
| 3.2.1 | Material and specimens | 81 |
| 3.2.2 | Displacement-controlled fatigue strength test for low cycle fatigue region | 81 |
| 3.2.3 | Finite element analysis | 82 |

| | | |
|------------------|--|-----|
| 3.3 | Results | 82 |
| 3.3.1 | Fatigue strength test results in low cycle fatigue region | 82 |
| 3.3.2 | Fracture surface observations | 86 |
| 3.3.3 | Stress distribution at the notch root under displacement-controlled condition for $R=0.1$ in elastic-plastic FEA of notched specimen | 88 |
| 3.4 | Discussion | 97 |
| 3.4.1 | Mechanism for local stress ratio variation at notch root | 97 |
| 3.4.2 | Fatigue life predictions of the notched specimen | 101 |
| 3.4.3 | Comparison of the predicted lives and experimental results | 104 |
| 3.5 | Conclusions | 106 |
| Chapter 4 | Notch fatigue behavior of A2024-T4 alloy in high cycle fatigue, transition and low cycle fatigue regions | |
| 4.1 | Introduction | 112 |
| 4.2 | Experiments and FEM analysis | 114 |
| 4.2.1 | Material and specimens | 114 |
| 4.2.2 | Tensile test | 116 |
| 4.2.3 | Load-controlled fatigue strength test | 116 |
| 4.2.4 | Strain-controlled fatigue strength test | 116 |
| 4.2.5 | Cyclic stress-strain curve | 117 |
| 4.2.6 | Finite element analysis | 117 |
| 4.3 | Result | 118 |
| 4.3.1 | Load-controlled fatigue strength test of the smooth and notched specimens | 118 |
| 4.3.2 | Cyclic stress-strain behavior | 121 |
| 4.3.3 | Strain-controlled fatigue test of the smooth specimen | 123 |
| 4.3.4 | Elastic-plastic FEA at notch root | 124 |
| 4.3.4.1 | Stress distribution at notch root for $R=0.1$ | 124 |
| 4.3.4.2 | Stress strain response hysteresis loop at notch root for $R=0.1$ | 126 |
| 4.3.4.3 | Stress distribution at notch root for $R=0.5$ | 133 |
| 4.3.4.4 | Stress strain response hysteresis loop at notch root for $R=0.5$ | 133 |
| 4.4 | Discussion | 141 |

Table of Contents

| | | |
|------------------|--|-----|
| 4.4.1 | Critical nominal stress amplitude | 141 |
| 4.4.2 | Variation of local stress ration at notch root | 141 |
| 4.4.3 | Comparison of S-N curve kinking behavior in A2024-T4 alloy and Ti-6Al-4V alloy | 143 |
| 4.4.4 | Fatigue life predictions of the notched specimen for A2024-T4 alloy | 147 |
| 4.4.5 | Comparison of the predictedlives and experimental results | 149 |
| 4.5 | Conclusions | 153 |
| Chapter 5 | Summary | |

List of Figures

Chapter 1

| | | |
|----------|--|----|
| Fig. 1.1 | Typical Wohler curve with stages: L- Low Cycle, H-High Cycle and I- Unlimited fatigue life | 5 |
| Fig. 1.2 | Elastic stress distribution in a notched bar subjected to a tensile load | 7 |
| Fig. 1.3 | S-N curves for smooth and notched specimens | 9 |
| Fig. 1.4 | The stress and strain concentration factors under plastic deformation | 13 |
| Fig. 1.5 | Terminology for alternating stress | 14 |
| Fig. 1.6 | High cycle fatigue data showing influence of mean stress | 14 |
| Fig. 1.7 | Reversed loading into compression | 20 |
| Fig. 1.8 | A complete stress-strain cycle: a hysteresis loop | 20 |

Chapter 2

| | | |
|----------|---|----|
| Fig. 2.1 | Microstructure of the Ti-6Al-4V alloy used | 42 |
| Fig. 2.2 | Geometry of the (a) smooth and (b) notched specimens | 42 |
| Fig. 2.3 | FEM model of the notched specimen | 46 |
| Fig. 2.4 | S-N curves for the smooth and notched specimens of the Ti-6Al-4V alloy | 49 |
| Fig. 2.5 | Fatigue fracture surfaces of the smooth specimens tested at (a) $\sigma_a = 280\text{MPa}$, $N_f = 2,839,763$ cycles (b) $\sigma_a = 340\text{MPa}$, $N_f = 577,026$ cycles and the notched specimen tested at (c) $\sigma_a = 280\text{MPa}$, $N_f = 44,756$ cycles (d) $\sigma_a = 180\text{MPa}$, $N_f = 4,376,196$ cycles under $R = 0.1$ | 50 |
| Fig. 2.6 | Fatigue fracture surfaces of the smooth specimens tested at (a) $\sigma_a = 200\text{MPa}$, $N_f = 564,203$ cycles (b) $\sigma_a = 220\text{MPa}$, $N_f = 93,766$ cycles and the notched specimen tested with (c) $\sigma_a = 140\text{MPa}$, $N_f = 1,897,399$ cycles (d) $\sigma_a = 200\text{MPa}$, $N_f = 78,201$ cycles under $R = 0.5$ | 51 |
| Fig. 2.7 | Cyclic stress strain curve for the Ti-6Al-4V alloy | 52 |
| Fig. 2.8 | The von Mises stress distribution near notch root in the first | |

| | | |
|-----------|--|----|
| | cycle (a) and the corresponding plastic strain distribution near notch root region, (b) under $R=0.1$ | 54 |
| Fig. 2.9 | The von Mises stress distribution near notch root in the first cycle (a) and the corresponding plastic strain distribution near notch root region, (b) under $R=0.5$ | 55 |
| Fig. 2.10 | Finite element analysis of notch specimen under load-controlled cyclic loading: von Mises stress distribution from notch root to notch center under $R=0.1$: (a) $\sigma_a = 240\text{MPa}$, (b) $\sigma_a = 260\text{MPa}$, (c) $\sigma_a = 280\text{MPa}$ | 57 |
| Fig. 2.11 | Finite element analysis of notch specimen under load-controlled cyclic loading: plastic strain distribution from notch root to notch center under $R=0.1$: (a) $\sigma_a = 240\text{MPa}$, (b) $\sigma_a = 260\text{MPa}$, (c) $\sigma_a = 280\text{MPa}$ | 58 |
| Fig. 2.12 | Cyclic stress strain hysteresis at notch root under $R=0.1$: (a) $\sigma_a = 240\text{MPa}$, (b) $\sigma_a = 260\text{MPa}$, (c) $\sigma_a = 280\text{MPa}$ | 59 |
| Fig. 2.13 | Cyclic stress strain hysteresis at notch root under $R=0.1$ at $\sigma_a = 240\text{MPa}$ | 60 |
| Fig. 2.14 | Cyclic stress strain hysteresis at notch root under $R=0.1$ at $\sigma_a = 260\text{MPa}$ | 61 |
| Fig. 2.15 | Cyclic stress strain hysteresis at notch root under $R=0.1$ at $\sigma_a = 280\text{MPa}$ | 62 |
| Fig. 2.16 | Finite element analysis of notch specimen under load-controlled cyclic loading: von Mises stress distribution from notch root to notch center under $R=0.5$: (a) $\sigma_a = 120\text{MPa}$, (b) $\sigma_a = 160\text{MPa}$, (c) $\sigma_a = 200\text{MPa}$ | 64 |
| Fig. 2.17 | Finite element analysis of notch specimen under load-controlled cyclic loading: plastic strain distribution from notch root to notch center under $R=0.5$: (a) $\sigma_a = 120\text{MPa}$, (b) $\sigma_a = 160\text{MPa}$, (c) $\sigma_a = 200\text{MPa}$ | 65 |
| Fig. 2.18 | Cyclic stress-strain hysteresis loops at notch root under the stress ratio of $R=0.5$: (a) $\sigma_a = 120\text{MPa}$ (b) $\sigma_a = 160\text{MPa}$ (c) $\sigma_a = 200\text{MPa}$ | 66 |
| Fig. 2.19 | Cyclic stress strain hysteresis at notch root under $R=0.5$ | |

| | | |
|----------------------|---|----|
| | at $\sigma_a = 120\text{MPa}$ | 67 |
| Fig. 2.20 | Cyclic stress strain hysteresis at notch root under $R= 0.5$ | |
| | at $\sigma_a = 160\text{MPa}$ | 68 |
| Fig. 2.21 | Cyclic stress-strain hysteresis loops at notch root under the stress ratio of $R= 0.5$ at $\sigma_a = 200\text{MPa}$ | 69 |
| Fig. 2.22 | Relationship between local stress ratio at notch root and applied nominal stress | 71 |
| Fig. 2.23 | Relationship between local stress ratio and distance from notch root under the remote stress ratio of 0.1 | 72 |
| Fig. 2.24 | Relationship between local stress ratio and distance from notch root under the remote stress ratio of 0.5 | 72 |
| Chapter 3 | | |
| Fig. 3.1 | S-N curves in the low cycle fatigue region of the smooth specimens at $R= -1$ for Ti-6Al-4V alloy | 83 |
| Fig. 3.2 | S-N curves in the low cycle fatigue region of the notched specimens at $R= 0.1$ for Ti-6Al-4V alloy | 84 |
| Fig. 3.3 | Cyclic stress-strain hysteresis loops obtained by the low cycle fatigue test for the Ti-6Al-4V alloy under $R= 0.1$: (a) $\epsilon_a = 0.3\%$, (b) $\epsilon_a = 0.7\%$ | 85 |
| Fig. 3.4 | Fatigue fracture surfaces of the notched specimens tested under $R= 0.1$: (a) High cycle fatigue region: $\sigma_a = 180\text{MPa}$, $N_f = 4,376,196$ cycles, (b) Transition region: $\epsilon_a = 280$ MPa, $N_f = 44,756$ cycles, (c) Transition region: $\epsilon_a = 0.4\%$, $N_f = 64,425$ cycles, (d) Low cycle fatigue region: $\epsilon_a = 0.7\%$, $N_f = 697$ cycles | 87 |
| Fig. 3.5 | The von Mises stress distribution near notch root in the first cycle under $R= 0.1$ in low cycle fatigue region | 89 |
| Fig. 3.6 | The corresponding plastic strain distribution near notch root region in the first cycle under $R= 0.1$ in low cycle fatigue region | 89 |
| Fig. 3.7 | Finite element analysis of notch specimen under displacement-controlled cyclic loading: von Mises stress | |

| | | |
|----------------------|---|-----|
| | distribution from notch root to notch center under R= 0.1: (a) $\epsilon_a = 0.2\%$, (b) $\epsilon_a = 0.5\%$, (c) $\epsilon_a = 0.7\%$ | 90 |
| Fig. 3.8 | Finite element analysis of notch specimen under displacement-controlled cyclic loading: plastic strain distribution from notch root to notch center under R= 0.1: (a) $\epsilon_a = 0.2\%$, (b) $\epsilon_a = 0.5\%$, (c) $\epsilon_a = 0.7\%$ | 91 |
| Fig. 3.9 | Cyclic stress-strain hysteresis at notch root under R= 0.1 in low cycle fatigue region: (a) $\epsilon_a = 0.2\%$, (b) $\epsilon_a = 0.5\%$, (c) $\epsilon_a = 0.7\%$ | 92 |
| Fig. 3.10 | Cyclic stress strain hysteresis at notch root under R=0.1 in low cycle fatigue region at $\epsilon_a = 0.2\%$ | 93 |
| Fig. 3.11 | Cyclic stress strain hysteresis at notch root under R=0.1 in low cycle fatigue region at $\epsilon_a = 0.5\%$ | 94 |
| Fig. 3.12 | Cyclic stress strain hysteresis at notch root under R=0.1 in low cycle fatigue region at $\epsilon_a = 0.7\%$ | 95 |
| Fig. 3.13 | Relationship between local stress ratio at notch root and applied nominal strain amplitude under the remote stress ratio of 0.1 | 96 |
| Fig. 3.14 | A schematic explanation of the local mean stress or local stress ratio variation mechanism: (a) transition region (b) low cycle fatigue region | 99 |
| Fig. 3.15 | Relationship between local stress ratio and distance from the notch root under the remote stress ratio of 0.1: (a) Transition region: $\sigma_a = 280\text{MPa}$ (b) Low cycle fatigue region: $\epsilon_a = 0.7\%$ | 100 |
| Fig. 3.16 | Comparison between experimental and predicted fatigue lives for the notched specimen under remote stress ratio of 0.1 for the wide range of fatigue from low cycle to high cycle | 106 |
| Chapter 4 | | |
| Fig. 4.1 | Microstructure of the A2024-T4 alloy used | 115 |
| Fig. 4.2 | Shape and dimensions of the smooth and notched specimens | 115 |
| Fig. 4.3 | S-N curves for the smooth and notched specimens of the A2024-T4 alloy | 119 |

| | | |
|-----------|--|-----|
| Fig. 4.4 | Fatigue fracture surfaces of the smooth specimens tested at (a) $\sigma_a = 180\text{MPa}$, $N_f = 150,235$ cycles (b) $\sigma_a = 200\text{MPa}$, $N_f = 49,703$ cycles and the notched specimen tested at (c) $\sigma_a = 120\text{MPa}$, $N_f = 780,000$ cycles (d) $\sigma_a = 180\text{MPa}$, $N_f = 11,500$ cycles under $R = 0.1$ | 120 |
| Fig. 4.5 | Fatigue fracture surfaces of the smooth specimens tested at (a) $\sigma_a = 110\text{MPa}$, $N_f = 601,495$ cycles (b) $\sigma_a = 120\text{MPa}$, $N_f = 167,576$ cycles and the notched specimen tested with (b) $\sigma_a = 90\text{MPa}$, $N_f = 458,014$ cycles (d) $\sigma_a = 145\text{MPa}$, $N_f = 15,489$ cycles under $R = 0.5$ | 121 |
| Fig. 4.6 | Cyclic stress strain curve for the A2024-T4 alloy | 122 |
| Fig. 4.7 | S-N curve for low cycle fatigue of the A2024-T4 alloy | 123 |
| Fig. 4.8 | The von Mises stress distribution near notch root in the first cycle; (a) $R = 0.1$, (b) $R = 0.5$ and the corresponding plastic strain distribution near notch root: (c) $R = 0.1$, (d) $R = 0.5$ | 125 |
| Fig. 4.9 | Finite element analysis of notch specimen under load-controlled cyclic loading: von Mises stress distribution from notch root to notch center under $R = 0.1$: (a) $\sigma_a = 90\text{MPa}$, (b) $\sigma_a = 140\text{MPa}$, (c) $\sigma_a = 180\text{MPa}$ | 127 |
| Fig. 4.10 | Finite element analysis of notch specimen under load-controlled cyclic loading: plastic strain distribution from notch root to notch center under $R = 0.1$: (a) $\sigma_a = 90\text{MPa}$, (b) $\sigma_a = 140\text{MPa}$, (c) $\sigma_a = 180\text{MPa}$ | 128 |
| Fig. 4.11 | Cyclic stress strain hysteresis at notch root under $R = 0.1$: (a) $\sigma_a = 90\text{MPa}$, (b) $\sigma_a = 140\text{MPa}$, (c) $\sigma_a = 180\text{MPa}$ | 129 |
| Fig. 4.12 | Cyclic stress strain hysteresis at notch root under $R = 0.1$ at $\sigma_a = 90\text{MPa}$ | 130 |
| Fig. 4.13 | Cyclic stress strain hysteresis at notch root under $R = 0.1$ at $\sigma_a = 140\text{MPa}$ | 131 |
| Fig. 4.14 | Cyclic stress strain hysteresis at notch root under $R = 0.1$ at $\sigma_a = 180\text{MPa}$ | 132 |
| Fig. 4.15 | Finite element analysis of notch specimen under load-controlled | |

| | | |
|------------------|---|-----|
| | cyclic loading: von Mises stress distribution from notch root to notch center under R= 0.5: (a) $\sigma_a = 80\text{MPa}$, (b) $\sigma_a = 100\text{MPa}$, (c) $\sigma_a = 150\text{MPa}$ | 134 |
| Fig. 4.16 | Finite element analysis of notch specimen under load-controlled cyclic loading: plastic strain distribution from notch root to notch center under R= 0.5: (a) $\sigma_a = 80\text{MPa}$, (b) $\sigma_a = 100\text{MPa}$, (c) $\sigma_a = 150\text{MPa}$ | 135 |
| Fig. 4.17 | Cyclic stress strain hysteresis at notch root under R= 0.5: (a) $\sigma_a = 80\text{MPa}$, (b) $\sigma_a = 100\text{MPa}$, (c) $\sigma_a = 150\text{MPa}$ | 136 |
| Fig. 4.18 | Cyclic stress strain hysteresis at notch root under R= 0.5 at $\sigma_a = 80\text{MPa}$ | 137 |
| Fig. 4.19 | Cyclic stress strain hysteresis at notch root under R= 0.5 at $\sigma_a = 100\text{MPa}$ | 138 |
| Fig. 4.20 | Cyclic stress strain hysteresis at notch root under R= 0.5 at $\sigma_a = 150\text{MPa}$ | 139 |
| Fig. 4.21 | Relationship between local stress ratio at notch root and applied nominal stress amplitude under the remote stress ratios of 0.1 and 0.5 | 140 |
| Fig. 4.22 | Relationship between local stress ratio and distance from notch root at $\sigma_a = 150\text{MPa}$ under the remote stress ratio of 0.5 | 140 |
| Fig. 4.23 | Comparison of local stress ratio variation under the remote stress ratio of 0.5 for two different materials | 145 |
| Fig. 4.24 | Comparison between experimental and predicted fatigue lives for notched specimens under R= 0.1 | 150 |
| Fig. 4.25 | Comparison between experimental and predicted fatigue lives for notched specimens under R= 0.5 | 150 |
| Fig. 4.26 | Comparison between experimental and predicted fatigue lives for notched specimens under the remote stress ratio of 0.1 for the wide range of fatigue from low to high cycle | 152 |
| Chapter 5 | | |
| Fig. 5.1 | Stress ratio effect on S-N curve in low cycle fatigue (a) and high cycle fatigue (b) as well as the intermediate uncertain | 159 |

| | | |
|----------|--|-----|
| | fatigue behavior region between low cycle fatigue and high cycle fatigue (c) | |
| Fig. 5.2 | Variation of local stress ratio at notch root | 161 |
| Fig. 5.3 | Estimated overall S-N curves for the remote stress ratios $R = -1$ and $R > -1$ by the proposed fatigue life prediction method with taking account of local stress ratio variation | 162 |

List of Tables

Chapter 1

| | | |
|-----------|---------------------------------|----|
| Table 1.1 | Classification of fatigue | 6 |
| Table 1.2 | R values and loading conditions | 16 |

Chapter 2

| | | |
|-----------|---|----|
| Table 2.1 | Chemical composition of the Ti-6Al-4V alloy used | 43 |
| Table 2.2 | Mechanical properties of the Ti-6Al-4V alloy used | 43 |
| Table 2.3 | Cyclic properties of the Ti-6Al-4V alloy | 53 |

Chapter 3

| | | |
|-----------|---|----|
| Table 3.1 | Low cycle fatigue properties of the Ti-6Al-4V alloy | 84 |
|-----------|---|----|

Chapter 4

| | | |
|-----------|--|-----|
| Table 4.1 | Chemical composition of the A 2024-T4 alloy used | 113 |
| Table 4.2 | Mechanical properties of the A2024-T4 alloy used | 114 |
| Table 4.3 | Cyclic properties of the A2024-T4 alloy | 122 |
| Table 4.4 | Low cycle fatigue properties of the A2024-T4 alloy | 124 |
| Table 4.5 | Characteristics values at the kinked point | 146 |

CHAPTER – 1
INTRODUCTION

Chapter-1

Introduction

1.1 Background

1.1.1 Importance of fatigue and cyclic deformation

According to the American Society for Testing and Materials (ASTM), fatigue is defined as the progressive, localized and micro-permanent structural change that occurs in a material when subjected to repeated loading or fluctuating strains at nominal stresses with maximum values less than the tensile strength of the material [1]. This localized and permanent micro-structural change induces crack nucleation and propagation and then failure of materials, which is defined as fatigue failure. The process that cause fatigue failure of a component may occur since the components are started to use in service application.

From monotonic tensile test, some of the mechanical properties can be obtained such as ultimate tensile strength, yield stress, Young's modulus and ductility. These monotonic properties are considered for components under static loads. However, most of the engineering components were designed to withstand cyclic loads for their service lives. Comparably to monotonic tensile properties, cyclic properties must be evaluated when designing for cyclic loading conditions since these properties would be significantly different from the monotonic properties. Structural components such as wings tension

member, shear webs, gears and suspension parts are some examples of designs which are subjected to cyclic loading.

Many books and articles have mentioned that 70 to 80 percent of mechanical failures are caused by fatigue failures [2]. Some of these failures have been due to poor design or accidentally created defects in production process or service in used. However, it has been discovered that many failures have been caused by pre-existing notches or flaws in structural components such as fillets, holes and keyways. It has been also known that stress concentration occurs at the tip of the notches or flaws. If the components are used under cyclic loading, these stress raisers act as the sites for crack nucleation and propagation, and then lead to fracture. Moreover, most of these failures occur suddenly with no obvious warning and in some cases result in catastrophic loss [3]. In consequence, considerable effort has been made to determine the physical nature of fatigue in notch structural members.

In order to account for all stress raisers in design, but maintain a simple fatigue analysis, designer often makes the assumption of elastic body where the local stresses remain below the yield strength. This, the stress-life method of fatigue analysis, is relatively simple and works well if the component is designed to withstand low stresses and the resulting lives are long for the case of high cycle fatigue. However, this method can not apply to low cycle fatigue where the local stress is higher than yield stress and the plastic strain controls fatigue behavior and in this case, strain-life method is widely used in fatigue analysis [4]. Between these two typical cases, the fatigue behavior is expected to be complicated and to indicate the transition behavior. However, this transition fatigue behavior of notch has not been well understood. Besides from stress-based and strain-based approach, fracture mechanics approach was also commonly used in design

components for stress raisers. In this approach, it assumes that a crack is initially included in material body, and when the crack length reaches to its critical values, failure occurred in the material.

1.1.2 The S-N curve

The Wohler curve or stress-life diagram (S-N curve) was first investigated in the 1860s by Wohler to analyze failure behavior of railroad axles. In the curve or diagram, specimens are subjected to rotating or reversed bending and uniaxial loading. In order to determine the shape of the so-called Wohler curve, many cyclic tests with various constant amplitude loads have to be undertaken as shown in Fig. 1.1 [5], which shows the relationship between amplitude (or maximum value, or mean value) of the applied stress and number of cycles to failure N_f while the vertical axis is commonly adopted the stress amplitude σ_a or the logarithm of σ_a . The strain-life diagram was investigated in 1950s by Coffin and Manson. In this diagram, reversal to failure was related to the total strain amplitude which accounts for elastic and plastic deformation. In both the stress-life and strain-life diagram, the life includes crack initiation and propagation lives. It is known that the crack initiation life is dominant in high cycle fatigue of smooth specimen, while the crack propagation life is dominant in notch specimen, fracture mechanic approach can be applied for predicting crack propagation life. The fracture mechanics was first proposed by Griffith and Irwin [6, 7]. Griffith proposed that fracture of crack body occurs when the energy release rate G reaches the critical value. Irwin proposed the stress intensity factor, K , as the driving force for unstable crack growth. It is known that G and K are equivalent as $G = \frac{K^2}{E}$, $E' = E/(1-\nu^2)$ for plane strain and $E' = E$ for plane stress.

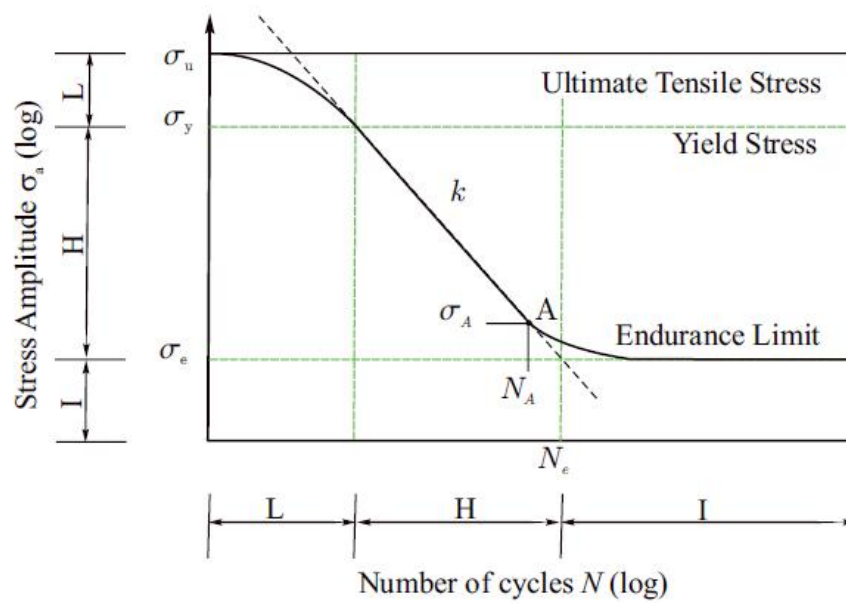


Fig. 1.1 Typical Wohler curve with stages: L- Low Cycle, H-High Cycle and I- Unlimited fatigue life, [5]

1.1.3 High cycle versus low cycle fatigue

Typically, there are two types of fatigue: one is that the applied cyclic stresses are lower than the elastic limit (yield stress) and the fatigue lives are longer than 10^4 cycles, which is known as high-cycle fatigue. The other is that the cyclic stresses are relatively large with significant amount of plastic strain and the fatigue lives are shorter than 10^4 cycles. This type of behavior has been commonly referred as low-cycle fatigue [8]. A classification of fatigue has been introduced by Dufailly and Lemaitre, as given in Table 1.1 [9]. Then, without repeated plastic deformation fatigue will not occur. Although the nominal behavior is typically elastic, cyclic plastic deformation commonly occurs at stress concentrations or at the microscopic level which is the main reason for fatigue crack nucleation [10].

Table 1.1 Classification of fatigue [9]

| | Number of cycles to failures | Stress range σ_r | Strain ratio $\Delta\epsilon^p/\Delta\epsilon^e$ | Energy ratio $\Delta W^p/\Delta W^e$ |
|-------------------------------|------------------------------|--------------------------|--|--------------------------------------|
| High Cycle Fatigue (HCF) | $>10^5$ | $<\sigma_y$ | ≈ 0 | ≈ 0 |
| Low Cycle Fatigue (LCF) | 10^2 to 10^4 | σ_y to σ_u | 1 to 10 | 1 to 10 |
| Very Low Cycle Fatigue (VLCF) | 1 to 20 | Close to σ_u | 10 to 100 | 10 to 100 |

1.1.4 Notch

In machines and structures, most of their components have discontinuities, in other term called notches, like shoulder and holes. When these machines and structures are loaded by external force, stress concentration will occur at notches, which depends on the geometry of holes. The maximum stress always occurs at the notch root. The maximum stress and the cyclic plastic strain at notch root enhance the crack nucleation, and then failure of components and structures. Therefore, in order to avoid sudden failure of the machines and structures, it is very important to assure the maximum stress at notch root should be smaller than the fatigue limit [10].

1.1.5 Stress concentration at notch root

Notches are prevalent in many different components at various scales. At the component scale, there are bolt holes and fillets, and at a micro structural scale, they are inclusions or voids, etc. Under loading, these notches induce a stress concentration and a stress gradient field emanating from the notch root. Therefore, the presence of a notch or any other geometrical discontinuity acts to locally disturb the stress field. Specifically, a

non-uniform triaxial stress field arises in the plane of the notch with the highest stress concentration near the discontinuity. This type of stress field exists even when a unidirectional tensile load is applied to an elastic body as shown in Fig. 1.2. At the notch tip, there is a constraint of local deformation in the direction transverse to the applied load. In response of the constraint, transverse stresses are induced at the notch tip [4].

As in any typical boundary value problem, the notch tip stress and strain components can be evaluated by locally satisfying the equations of equilibrium, the material constitutive relation, the compatibility equation and boundary conditions. In this case, numerical techniques such as the finite element or the boundary element methods can be used to simultaneously satisfy the field equation at the notch tip. However, the local stress-strain behavior at notch root under cyclic loading has not been always clarified yet. As indicated in the section 1.3, one of the goals of this research is to identify the local stress strain behavior at notch root under cyclic loading by using finite element analysis.

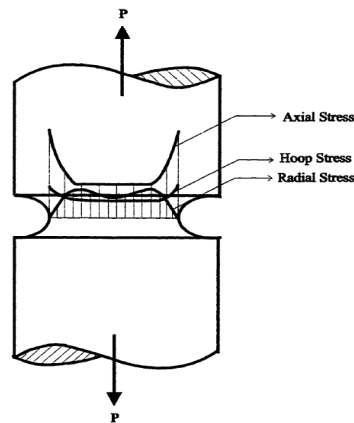


Fig. 1.2 Elastic stress distribution in a notched bar subjected to a tensile load [4]

The maximum local stress near the notch root, σ_{\max} is larger than the remote applied stress, S_a . For linear elastic body, the ratio of these two stresses is called as elastic concentration factor and given as:

$$K_t = \frac{\sigma_{max}}{S_a} \quad (1.1)$$

The elastic stress concentration factor depends on geometry of the specimen and the nature of the loading condition (bending, tensile, torsional, etc). Handbooks of stress concentration factors have been published [11].

1.1.6 Effect of notch on fatigue

Generally, there are two factors to discuss the notch size effect: the statistical size effect and the geometrical size effect. The statistical size effect is evolved when a component is subjected under an alternating load. Number of nucleated micro-cracks will depend on the volume of high stress. In case of larger specimen, there will be higher possibility of larger number of micro-cracks which results in lower fatigue strength. The statistical size effect can be found mainly in the smooth specimen with no stress concentration.

The geometrical size effect, which is also called as the stress gradient effect is considered for the specimens with notch. The maximum stress, stress gradient and plastic deformation at notch root are strongly dependent on the geometry and size of notch. Therefore, fatigue crack nucleation and then fatigue strength of notch body depend on the geometry and size of notch.

Figure 1.3 shows the effect of notch on fatigue behavior. As seen from the figure, fatigue strength is significantly reduced by the presence of a notch. It is also known that, the fatigue strength of notched members not only depends on the stress concentration but also on other mechanical factors such as the notch radius, stress ratio and mean stress, etc. The notch effect is also depending on materials. Therefore, it is important to understand the effect of notch on S-N curve for different materials.

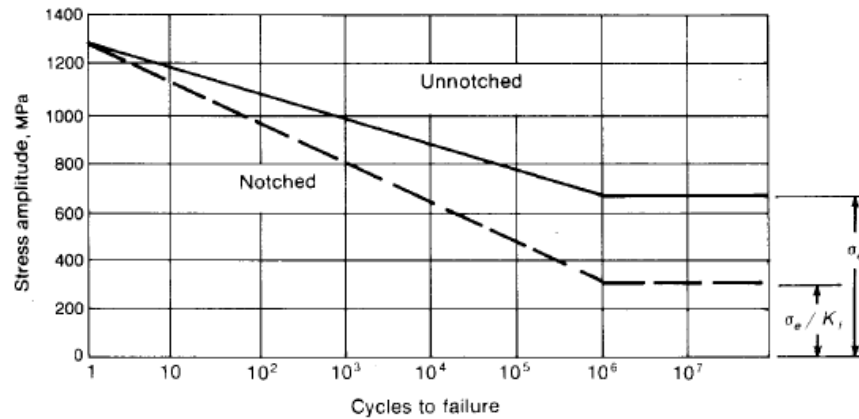


Fig. 1.3 S-N curves for smooth and notched specimens [12]

1.1.7 Traditional notch root analysis and fatigue life prediction

Traditional simplified notch root analysis techniques employ a global-local approach to analyze fatigue response of notched specimens. If the local stress and strain components due to a remote applied stress are known within the notch root field, the fatigue life can be estimated using stress-life or strain-life approaches based on smooth specimen experimental results. Therefore, extensive studies for estimating stress and strain states near the notch root under cyclic loading are needed while lots of studies under monotonic loading have been available.

1.1.8 Fatigue notch factor and notch sensitivity

When fatigue is considered in the Stress-Life approach, the effect of notch is accounted through the fatigue notch factor, K_f . This factor is defined as the ratio of fatigue strength of smooth specimen to that of notched specimen:

$$K_f = \frac{\sigma_f^{unnotched}}{\sigma_f^{notched}} \quad (1.2)$$

The fatigue notch factor is usually equal to or less than the stress concentration factor. The relationship between the elastic stress concentrations factor, K_t and the fatigue notch factor, K_f is given as:

$$q = \frac{K_f - 1}{K_t - 1} \quad (1.3)$$

The value of q is ranged from 0 (for the case of no notch effect, $K_f=1$) to 1 (for the case of $K_f = K_t$).

1.1.9 Strain-life approaches for notch

In the low cycle fatigue (LCF) regime, the strain-life approach is used. When the stress at notch root is lower than yield stress, the local stresses and strains at the notch root are linearly related to the remote applied loads, through the stress concentration factor. For notches with localized plastic zone in the notch root region, it is difficult to evaluate the local stresses and strains in the notch root region. Due to the constraint imposed by the elastic material surrounding the plastic zone, the deformation at notch root is expected to be under a strain-controlled condition. Therefore, the strain-life approach is applied to estimate the material response at the notch root in low cycle fatigue

regime. Thus, the basic assumption of the strain-life approach is that a smooth specimen tested under strain-control can simulate the notch root region, specimen exposed to a remote applied load, where deformation is under strain-controlled. When the plastic strain of the notch root region is the same as that of the smooth specimen, the fatigue life of the notch specimen is assumed to be the same as that of the smooth specimen.

1.1.10 Elastic-plastic stress concentration factor

In order to evaluate the stress and strain histories near the notch root under elastic-plastic conditions, several estimation techniques have been proposed by such as Neuber [13] and Molski and Glinka [14]. Under fully elastic conditions in the uniaxial case, stress and strain are linearly related through Hooke's Law. When plasticity occurs, the uniaxial stress-strain response becomes non-linear and is modeled through other techniques such as the Ramberg-Osgood relationship [15],

$$\varepsilon = \frac{\sigma}{E} + \left(\frac{\sigma}{H} \right)^{1/n} \quad (1.4)$$

where H is monotonic strength coefficient and n is the strain hardening exponent which is usually ranged from 0 to 0.5 [16]. The first and second terms on the right hand side of Eq. 1.4 are the elastic strain and the plastic strain, respectively. The cyclic hysteresis curve can be described as:

$$\frac{\Delta\varepsilon}{2} = \frac{\Delta\sigma}{2E} + \left(\frac{\sigma}{2K'} \right)^{1/n'} \quad (1.5)$$

where K' and n' are the cyclic strength coefficient and the cyclic strain hardening exponent, respectively. The Massing hypothesis of tension-compression symmetry is also assumed. These constants are generally not equal to those of under monotonic loading.

Prior to yielding, the elastic stress concentration factor, K_t , is equal to the local stress concentration factor $K_\sigma = \sigma/S$ and the local strain concentration factor K_ϵ is given as: $K_\epsilon = \epsilon/e$. When yielding occurs, the local strain is higher than that predicted by K_t and the local stress is lower than that predicted by K_t , as shown in Fig. 1.4. The theoretical stress concentration should lie somewhere in between K_σ and K_ϵ . Based on the nonlinear elastic analysis, Neuber [13] proposed that the theoretical stress concentration is the geometric mean of the stress and strain concentration factors:

$$K_t = \sqrt{K_\sigma \cdot K_\epsilon} \quad (1.6)$$

Molski and Glinka [14] introduced an energy-based method to estimate the local stress-strain history near the notch root. Using the Ramberg-Osgood relationship, Eq. 1.4, the local strain energy in the notch root region can be calculated as:

$$W = \int_0^\epsilon \sigma(\epsilon) d\epsilon = \frac{\sigma^2}{2E} + \frac{\sigma}{n+1} \left(\frac{\sigma}{H} \right)^{1/n} \quad (1.7)$$

Assuming the localized plasticity near the notch root does not influence the overall strain energy distribution within the notch root, the stress concentration factor can be estimated as,

$$K_t = \left(\frac{W_\sigma}{W_s} \right)^{1/2} \quad (1.8)$$

where W_σ is the strain energy per unit volume due to local stress and strain at the notch root and W_s is the elastic strain energy per unit volume due to remote applied nominal stress S .

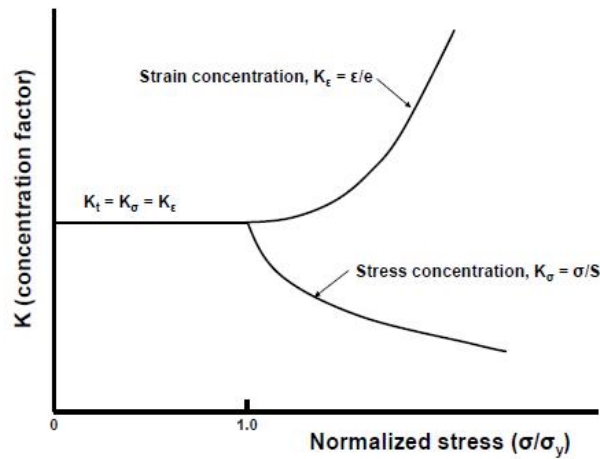


Fig. 1.4 The stress and strain concentration factors under plastic deformation [17]

1.1.11 Influence of mean stress on fatigue behavior

Most of the basic fatigue data are collected in the laboratory under fully reversed loading (i.e., $R = -1$). However, many actual service situations include non-zero mean stresses, for example, piping systems in the nuclear power plant and pre-strain bolts on pressure vessel. Generally, tensile mean stress was detrimental effect to high cycle fatigue life while compressive mean stress was beneficial to fatigue life [18]. Therefore, it is very important to know the effect of mean stress on fatigue behavior so that the fully reversed laboratory data can be usefully employed in practical situations. Therefore, effect of mean stress on fatigue behavior should be investigated. Figure 1.5 illustrates the relationships and definitions of mean stress σ_m and alternating stress σ_a .

Figure 1.6 shows the mean stress effect on fatigue strength. Several equations and diagrams proposed for simulating the effect of mean stress on fatigue strength such as Goodman and Gerber diagrams [12]. As seen from the Fig. 1.6, the fatigue strength decrease with increasing mean stress in the tensile mean stress region.

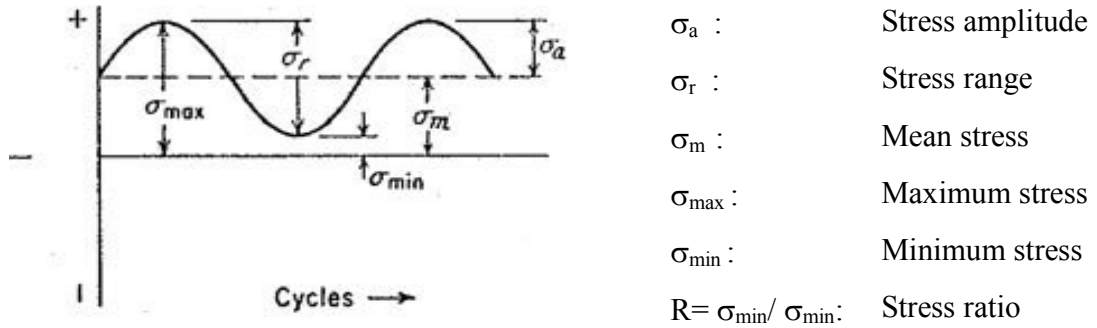


Fig. 1.5 Terminology for alternating stress [12]

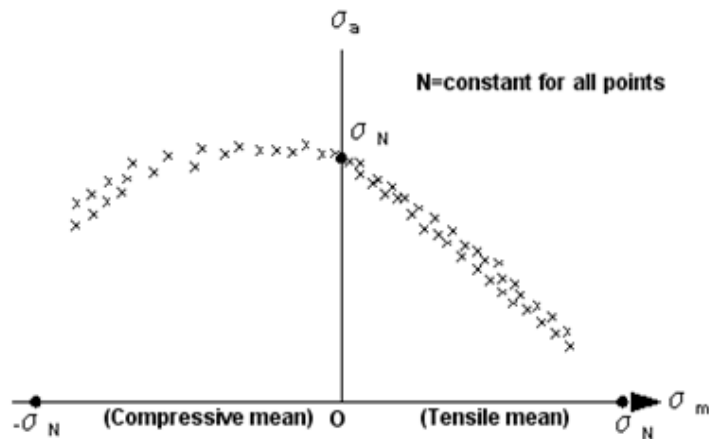


Fig. 1.6 High cycle fatigue data showing influence of mean stress [19]

In Fig. 1.5, it is possible to distinguish different loading forms for different values of stress ratio and mean stress, as shown in Table 1.2. Within the present study, only repeated loading ($-1 < R < 1$) is considered for conducting fatigue tests for the notch and smooth specimens. The following equations are used to correlate mean stress (R ratio) to stress amplitude.

The stress range σ_r is defined as:

$$\sigma_r = \sigma_{\max} - \sigma_{\min} \quad (1.9)$$

The stress amplitude, σ_a , is half of the stress range as:

$$\sigma_a = \frac{\sigma_r}{2} = \frac{(\sigma_{\max} - \sigma_{\min})}{2} \quad (1.10)$$

The mean stress is the algebraic mean of the maximum and minimum stress during the cycle and given as:

$$\sigma_m = \frac{(\sigma_{\max} + \sigma_{\min})}{2} \quad (1.11)$$

Two ratios are often defined for the representation of mean stress, the stress or R ratio and the amplitude ratio A .

$$R = \frac{\sigma_{\min}}{\sigma_{\max}} \quad (1.12)$$

$$A = \frac{\sigma_a}{\sigma_m} = \frac{1 - R}{1 + R} \quad (1.13)$$

Table 1.2 R values and loading conditions [12]

| R ratio | Loading Condition |
|--------------|--|
| $R > 1$ | Both σ_{\max} and σ_{\min} are negative. Negative mean stress. |
| $R = 1$ | Static loading. |
| $0 < R < 1$ | Both σ_{\max} and σ_{\min} are positive; Positive mean stress, $ \sigma_{\max} > \sigma_{\min} $. |
| $R = 0$ | Zero to tension loading, $\sigma_{\min} = 0$ |
| $R = -1$ | Fully-reversed loading, $ \sigma_{\max} = \sigma_{\min} $; zero mean stress. |
| $R < 0$ | $ \sigma_{\max} < \sigma_{\min} $, σ_{\max} approaching zero. |
| R infinite | σ_{\max} equal to zero. |

1.1.12 Models for predicting mean stress effect

Some of the most popular stress based equations that taking into account mean stress effect can be found in the literature such as Goodman (Modified Haigh), Gerber, Morrow and SWT (Smith-Waston-Topper) equations [12,20,21].

The Goodman's equation is stated by:

$$\frac{\sigma_a}{\sigma_{ar}} + \frac{\sigma_m}{\sigma_u} = 1 \quad (1.14)$$

where σ_a is the alternating stress, σ_m is the mean stress, σ_{ar} is fatigue limit for completely reversed loading and σ_u is the ultimate tensile strength. From the equation, one can study when the ultimate tensile strength of a material increase, σ_{ar} is becomes less significant to mean stress.

The Gerber approach is stated by the following equation but most of the studies reported that the Gerber approach over-predicts the fatigue life and it does not take into account the compressive mean stress effect [22]. It is mentioned that ninety percent of the

results for ductile metals are above the Goodman line and two-third of the way to the Gerber parabola [23].

$$\frac{\sigma_a}{\sigma_{ar}} + \left(\frac{\sigma_m}{\sigma_u}\right)^2 = 1 \quad (1.15)$$

The next model was investigated by Morrow: he used the true fracture stress instead of the ultimate tensile strength in Goodman equation. Morrow and Goodman equations gave similar results when the materials do not show significant necking due to the difference between tensile strength and the true fracture strength is quite small. On the other hands, for material that shows significant necking, the difference between tensile strength and true fracture strength is significant. Dowling reported that for ferrous metals, especially, various steels and aluminum alloys, the Morrow equation can provide satisfactory results compared to Goodman equation [24]. However, in case of non-ferrous metals, using the fatigue strength coefficient can provide unsatisfactory results. The Morrow equation is stated as below;

$$\frac{\sigma_a}{\sigma_{ar}} + \frac{\sigma_m}{\sigma_f} = 1 \quad (1.16)$$

The other famous approach used by many researchers in the fatigue field for taking into account mean stress effect is a simple model of SWT damage approach. Based on this approach, many researchers got conservative results for a wide range of materials. Every prediction damage models have its own unique characteristics and can get better results for certain application. Most damage parameters were considered under a strain based approach. The SWT damage were also considered under a strain based approach and used to apply the stress and strain response of a material in the presence of mean stress under

cyclic loading. In this parameter, it consist the relationship between the cyclic strain amplitude $\Delta\varepsilon/2$ and the maximum stress σ_{max} . This damage parameter gives accurate predictions results for a uniaxial loading situation in which mean stress correction is needed. This SWT approach can produce a very conservative fatigue life prediction results for most of the aluminium alloy and it is also suitable for the use of the specimens which failure occur due to tensile loading [25]. The following equation shows the relationship between variables in the SWT model and stated by:

$$\sigma_{ar} = \sqrt{\sigma_a \sigma_{max}} \quad (1. 17)$$

where σ_{ar} is the equivalent fully reversed stress amplitude which resulting in the similar fatigue life as the combination of σ_a - σ_m , σ_a is the stress amplitude and σ_{max} is the maximum stress. This SWT parameter can be applied to strain-life equation and can be written as:

$$\sigma_{max} \varepsilon_a = \frac{(\sigma'_f)^2}{E} (N_f)^{2b} + \sigma'_f \varepsilon'_f (N_f)^{b+c} \quad (1. 18)$$

where σ_{max} is given by $\sigma_{max} = \sigma_m + \sigma_a$ for given cycle and the product of the maximum stress and the strain amplitude in the strain-life parameter controls the both mean stress and the strain amplitude. The SWT damage parameter assumes that the product of stress-strain $\sigma_{max} \varepsilon_a$ parameter at a designated life was remained constant for different combination of the maximum stress and the strain amplitude. Determination of the basic low cycle properties such as fatigue ductility exponent c and fatigue strength coefficient b and the variables σ'_f , ε'_f can be obtained from the strain-controlled low-cycle fatigue experiment data by evaluating the log-log plot of the relation between slopes of the plastic and elastic strain life curves with strain amplitude, respectively. In our investigation, SWT approach will try to apply to predict the fatigue lives of notched specimens.

The Walker equation is also widely used to investigate the mean stress effect where the adjustable curve fitting parameter γ is introduced as;

$$\sigma_{ar} = \sigma_{max}^{1-\gamma} \sigma_a^\gamma \quad (1.19)$$

The parameter γ is a mean stress sensitivity indicator that valid range for γ is from 0 to 1. If the value of γ is lower, the material is more sensitive to tensile mean stress. But some researchers assumed the γ value as 0.5 for unknown case. If γ value is assumed to be 0.5, the Walker equation coincides with the SWT damage approach. The method for finding of γ can be found in [26].

1.1.13 Cyclic stress-strain behavior

For the case that loading process is started from zero stress to the maximum stress, the stress-strain hysteresis is shown as in Fig. 1.7(a). During the reversed loading, the yielding is occurred, as shown in Fig. 1.7(b). The complete loop will be obtained as shown in Fig. 1.8. The stress-strain loop illustrated in Fig. 1.7 is called hysteresis loop. Generally, such loops are generated under strain controlled experiments.

During the reversed loading, yielding in compression begins at point C due to Bauschinger effect. By reloading, in tension the hysteresis loop is completed as shown in Fig. 1.8. The characteristic of the loop is described by its width (the total strain range $\Delta \varepsilon$) and its height,(the total stress range $\Delta \sigma$).

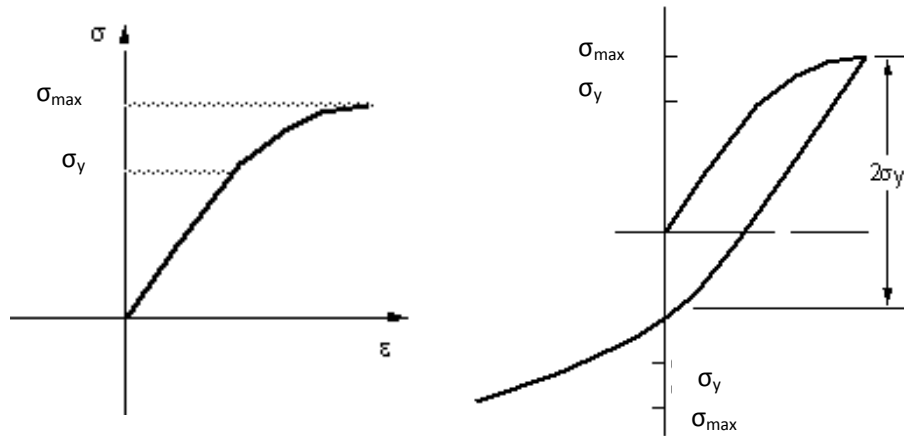


Fig. 1.7 Reversed loading into compression [19]

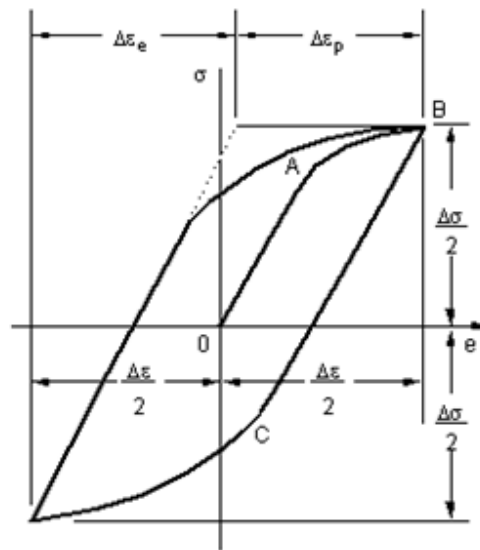


Fig. 1.8 A complete stress-strain cycle: a hysteresis loop [12]

The total strain range consists of the elastic and plastic components:

$$\Delta \varepsilon_t = \Delta \varepsilon_e + \Delta \varepsilon_p \quad (1.20)$$

Eq. 1.19 can be written as:

$$\Delta\varepsilon_t = \frac{\Delta\sigma}{E} + \Delta\varepsilon_p \quad (1.21)$$

It is well understood that the fatigue process depends on the stress-strain behavior. However, different materials show different mechanical behavior and response. So, it is needed to study the stress strain behavior for various materials with notch.

There have been lots of experimental results on the cyclic stress-strain behavior of smooth specimen [27, 28, 29]. However, almost no information about the cyclic stress-strain behavior at notch root. Therefore, it is important to clarify the cyclic stress-strain behavior at notch root to understand the fatigue behavior of notched specimen in detail.

1.2 Current status of research on notch fatigue behavior

1.2.1 Life prediction of notch specimen

In the present section, current research status of notch fatigue behavior focusing on (1) life prediction of notched specimen and (2) effect of mean stress on notch fatigue behavior, has been reviewed.

Bache and Tasleem [30] proposed the fatigue life prediction techniques for different notch geometries in titanium alloys. They conducted the strain-controlled low cycle fatigue experiments using plain specimens and correlated the data obtained on a variety of notch geometries with the stress concentration factors in the range from 1.4 to 4.7. Based on the parameter K_t , $\Delta\sigma$ for each notch and $\Delta\sigma$ for plain specimens where $\Delta\sigma$ is the stress range defined at stabilized condition as used to correlate the data for life prediction of notch. Although their technique can correlate the fatigue life for some notch geometries, it can be observed that notch fatigue behavior is not consistent with this

correlation and it is also influenced by microstructure condition, cyclic yield strength, shape of the cyclic stress strain curve and material response during cyclic loading.

Hurley et al., [31] reported on the application of numerical models to predict low cycle fatigue initiation lives of the notched Ti6264 specimen tested under ambient condition. Their prediction methods are based on the results of strain controlled fatigue test of plain specimen and they assumed in prediction that for an equivalent stress-strain state, both notch and plain specimens reveal the similar fatigue initiation lives. Their estimation of fatigue life is based on the strain based parameter such as SWT, Walker strain-based parameter and strain energy density fatigue parameter of Golos and Ellyin. They used both the Neuber rule and non-linear finite element analysis to get the material stress strain state at notch root. Results showed that three models can give accurate fatigue life predictions at room temperature under $R=0$ and -1 . For other cases, the model can not give accurate predictions at lower stress levels, which is caused by the high sensitivity of curve fitting in the high cycle fatigue region.

Medekshas and Balina [32] attempted to assess low cycle fatigue life prediction of notched components by using the von Mises stress as a proven design parameter. They used different geometry with stress concentration factor ranged from 1.39 to 7.8. They used both the results of finite element analysis and the experimental results obtained by low cycle fatigue tests of two alloy steels and two titanium alloys. From their study, it can be found that by using the stabilized cyclic stress strain and Neuber's rule, the low cycle fatigue life can be predicted by using the von Mises stress or strain at notch root.

Adib and Pluvinaige [33] proposed the volumetric approach to predict fatigue life for various notch components. Their volumetric method considers the elastic-plastic stress distribution at notch root, using the relative stress gradient and loading modes.

They used finite element analysis to determine the effective stress, effective plastic zone and relative stress gradient. They also determined the whole effective plastic zone and the stress field intensity in this zone was also computed. However, they suggested that this method is macromechanical method and it requires the special condition in crack (non-propagating cracks), but this method is easy to use and it can give conservative results for for different kinds of notch geometry.

Nicole et al., [34] proposed a probabilistic model of mean stress effects in strain-life fatigue. They added a probabilistic framework to deal with the experimental scatter to the Walker model to consider for the mean stress effect. They also included a parameter Υ that is related to the mean stress sensitivity of material. This addition made their model versatility that is not possessed by the other proposed mean stress methods. Their proposed method gave an improvement relative to the SWT model for materials which are significantly influence or less influence by mean stress.

Wang et al., [35] reported about the fatigue damage model for high cycle fatigue life prediction. In their report, they assumed the quasibrittle failure under high cycle fatigue, therefore the damage constitutive equation and the modified damage evolution equation are obtained with continuum damage mechanics. In order to describe the failure process of metallic material, they used the numerical analysis of FEM. The increment of specimen fatigue life and damage stage evolution was observed using damage mechanics-finite element analysis. At last, they can estimate the fatigue life of the specimen at the given stress level.

Susmel et al., [36] attempted to estimate the fatigue life of notched components by directly taking the multiaxiality into account of the local elasto-plastic stress-strain fields

acting on the fatigue deformation process zone. For more detail, they assumed that Stage I is the most significant stage to do modelling to exact estimation of fatigue damage and regardless of the sharpness of geometrical feature. According to their initial idea and by considering the advantage of modified Manson-Coffin curve method, their hypothesis formed that the crack initiation plane is always coincident with the material plane subjected the maximum shear strain amplitude. From their results, it can be concluded that their proposed multiaxial elasto-plastic approach seems to significantly support the idea that both the notch effect and the mean stress effect can be considered as problems of elasto-plastic inherent multiaxiality. The use of modified Manson-Coffin curve method under uniaxial cyclic loading in the presence of superimposed static loading seems to estimate as exact as fatigue lives obtained by applying both the Morrow corrections and the SWT parameter. But they suggested that more work should be done in this area to check the validity of such a modus operandi also in the sharp notches loaded to complex systems of variable amplitude cyclic forces and external constants by considering in full effect of non-proportional hardening.

Nicholas and Fatemi [37] studied the effect of notch on multiaxial fatigue behavior using thin tubular 2024-T3 aluminium specimens with a circular transverse hole. They performed the constant amplitude fully reversed axial, torsion and 90 degree out of phase axial torsion and in phase tests under load control. They used both Neuber's and FEA analysis to calculate the local stress distribution. Based on their analysis and experimental data, it can be found that when calculating the K_t values for multiaxial loading, it is necessary to select the suitable nominal and local stress definition as well as suitable location at the notch. In case of blunt notches, the location and maximum stress concentration values are changed with changing of nominal stresses. It was found that

predicted lives based on the Neuber's rule are in very good agreement with the results obtained from elastic-plastic analysis for torsion, axial and combined axial-torsion loadings. When compared the experimental life in pure torsion with pure axial loading at the same equivalent nominal strain, longer fatigue lives were obtained under pure torsion loading. Out-of-phased fatigue lives were shorter than in-phase fatigue lives at the same equivalent stress. Moreover, nominal stress life prediction based on von-Mises equivalent stress gave a better life estimation than maximum principal stress predictions. However, the ratios of their experimental and predicted lives were over a factor of 10.

Wang and Yang [38] estimated the high cycle fatigue strength of Ti-6Al-4V notched specimens considering the critical size effect. They tried to study not only the material effect but also notch geometry effect on high cycle fatigue strength. By assuming the product of critical distance and stress concentration factor was constant, they modified Theory of Critical Distance method. Their predicted high cycle fatigue strengths were fallen in an error interval of about $\pm 15\%$.

Joadder et al., [39] investigated the fatigue failure of notched round specimen under strain-controlled cyclic loading. Then fatigue life of notched round specimen was predicted by using the experimental strain-life relation obtained from smooth fatigue round specimen. In this study, they calculated the maximum strain by appropriate finite element analysis using the Armstrong, Frederick 1966 kinematic hardening model and cyclic hardening material model with ABAQUS software. It was reported that the maximum strain occurred at notch tip and the value of the maximum strain depended on the applied strain. For the validation of FE model, they compared the finite element results and experimental results of low cycle fatigue tests of round specimens. The obtained maximum strain values were utilized for prediction of fatigue life. Their

conclusions suggested that the total strain-life curves obtained by fatigue test of smooth round specimen can also be used for the prediction of fatigue life for notched specimen based on the maximum strain value at notch root. Moreover, if the maximum strain is compared with the fatigue life, the similar relationship can be obtained for the same material for any notch geometry. From the results, it is also found that the most predicted fatigue lives are shorter when compared to the experimental lives for all kinds of notched specimens. This may result from that the lives are predicted based upon the maximum strain at notch root. However, the actual failure may be influenced by the overall stress-strain state in notch cross section.

1.2.2 Effect of mean stress on smooth and notch fatigue behavior

It is known that mean stress effect on fatigue behavior is significant and important to consider in fatigue design. Therefore, extensive researches have been performed until now. In this section, papers related to the mean stress effect are reviewed.

Fatemi et al., [40] investigated fatigue behavior of notched specimen using QT and forged micro-alloyed steels. Mean stress tests were performed with K_t of 1.8 or 2.8. the modified Goodman equation was utilized to convert the test results to $R=-1$ and good correlation were obtained for specimen geometry with $K_t= 1.8$. The modified Goodman equation could provide the underestimate fatigue behavior because of a milder notch and crack growth was a significant portion until failure of specimen. The results of prediction gave small difference compared to the experimental results for both notched specimens. Notch effects were most significant at long life while not much at short life where the effects of notch blunting and localized plastic deformation would influence fatigue life.

Ince and Glinka [41] proposed the modification of the Morrow and the SWT mean stress correction models to take account of the mean stress effect on fatigue life. For

Morrow model, mean stress correction was applied only into the elastic term of the strain life equation. In case of the SWT model, mean stress correction also applied only to the elastic part of the strain cycles. Then, these two corrected models were used to compare with those of original Morrow and SWT model using existed mean stress fatigue test data. They attempted to apply to four different materials. The proposed model gave superior result for Incoloy 901f superalloy and ASTM A723 steel. In addition, both proposed and original models could be provided equally good correlation with experimental fatigue lives for 7075-T561 aluminium alloy and 1045 HRC steel. However, Morrow model gave less accurate predicted results for four materials compared to SWT models.

Yu et al., [42] investigated the effect of mean stress and effect of notch diameter on notch fatigue behavior of an SAE 1045 steel for $R=0$. Then, the results of notch effects were compared to completely reversed loading test. It was observed that the fatigue notch factor was larger for $R=-1$ tests compared to $R=0$ tests and the effect of fatigue notch factor more significantly influenced at longer life compare to shorter life. For predicting of fatigue notch factor, K_f , a computational method based on Neuber's rule was used due to the significant plastic deformation occurred at the notch root. For the blunt notch case, predictions were more accurate than the sharp notch. However, accurate predictions were obtained under $R=-1$ for both sharp and blunt notches.

Koh et al., [43] examined and documented the mean stress-strain effect on low cycle fatigue for a high strength A 723 quenched and tempered steel which is mainly used for pressure vessel. In their study, they used smooth specimens under axial strain-controlled low cycle fatigue conditions with various strain ratios R of -2, -1, 0, 0.5 and 0.75. Their target numbers of cycles to failure were ranged from 15 to 10^5 cycles. From

the results, it was found that cyclic stress-strain response under strain-controlled test were similar for all strain ratios. Mean stress relaxation was observed for all R ratio except under completely reversed loading $R = -1$. Moreover, it occurred only when plastic strain amplitudes were appeared during testing. Thus, they clearly pointed out that mean stress relaxation was dependent upon the cyclic plasticity. Tensile mean stress was deleterious to low cycle fatigue life, conversely compressive mean stress was beneficial effect to fatigue life. However, these effects happened only at the longer life with strain amplitude lower than 0.005. Then, their mean stress-strain relation was applied to Morrow model, the Lorenzo-Laird model and the SWT parameter. They suggested based on their results among three applied models, the log-log linear SWT model can give the best approximation of their mean stress data.

Hong Hao et al., [44, 45] studied the mean stress relaxation behaviour of 2124-T851 aluminium alloy under strain-controlled axial fatigue test with different strain ratios. The experimental results indicated that the material exhibited cyclic softening behavior in whole fatigue life and the mean stress was relaxed for all applied strain ratios except for the case of strain ratio $R=-1$. The tendency of cyclic softening linearly decreased with increasing applied strain amplitude and the decreasing strain ratio. It was observed that the decrease in fatigue life and ductility of material was corresponding to the higher strain ratios with increasing the density and length of the slip bands.

From their results, it can be understood that the mean stress relaxation depended not only on applied strain amplitude but also on applied strain ratio. Decreased fatigue life with increasing strain ratio was observed especially at lower strain amplitude due to accompany of mean stress and its relaxation during fatigue cyclic loading. Based on their quantitative analyses of the mean stress relaxation behavior, they developed a modified

empirical mean stress model which takes the strain ratio effect on strain-life relationship into account. Their proposed model can predict the mean stress relaxation at different strain ratio during strain-life fatigue cyclic loading.

As mentioned above, many researchers have tried to predict the fatigue life of notched specimen based on the conventional stress-life approach and strain-life approach in high cycle and low cycle fatigue regions. They have also taken account of the mean stress effect with existing mean stress models and modified ones. However, their predictions have been conducted using the remote applied stress ratio estimated notch stress-strain values obtained from analytical models under assumption of the constant mean stress (stress ratio) at notch root. However, they have not extended to study the local mean stress (stress ratio) variation on notch fatigue behavior and then there was almost no report on fatigue life prediction with taking account of variation of local stress ratio in wide range of fatigue from low cycle to high cycle fatigue regions. Therefore, it is important to study the variation of local mean stress (stress ratio) on notch fatigue behavior and necessary to consider the fatigue life prediction method for notch when the local mean stress (stress ratio) can not be kept constant during cyclic loading.

1.3 Objective of the present study

Based on the above survey of literature, there have been many researches on notch fatigue behavior in low cycle fatigue and high cycle fatigue regions. As discussed above, the strain-life curves under various remote stress ratios coincide each other and with that under $R=-1$ at high strain amplitudes in low cycle fatigue region. However, the stress-life curves under various stress ratios are separated each other in high cycle fatigue region where fatigue strength decreases with increasing stress ratio. When considering wide range of fatigue behavior extended over two typical regions, the stress ratio would be

varied from the remote stress ratio in high cycle fatigue region to $R = -1$ in low cycle fatigue region. For example, mean stress correction is applied only to the elastic term of the total strain-life curve in Morrow's model and mean stress correction is also applied only to elastic part of the strain cycle in SWT model. The ideas for these two assumptions are that the intermediate stress ratio is obtained by combining elastic strain with the remote stress ratio and plastic strain with $R = -1$ at each total strain amplitude. On the other hand, Koh et al., [43] pointed out that the mean stress relaxation is dependent on the cyclic plasticity. However, details of stress ratio variation in the transition region extended over the low cycle and high cycle fatigue regions have not yet been clarified.

Fatigue life predictions including mean stress effect in low cycle fatigue and high cycle fatigue regions have been successfully performed based on the proposed models, such as Neuber rule, Morrow model, Molski-Glinka model, Goodman diagram, Gerber equation, SWT model, etc. However, they are useful in low cycle fatigue region or in high cycle fatigue region. No intrinsic life prediction model in the transition region with change of stress ratio has not yet been developed, since detailed stress ratio variation behavior and mechanism have not yet been clarified.

Therefore, in the present study, for considering wide range of notch fatigue behavior including low cycle fatigue, transition and high cycle fatigue regions, load-controlled high cycle fatigue tests with various remote stress ratios and displacement-controlled low cycle fatigue tests of Ti-6Al-4V notched specimens have been carried out. Elastic-plastic finite element analysis of notched specimen under cyclic loading has been also carried out to estimate the cyclic stress strain distributions near notch region, local hysteresis loop at notch root, local stress ratio at notch root which have been combined with the SWT model and fracture mechanics approach for fatigue life prediction. And

then similar fatigue tests and FEA have been also carried out for A2024-T4 alloy to investigate the effects of material on notch fatigue behavior and local stress ratio variation. The present thesis consists of following five chapters:

Chapter 1 **Introduction:** The importance of fatigue, basic definition and stress strain behavior and literature review on previous research are briefly explained. The scope and objective of the present work is also addressed.

Chapter 2 **Notch fatigue behavior of Ti-6Al-4V alloy under load controlled high cycle fatigue tests:** Notch fatigue behavior of Ti-6Al-4V titanium alloy has been investigated under load-controlled high cycle fatigue tests and elastic-plastic finite element analysis was carried out in order to study the local stress strain behavior at the notch root. Based on analysis results, the kinking behavior of S-N in notched specimen was discussed. Fracture surface behaviors are also investigated for observed titanium alloy.

Chapter 3 **Notch fatigue behavior of Ti-6Al-4V alloy under displacement-controlled low cycle fatigue tests:** Notch fatigue behavior in the transition region between high and low cycle fatigue regions has been investigated by carrying out the displacement-controlled low cycle fatigue test of the Ti-6Al-4V alloy notched specimen combined with the results in the previous chapter under load-controlled high cycle fatigue test. The elastic-plastic finite element analysis of notched specimen under cyclic loading has been also carried out to investigate the local stress ratio variation at notch root depending on the applied nominal strain amplitude as well as stress-strain states during cyclic loading in detail. Based on the results of experiment and finite element analysis, local stress ratio variation regions and mechanisms of local stress ratio variation at the notch root were discussed. Fatigue life predictions with and without taking account of the

local stress ratio variation have been also performed for the whole range of the low cycle and high cycle fatigue regions including the transition region.

Chapter 4 **Notch fatigue behavior of A2024-T4 alloy in high cycle fatigue, transition and low cycle fatigue regions:** The detail of local stress ratio variation and its effects on notch fatigue behavior of different materials have been clarified. Based on the results of experiment and finite element analysis, aluminum alloy notch fatigue behavior were compared with the notch fatigue behavior of titanium alloy especially in transition region of S-N curve. The material dependence of local stress ratio variation was also discussed. Fatigue life prediction with and without taking account of the local stress ratio variation will make for the purpose of discussing the effect of local stress ratio variation on fatigue life prediction. Fracture surface behaviors are also investigated for observed aluminum alloy.

Chapter 5 **Summary:** Summarized the thesis and proposed for future work.

References

- [1] ASTM E 1150-1987, Standard Definitions of Fatigue, Annual Book of Standards, (1995) 753-762
- [2] R. I. Stephens, A. Fatemi, R.R. Stephens, H.O. Fuchs, Metal Fatigue in Engineering, 2nd John Wiley and Sons Inc., New York(2000)
- [3] G. Joadder, J. Shit, Fatigue Failure of Notched Specimen-A Strained-Life Approach, Mater Sci App 2 (2011)1730-1740
- [4] Meera N and Kaur Singh, Notch Tip Stress Strain Analysis in Bodies Subjected to Non-Proportional Cyclic Loads, Mechanical Engineering Thesis, Waterloo Onatario Canada (1998)
- [5] E. Haibach, H. DasLehrke,Verfahren Der Amplitude transformation zur Lebensdauerberechnung bei Schwingbeanspruchung, in: Archiv furr Eisenhüttenwesen 74(10) 623-638
- [6] A. A. Griffith, The Phenomena of Rupture and Flow in Solids, Philosophical Transactions of the Royal Society of London 221(1921) 163-198
- [7] G. Irwin, Analysis of Stresses and Strains Near The End of A Crack Traversing A Plate, J App Mech 24 (1957) 361-364
- [8] ASM Chapter 14, Element of Metallurgy and Engineering Alloys, Fatigue, ASM International (2008)
- [9] J. Lemaitre, J. Lemaitre, Modeling Very Low Cycle Fatigue, Int J Damage Mech 4 153-170
- [10] M. Makkonen, Statistical Size Effect in the Fatigue Limit of Steel, Int J Fatigue 23 (2001) 395-402

- [11] G.E. Dieter, Mechanical Metallurgy, McGraw-Hill United Kingdom (1988)
- [12] W. D. Pilkey, Peterson's Stress Concentration Factors 3rd, J. Wiley & Sons, New York (2007)
- [13] H. Neuber, Theory of Notch Stresses, Principles for Exact Stress Calculation, J. W. Edwards Ann Arbor (1946)
- [14] K. Molski, G. Glinka, A Method of Elastic-Plastic Stress and Strain Calculation At A Notch Root, Mat Sci Eng 50(1981) 93-100
- [15] W. Ramberg, W. Osgood, Description of Stress-Strain Curves By Three Parameters, National Advisory Committees for Aeronautics, Washington, D.C.(1943)
- [16] S. Suresh, Fatigue of Materials 2nd, Cambridge University Press Cambridge (1998)
- [17] J. A. Bannantine, J. J. Comer, J. L. Handrock, Fundamental of Metal Fatigue Analysis, Prentice Hall (1990)
- [18] R. Gary, Halford, P. Joseph, Gallagher, Fatigue and Fracture Mechanics 3 1st, ASTM, Chelsea (2000)
- [19] MSC Fatigue information, Fatigue User's Guide, Fatigue Theory, Total Life (S-N) Analysis, Crack Initiation/Strain-Life Analysis. URL www.mscsoftware.com
- [20] J. Morrow, Fatigue Properties of Metals, Fatigue Design Handbook, Warrendale (1968)
- [21] K. N. Smith, P. Watson, T. H. Topper, A Stress-Strain Function For The Fatigue of Metals, J. Mater 5 (1970) 767-778
- [22] T. Wehner, A. Fatemi, Effects of Mean Stress on Fatigue Behavior of A Hardened Carbon Steel, Intl J Fatigue 13, (1991) 241 - 248

- [23] S. J. Wang, M. W. Dixon, C. O. Huey Jr, and S. C. Chen, The Clemson Limit Stress Diagram For Ductile Parts Subjected To Positive Mean Fatigue Loading, *J Mech Design* 122 (2000) 143-146
- [24] N.E. Dowling, Mean Stress Effects In Stress-Life and Strain-Life Fatigue, 2nd SAE Brasil International Conference on Fatigue, São Paulo Brazil (2004)
- [25] N. E Dowling, C. A. Calhoun ,A .Arcari, Mean Stress Effects in Stress-Life Fatigue and The Walker Equation, *Fatigue Fract Eng M* 32 (2009) 163-179
- [26] R. Burger, Y.L Lee, Assessment of the Mean-Stress Sensitivity Factor Method in Stress-Life Fatigue Predictions, *J Test Eval* 41 (2013) 1-7
- [27] R.Wang, H. Cheng, J. Li, Stress Strain Analysis Of Notched Specimen Based On Material Property Gradient, *P Eng* 31 (2012) 360-365
- [28] A. Fatemi, Z. Zeng, A. Plaseied, Fatigue Behavior and Life Predictions of Notched Specimens Made of QT and Forged Microalloyed Steels, *Int J Fatigue* 26 (6) (2004) 663-672
- [29] B.N. Leis, T.H. Topper, Cyclic Deformation And Fatigue Analysis For Notched Components, *Nucl Eng Des* 29(3) (1974) 370-383
- [30] M.R. Bache, M. Tasleem, Fatigue Life Prediction Techniques For Notch Geometries In Titanium Alloys, *Int J Fatigue* 21(1999) 187-197
- [31] P.J. Hurley, M.T. Whittaker, S.J. Williams, W.J. Evans, Prediction Of Fatigue Initiation Lives In Notched Ti 6246 Specimens, *Int J Fatigue* 30 (2008) 623-634
- [32] H. Medekshas, V. Balina, Assessment of Low Cycle Fatigue Strength of Notched Components, *Mater Des* 27 (2006) 132-140

- [33] H. Adib, G. Pluinage, Theoretical and Numerical Aspects of The Volumetric Approach for Fatigue Life Prediction in Notched Components, *Int J Fatigue* 25 (2003) 67-76
- [34] P.M.G.P. Moreira, P.J. Tavares, N. Apetre, A. Arcari, N. Dowling, N. Iyyer, N. Phan, Probabilistic Model of Mean Stress Effects in Strain-Life Fatigue, *P Eng*, 114 (2015) 538-545
- [35] M.Wang, Q.Fei, P.Zhang, A Modified Fatigue Damage Model for High-Cycle Fatigue Life Prediction, *Adv Mater Sci Eng* (2016)
<http://dx.doi.org/10.1155/2016/2193684>
- [36] L. Susmel, B. Atzori, G. Meneghetti, D. Taylor, Notch and Mean Stress Effect in Fatigue As Phenomena of Elasto-Plastic Inherent Multiaxiality, *Eng Fract Mech* 78 (2011) 1628-1643
- [37] N. Gates, A. Fatemi, Notched Fatigue Behavior and Stress Analysis Under Multiaxial States of Stress, *International Journal of Fatigue* 67 (2014) 2-14
- [38] J. Wang, X. Yang, HCF Strength Estimation of Notched Ti-6Al-4V Specimens Considering The Critical Distance Size Effect, *Int J Fatigue* 40 (2012) 97-104
- [39] BikashJoadder, Jagabandhu Shit, SanjibAcharyya, SankarDhar, Fatigue Failure of Notched Specimen-A Strain-Life Approach, *Mater Sci App* 2 (2001) 1730-1740
- [40] A. Fatemi, Z. Zeng, A. Plaseied, Fatigue Behavior and Life Predictions of Notched Specimens Made of QT And Forged Microalloyed Steels, *Int J Fatigue* 26 (2004) 663-672
- [41] A.Ince, G.Glinka, A Modification of Morrow And Smith-Waston-Topper Mean Stress Correction Models, *Fatigue Frac Engng Mater Struct* 34 (2011) 854-861

- [42] M.T. Yu, D.L. DuQuesnay, T.H. Topper, Notch Fatigue Behaviour of SAE1045 Steel, *Int J Fatigue*, 10 (1988) 109-116
- [43] S.K.Koh, Stephens, Mean Stress Effects on Low Cycle Fatigue for A High Strength Steel, *Fatigue Fract. Engng Mater Struct* 14 (1991) 413-428
- [44] H. Hao, D. Ye, Y. Chen, M. Feng, J. Liu, A Study on The Mean Stress Relaxation Behavior of 2124-T851 Aluminum Alloy During Low-Cycle Fatigue at Different Strain Ratios, *Mater Design* 67 (2015) 272-279
- [45] H. Hao, D. Ye, C. Chen, Strain Ratio Effects on Low-Cycle Fatigue Behavior and Deformation Microstructure of 2124-T851 Aluminum Alloy, *Mater Sci Eng: A*, 605 (2014) 151-159

CHAPTER – 2

NOTCH FATIGUE BEHAVIOR OF

TI-6AL-4V ALLOY UNDER LOAD-

CONTROLLED HIGH CYCLE FATIGUE

TESTS

Chapter-2

Notch Fatigue Behavior of Ti-6Al-4V Alloy Under Load-Controlled High Cycle Fatigue Tests

2.1 Introduction

When the fatigue behavior of smooth specimen is presented in wide range of fatigue life (for example, $10 - 10^7$ cycles), the total strain-life curve is generally adopted which is given by the sum of the two curves: one is the elastic strain-life curve which dominates in high cycle fatigue regime and the other is the plastic strain-life curve which dominates in low cycle fatigue regime. Examples of the total strain-life curve are available in many reports and textbooks [1, 2, 3, 4, 5]. In the high cycle fatigue regime, the stress-life curve is generally adopted instead of the elastic strain-life curve.

For the fatigue behavior of notched specimen, the stress-strain level at the notch root becomes high and local plastic deformation can occur at the notch root even if the applied nominal stress is lower than the yield strength. In the low cycle regime, the total strain-life curve of the smooth specimen has been applied to predict the crack initiation life at notch root. Various prediction methods, such as Neuber [6] and Glinka [7] approaches to relate local stress and strain to their remote values, and

Morrow [8], Walker [9] and SWT [10] models to take account of mean stress effect, have been proposed and successfully applied to the various specimen geometries and loading modes.

However, most of research works have assumed that the local stress-strain state is stable and the mean stress (that is, the stress ratio) at notch root is also constant during fatigue loading. These assumption will be satisfied in the high cycle fatigue regime with small amount of local plastic deformation at the notch root and in the low cycle fatigue regime with fully plastic in the notch section. But between these two regions with a certain amount of local plastic deformation at notch root it is not sure whether the mean stress and the stress ratio can be constant during fatigue loading under a constant remote stress ratio. Knop et. al., [11] reported that if the plastic deformation occurred at the notch root, the mean stress relaxation could be induced which can influence fatigue life. Therefore, unless the variation of local mean stress is taken into account, the accuracy of life prediction will be low. However, only few research on the variation of local mean stress or local stress ratio at the notch root has been available until now. Therefore, details of the local stress ratio variation and its effect on fatigue life prediction have not yet been clarified.

In the present chapter, as the first step of detailed research on notch fatigue behavior focused on local stress ratio variation at notch root and its effect on fatigue life prediction of notched body, fatigue behavior of Ti-6Al-4V alloy notched specimens under load-controlled high cycle fatigue tests have been investigated. The stress-strain behavior at the notch root under cyclic loading has been also analyzed by using the elastic-plastic finite element method for detailed discussion about local stress ratio variation at notch root.

2.2 Experimental and analytical procedures

2.2.1 Material and specimens

The material used was Ti-6Al-4V alloy for the present investigation. The chemical composition and mechanical properties of the Ti-6Al-4V alloy are shown in Tables 2.1 and 2.2, respectively. The microstructure of the Ti-6Al-4V alloy consisted of the bimodal structure with equiaxed primary alpha phase and secondary phase in which acicular alpha phase is embedded in the beta matrix, as shown in Fig. 2.1. The average grain size measured by the line intersect method (ASTM E112) was 15 μm .

The smooth and notched specimens were prepared. Shapes and dimensions of the smooth and notched specimens are shown in Fig. 2.2 which were designed according to the ASTM-E606[12]. The notched specimen had a U-shaped circumferential notch with a notch root radius of 2 mm and a depth of 3 mm. Elastic stress concentration factor of the notch was 1.55[13]. After machining the specimens, surfaces of the specimen gage part were polished by using emery papers with the grades from #400 to #1000 in order to eliminate the effects of residual stress and surface roughness induced by the machining on fatigue behavior. After the polishing, the diameter of notched specimen at minimum section and the gage section diameter of smooth specimen were measured by using a travelling microscope with an accuracy of 10 μm .

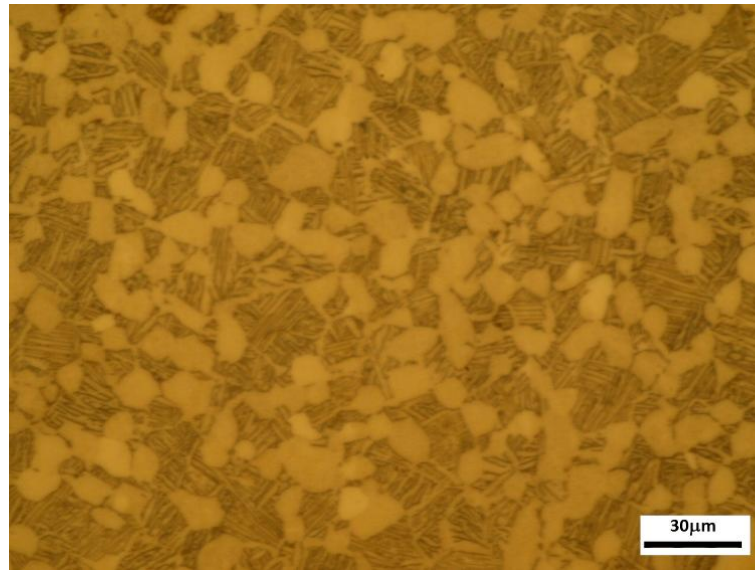


Fig. 2.1 Microstructure of the Ti-6Al-4V alloy used

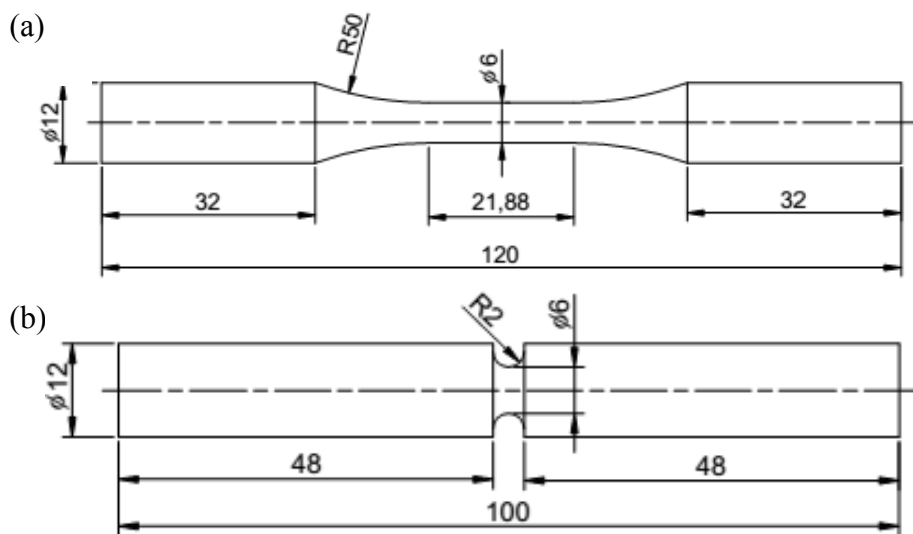


Fig. 2.2 Geometry of the (a) smooth and (b) notched specimens (in mm)

Table 2.1 Chemical composition of the Ti-6Al-4V alloy used

| Al | V | Ti | Fe | O | C | N | H | Y |
|------|------|-----|------|-----|------|--------|--------|--------|
| 6.32 | 4.34 | Bal | 0.17 | 0.2 | 0.03 | 0.0027 | 0.0024 | <0.001 |

Table 2.2 Mechanical properties of the Ti-6Al-4V alloy used

| | |
|-------------------------------|---------|
| Tensile Strength, σ_u | 967 MPa |
| 0.2% Proof Stress, σ_y | 885 MPa |
| Elongation at Break | 16.4% |
| Young's Modulus, E | 120 GPa |
| Reduction in Area | 43.5% |

2.2.2 Load-controlled fatigue strength test for high cycle fatigue region

Conventional load-controlled fatigue strength tests in the high cycle region to obtain S-N curves were carried out at a frequency of 20 Hz under a sinusoidal wave form of loading with two different stress ratio (R) of 0.1 and 0.5 by using a servo-hydraulic fatigue testing machine with a load capacity of 50 kN. Test method was followed the ASTM standard E468-11[14] and the loading alignment was carefully adjusted before conducting the tests according to the ASTM E606 [12]. The numbers of smooth specimens tested were 10 and 7 for $R=0.1$ and 0.5, respectively. Those of notched specimens were 13 for both $R=0.1$ and 0.5. All the tests were performed in

laboratory air at room temperature. Fracture surfaces of the specimens were examined in detail by using a scanning electron microscope (SEM).

2.2.3 Cyclic stress-strain curve

To obtain a cyclic stress-strain curve of the present material, which was used in the FEA, strain-controlled tests were performed for the smooth specimen. The specimen was subjected to fully reversed loading with triangular waveform according to a standard incremental step test method [15, 16] in a servo-hydraulic fatigue testing machine with a load capacity of 50 kN. An extensometer with 13 mm gauge length was used for the strain-controlled test. In this method, the specimen was subjected to block loading with gradually increasing and decreasing strain amplitudes. Details of the block loading with the maximum strain amplitude of 1.2% were as follows: the starting strain amplitude was 0.4% and increased up to 1.2% with a strain increment step of 0.1% under a strain rate of 0.05% per second. The strain decreasing process was symmetrically reversed to the strain increasing process. After repeated few loading blocks, the stress-strain response was stabilized. By connecting the peak stresses at each hysteresis loops in the stabilized block, cyclic stress-strain curve was obtained.

2.2.4 Finite element analysis

Finite element analysis of stress and strain across the notch has been carried out using the commercial finite element method (FEM) software MARC (Mentat 2013) [17]. 2D axisymmetric analysis was adopted due to the geometrical and loading symmetry. Four noded axisymmetric solid elements were used to model the quarter of the specimen in the analysis. Appropriated boundary conditions were incorporated in the model as shown in Fig. 2.3. In order to confirm mesh size effect on stress distribution at the notch root, elastic model was used to make by defining Young's modulus of 73 GPa and Poisson's ratio of 0.33. Tensile loading was applied to the elastic model to study the elastic stress concentration at the notch. Because large variation would occur stresses and strains near the notch root due to stress concentration, the mesh was refined close to the notch root to get the theoretical stress concentration factor at the notch root.

The mesh size at the notch root was determined when the stress concentration factor obtained by the elastic FEA with refined mesh size under monotonic tensile loading coincided with that obtained by the elasticity theory. When the mesh size at the notch root was 57 μm , the elastic stress concentration factor estimated by the elastic FEA was 1.55 and in good agreement with the theoretical elastic stress concentration factor. Therefore, the mesh size of 57 μm at the notch root was adopted for eliminating the mesh size effect in the FE model.

As results, the total numbers of elements and nodes of the FE models employed in the present work were 5500 elements and 5671 nodes, respectively. A FE model of notched specimen and final mesh type are also presented in Fig. 2.3.

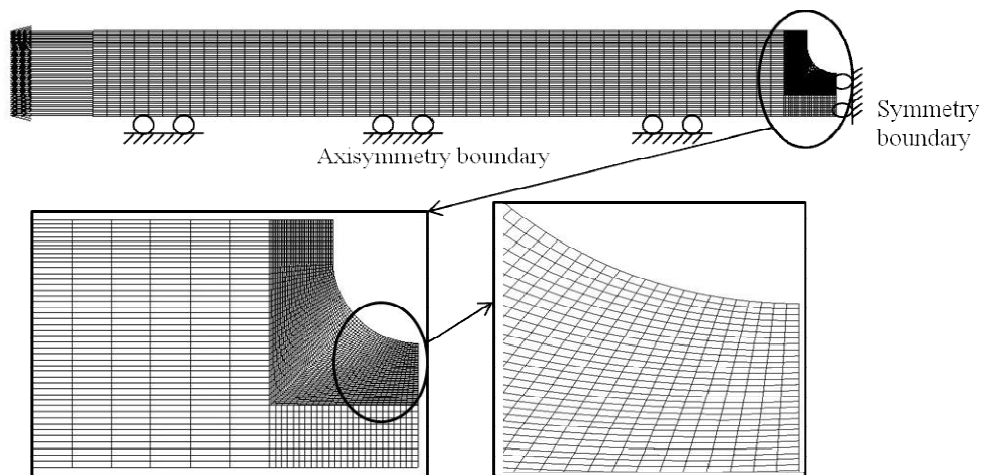


Fig. 2.3 FEM model of the notched specimen

After the mesh size effect was confirmed by the elastic analysis, the elastic-plastic FEA was carried out. The material properties used for the elastic-plastic FEA were obtained from the experimental results of incremental step test explained in the section 2.2.3 and listed in Table 2.3. The analysis was performed with Poisson's ratio of 0.5 in the plastic region of notched specimen with isotropic hardening rule to study the cyclic stress-strain behavior at the notch root.

The cyclic loading was applied to the FEM model in two steps. In the first step, an initial mean load was applied. In the second step, the cyclic loading of sinusoidal waveform as the experiment was applied. The analysis time to apply the sinewave form is chosen to be 100 seconds for total 100 cycles and the number steps is 1000. Therefore, the fixed constant time step is 0.1 in this elastic-plastic analysis. Moreover, the analysis was performed with two different stress ratios of 0.1 and 0.5. Von-Mises

yield criterion was applied for plastic deformation where von Mises stress is defined as:

$$\sigma_{vm} = \sqrt{1/2 ((\sigma_1 - \sigma_2)^2 + (\sigma_2 - \sigma_3)^2 + (\sigma_3 - \sigma_1)^2)} \quad (2.1)$$

where σ_1 , σ_2 and σ_3 are the principal stresses. The effective plastic strain according to the isotropic yield criterion which is defined as the following equation:

$$\sigma_y = A(\varepsilon_0 + \bar{\varepsilon})^n + B\dot{\bar{\varepsilon}}^m \quad (2.2)$$

where ε_0 is the strain corresponding to the initial yield stress, $\bar{\varepsilon}$ is the equivalent strain, $\dot{\bar{\varepsilon}}$ is the rate of equivalent strain and A and n are the strength coefficient and the hardening exponent, respectively. Since the deformation behaviour in the present study is not time dependent, the second term of Eq. (2.2) can be neglected and the material constants B and m are assumed to be zero.

2.3 Results

2.3.1 Load-controlled fatigue strength tests of the smooth and notched specimens

Figure 2.4 shows relationships between applied nominal stress amplitude and number of cycles to failure for the smooth and notched specimens under two different R of 0.1 and 0.5. The nominal stress for the notched specimen was evaluated by the applied load divided by the minimum cross-sectional area at notch root. As can be seen from the figure, significant reduction of fatigue strength was observed in the notched specimen compared to the smooth specimen, which is commonly known as the effect of notch [18]. It is also well known that fatigue strength decreased with increasing stress ratio R (that is, mean stress, σ_m) [19], where the relationship between mean stress and stress ratio is given as: $\sigma_m = (1+R)\sigma_{max}/2$, where σ_{max} is the maximum stress. As seen from the Fig. 2.4, the S-N curve is not smooth and kinked due to the development of plastic deformation at the notch root where the kinked point is hereafter called as the critical nominal stress amplitude.

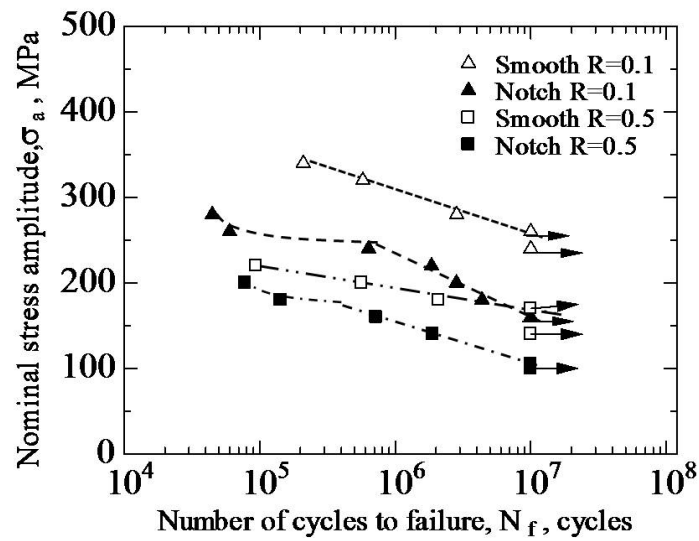


Fig. 2.4 S-N curves for the smooth and notched specimens of the Ti-6Al-4V alloy

2.3.2 Fracture surface observation

Overall fracture surface observations for the smooth and notched specimens tested under two different stress ratios showed only single crack nucleation for the smooth and notched specimens regardless of applied stress level and stress ratio as shown in Fig. 2.5 and 2.6. From the detailed observations of the crack nucleation sites at higher magnifications, it was confirmed that there was no internal or subsurface crack nucleation from inclusions or precipitates.

To investigate more detail of the transition behaviour of S-N curve in notched specimen, elastic-plastic finite element analysis is performed for notched specimen.

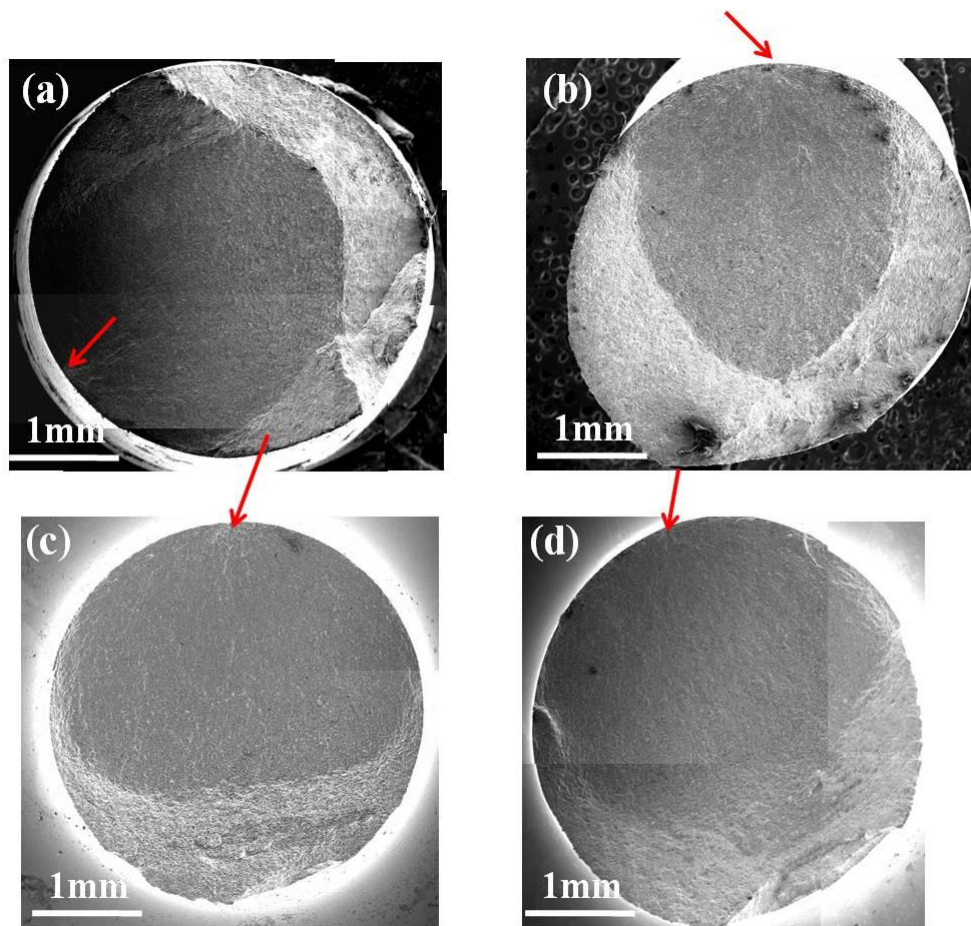


Fig. 2.5 Fatigue fracture surfaces of the smooth specimens tested at (a) $\sigma_a = 280\text{MPa}$, $N_f = 2,839,763$ cycles (b) $\sigma_a = 340\text{MPa}$, $N_f = 577,026$ cycles and the notched specimen tested at (c) $\sigma_a = 280\text{MPa}$, $N_f = 44,756$ cycles (d) $\sigma_a = 180\text{MPa}$, $N_f = 4,376,196$ cycles under $R = 0.1$

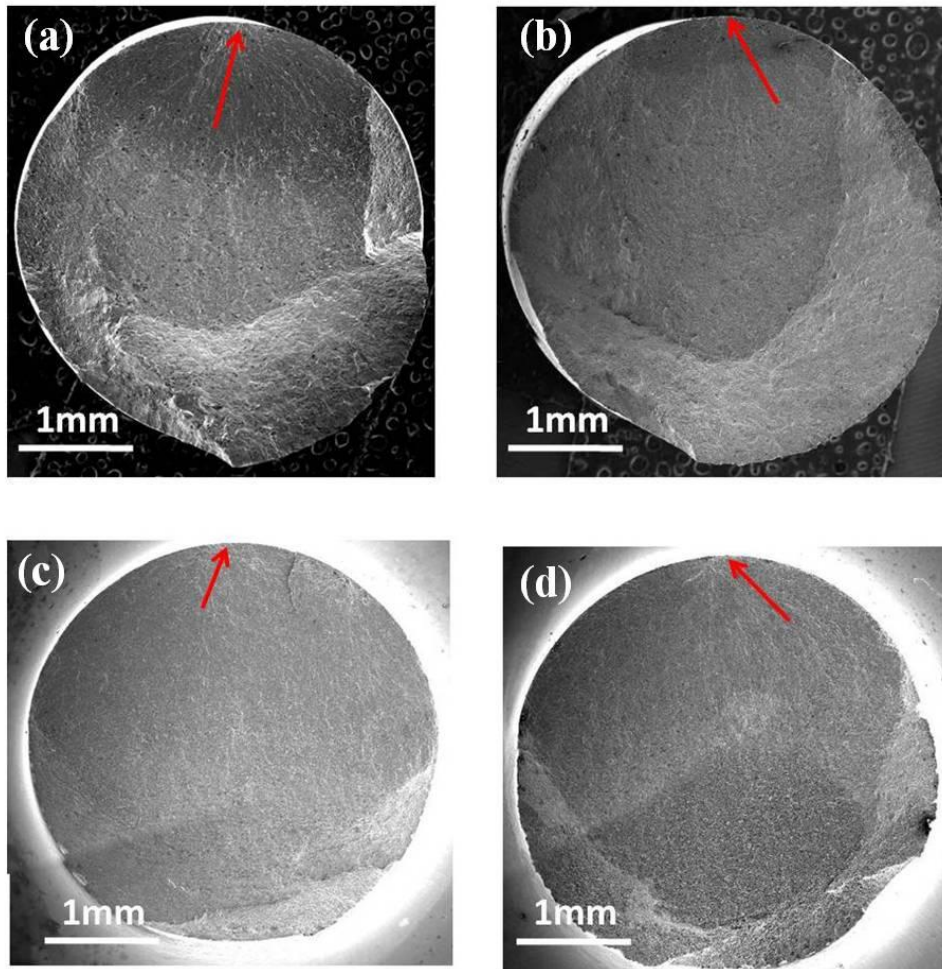


Fig. 2.6 Fatigue fracture surfaces of the smooth specimens tested at (a) $\sigma_a = 200\text{MPa}$, $N_f = 564,203$ cycles (b) $\sigma_a = 220\text{MPa}$, $N_f = 93,766$ cycles and the notched specimen tested with (c) $\sigma_a = 140\text{MPa}$, $N_f = 1,897,399$ cycles (d) $\sigma_a = 200\text{MPa}$, $N_f = 78,201$ cycles under $R = 0.5$

2.3.3 Cyclic stress-strain behavior

The cyclic stress-strain curve determined by using the incremental step method under a strain-controlled cyclic loading test is shown in Fig.2.7. The static stress-strain relationship is also presented in the figure [20]. By comparing the two stress-strain curves, it is found that the cyclic softening occurs during cyclic loading in the present Ti-6Al-4V alloy which has been commonly observed in the Ti-6Al-4V alloy [21, 22]. The relationship between cyclic strain amplitude $\Delta\varepsilon/2$ and cyclic stress amplitude $\Delta\sigma/2$ can be expressed in the following equation [23]:

$$\frac{\Delta\varepsilon}{2} = \frac{\Delta\sigma}{2E} + \left(\frac{\Delta\sigma}{2K'}\right)^{(1/n')} \quad (2.3)$$

where K' is the cyclic strength coefficient, n' the cyclic strain hardening exponent and E the Young's modulus. The cyclic properties determined from the cyclic stress-strain curve are listed in Table 2.3. The obtained cyclic stress-strain relationship was utilized in the FEA simulation under cyclic loading.

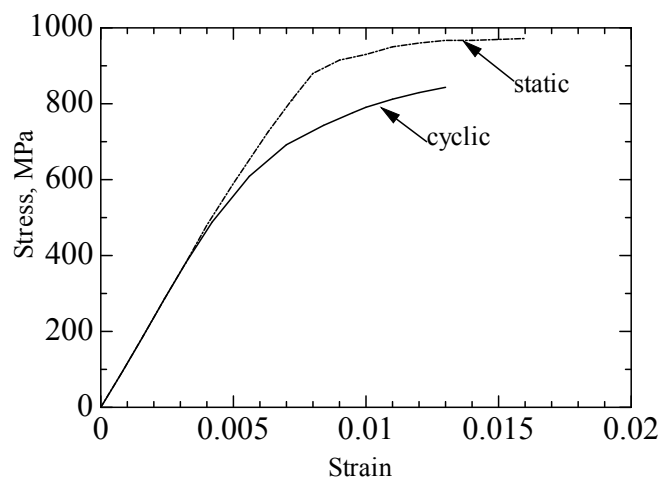


Fig.2.7 Cyclic stress strain curve for the Ti-6Al-4V alloy

Table 2.3 Cyclic properties of the Ti-6Al-4V alloy

| | |
|-----------------------------------|---------|
| Cyclic yield strength, σ_y | 720 MPa |
| Young's modulus, E | 113 GPa |
| Cyclic strength coefficient, K' | 1439 |
| Cyclic hardening exponent, n' | 0.106 |

2.3.4 Elastic-plastic FEA for the notched specimen

To investigate more detail of the kinked behavior in S-N curve of a notched specimen, elastic-plastic finite element analysis has been performed for a notched specimen. Figure 2.8 and 2.9 show von Mises stress and corresponding plastic strain distributions around the notch root under $R=0.1$ and 0.5 . As seen from the figure, for all applied nominal stress amplitudes, von Mises stress at the maximum load is the highest at the notch root and decreased toward the center of the specimen. Localized plastic deformation occurred around the notch root when the applied nominal stress amplitudes were higher than 160MPa and 240 MPa for $R=0.1$ and 0.5 , respectively. The plastic strain region at the notch root increased with an increase in applied nominal stress amplitude as shown in Fig. 2.8 (b) and 2.9 (b) .

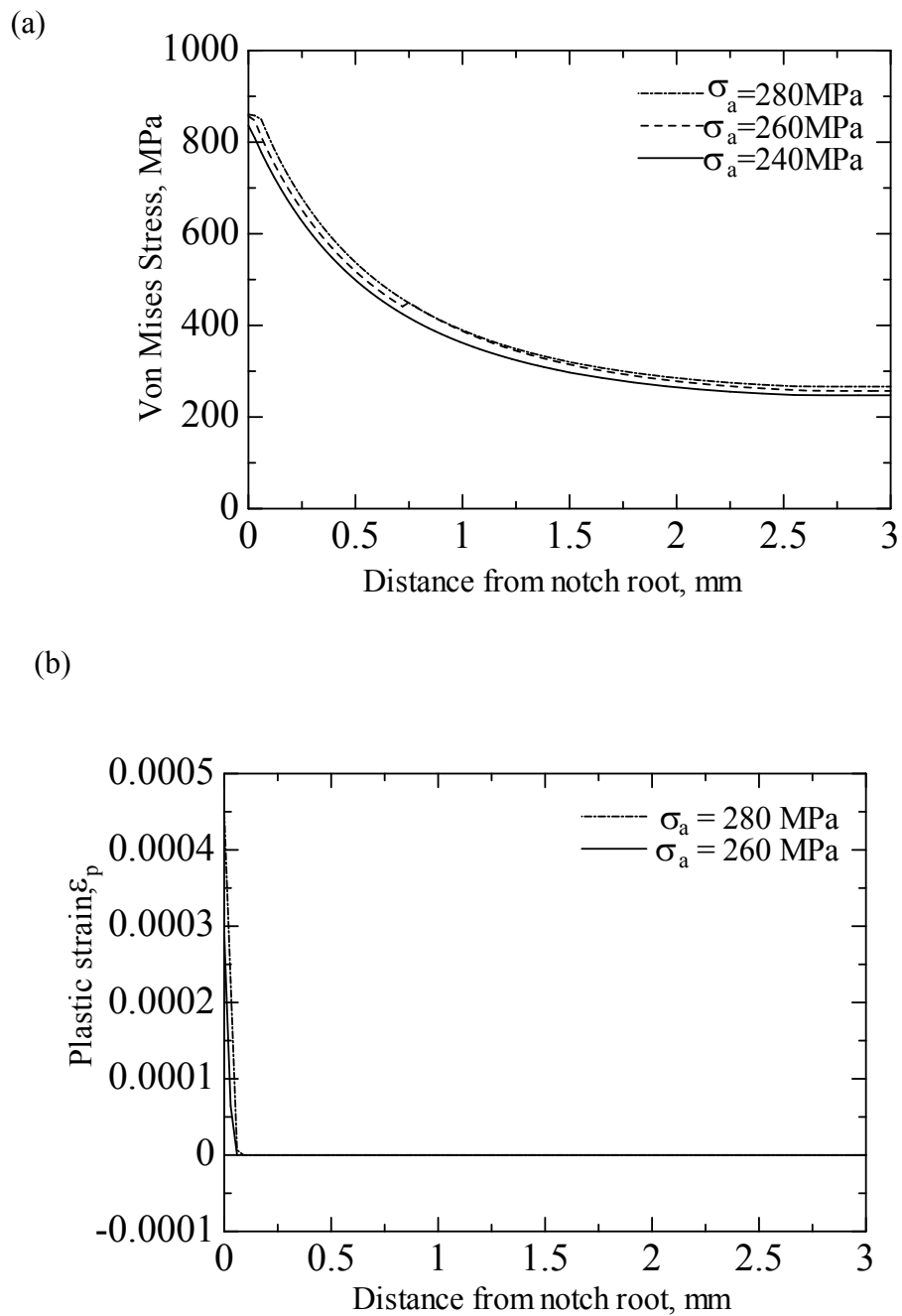
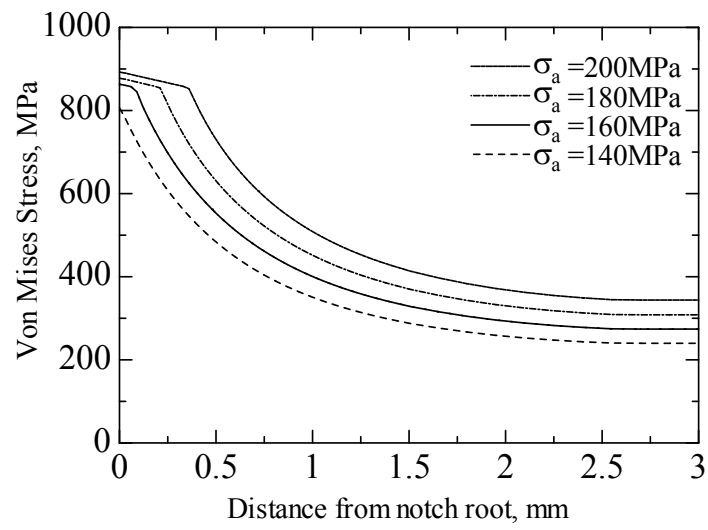


Fig. 2.8 The von Mises stress distribution near notch root in the first cycle (a) and the corresponding plastic strain distribution near notch root region, (b) under $R=0.1$

(a)



(b)

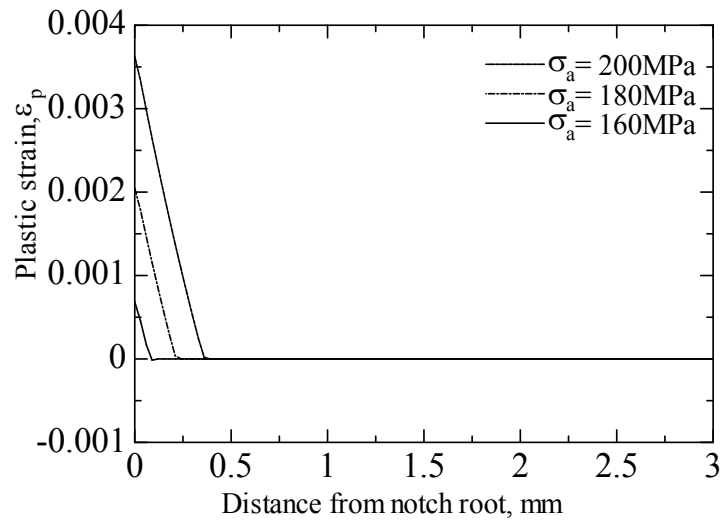


Fig. 2.9 The von Mises stress distribution near notch root in the first cycle (a) and the corresponding plastic strain distribution near notch root region, (b) under $R=0.5$

2.3.4.1 Stress distribution at notch root for R=0.1

Contour plots of von Mises stress distribution induced by the cyclic loading at the notch root from FEA results are given in Fig. 2.10. These contour plots are taken at the maximum stress applied to the model. For all applied stress levels, von Mises stress is the highest at the notch root and decreased toward the center of the notch plane. When the applied stress amplitude is lower as $\sigma_a = 240\text{MPa}$, the highest von Mises stress values is lower than the yield strength and fully elastic deformation occurred at the notch root to notch center as shown in Fig. 2.10(a). But when stress amplitude is $\sigma_a = 260\text{MPa}$, von Mises stress at the notch root were higher than the yield stress but it decreased toward the notch center and elastic-plastic deformation behavior was obtained as shown in Fig. 2.10(b). When stress amplitude was higher as $\sigma_a = 280\text{MPa}$ in Fig. 2.10(c), von Mises stress value at the notch root and notch center was higher than the yield stress and fully plastic deformation behavior was observed. Figure 2.11 shows the comparison of evolution of localized plastic strain at the notch root for three different stress amplitude levels.

2.3.4.2 Stress strain response hysteresis loop at notch root for R=0.1

Examples of stress-strain hysteresis at notch root during cyclic loading under R=0.1 estimated by the elastic-plastic FEA are shown in Fig. 2.12. These stress-strains relationships were taken at the notch root of the comp 11 loading direction when maximum stress applied to the model. As found from the figure, when the nominal stress amplitude was in the lower range of 240 MPa, the stress-strain hysteresis was fully elastic. When the stress level was increased up to 260 MPa, plastic deformation was found at the first cycle and then the stress-strain response became linear elastic in

the following cycles. With further increasing the nominal stress amplitude up to 280 MPa, plastic deformation occurred at the first loading cycle and then small plastic deformation was repeated in a few cycles and finally the stress-strain response became linear elastic. It was also found from Fig. 2.12(c) that after localized plastic straining at notch root, the local mean stress decreased and the local stress ratio at notch root became low from the applied remote stress ratio of 0.1.

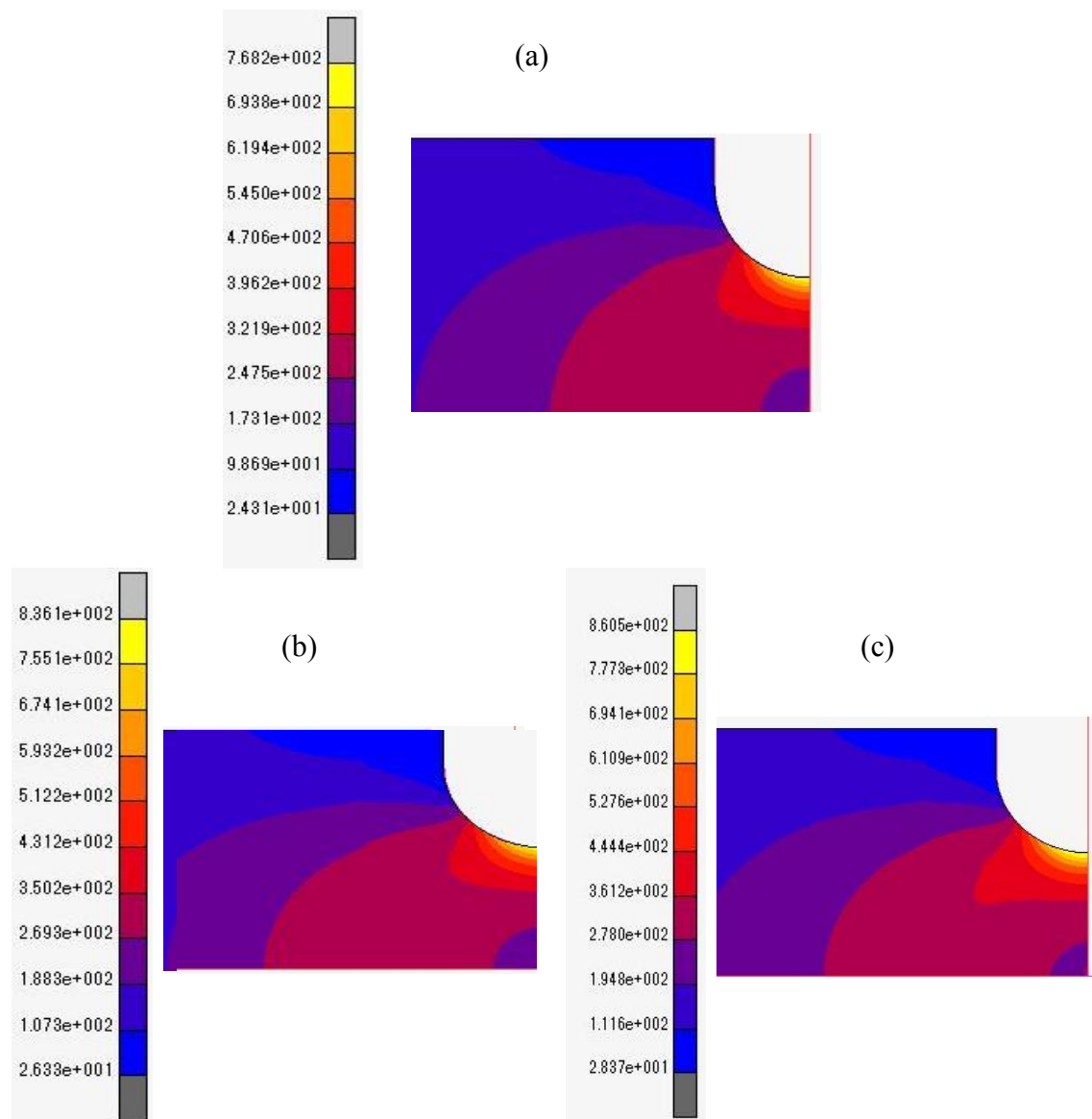


Fig. 2.10 Finite element analysis of notch specimen under load-controlled cyclic loading: von Mises stress distribution from notch root to notch center under $R = 0.1$: (a) $\sigma_a = 240$ MPa, (b) $\sigma_a = 260$ MPa, (c) $\sigma_a = 280$ MPa

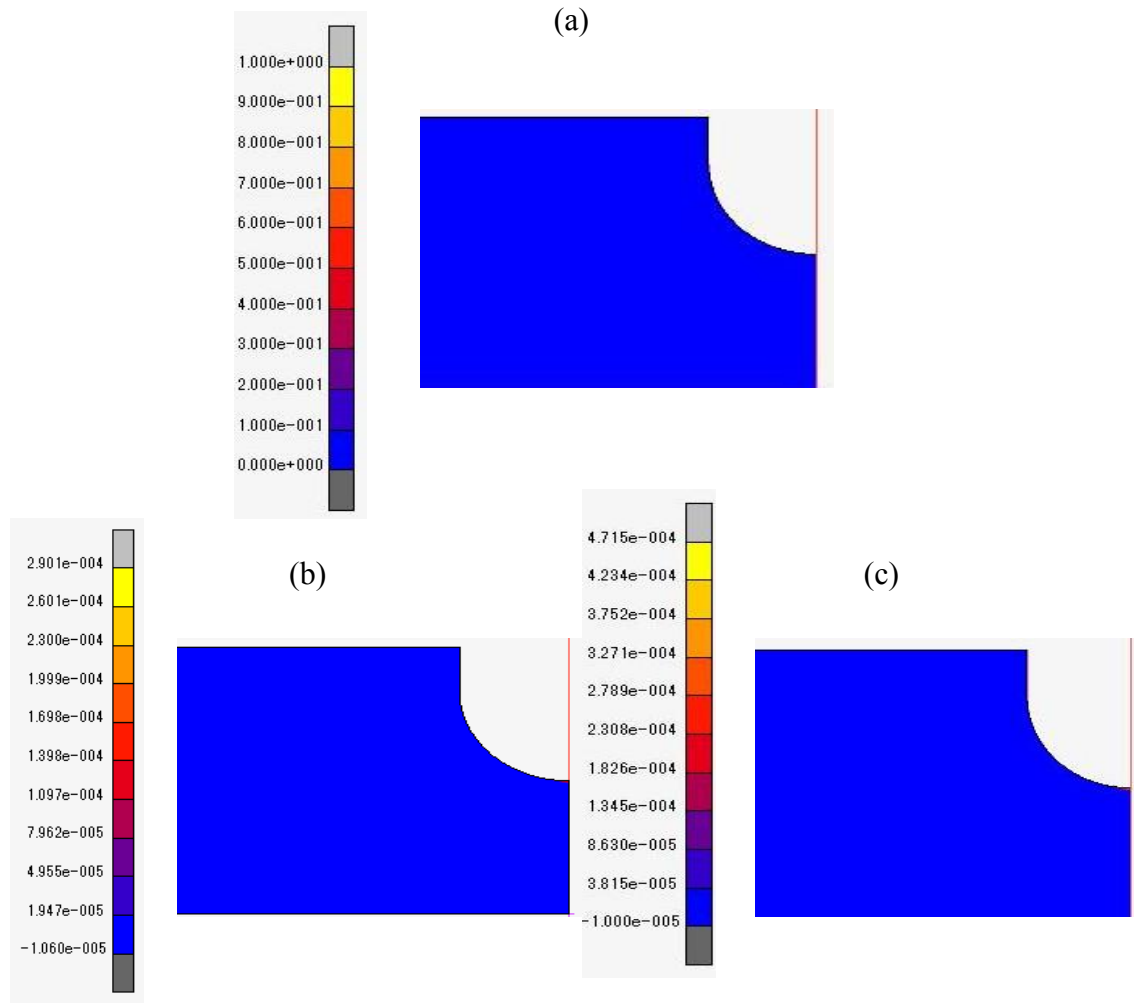


Fig. 2.11 Finite element analysis of notch specimen under load-controlled cyclic loading: plastic strain distribution from notch root to notch center under $R=0.1$: (a) $\sigma_a = 240$ MPa, (b) $\sigma_a = 260$ MPa, (c) $\sigma_a = 280$ MPa

Stress-strain curves at the notch root determined from the stress-strain analysis are presented from Fig.2.13 to Fig.2.15 for three stress amplitude levels 240MPa, 260MPa and 280MPa. In order to understand the total stress-strain history cycles and subsequent following cycles at notch root during cyclic loading, total cycles and each cycles behavior was taken out and also plotted as shown in figures.

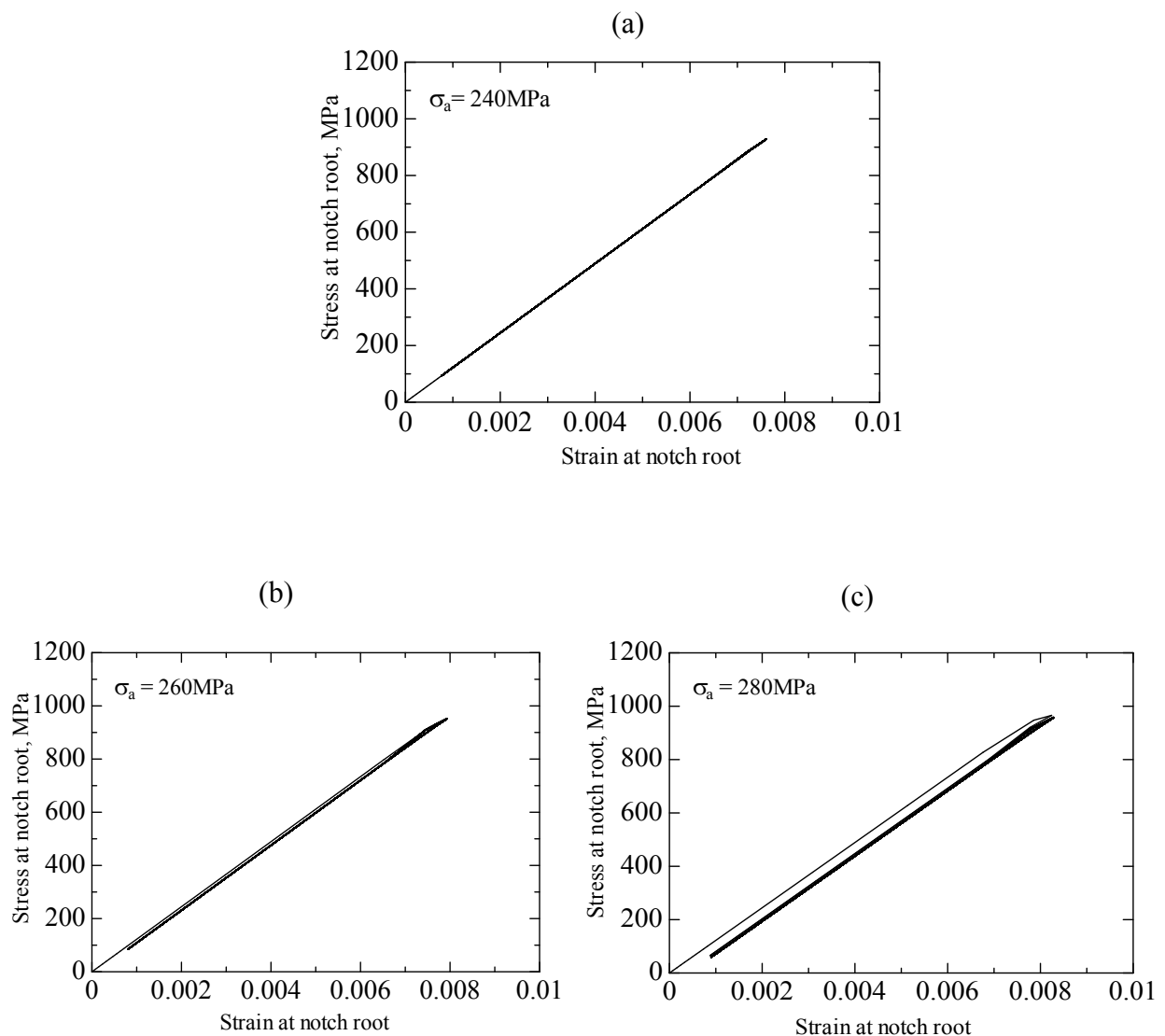


Fig. 2.12 Cyclic stress strain hysteresis at notch root under $R=0.1$: (a) $\sigma_a = 240\text{MPa}$, (b) $\sigma_a = 260\text{MPa}$, (c) $\sigma_a = 280\text{MPa}$.

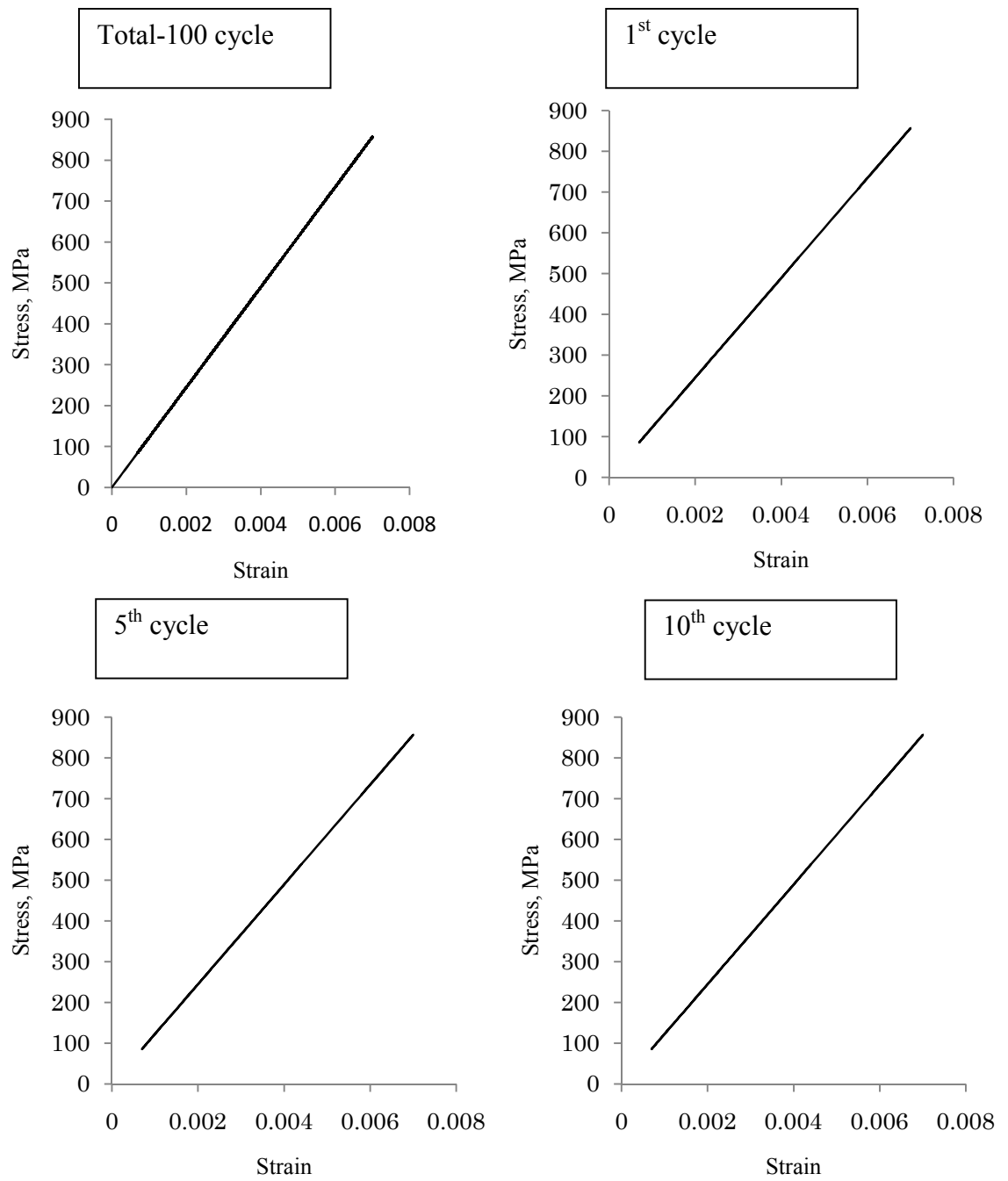


Fig. 2.13 Cyclic stress strain hysteresis at notch root under R=0.1 at $\sigma_a = 240\text{MPa}$

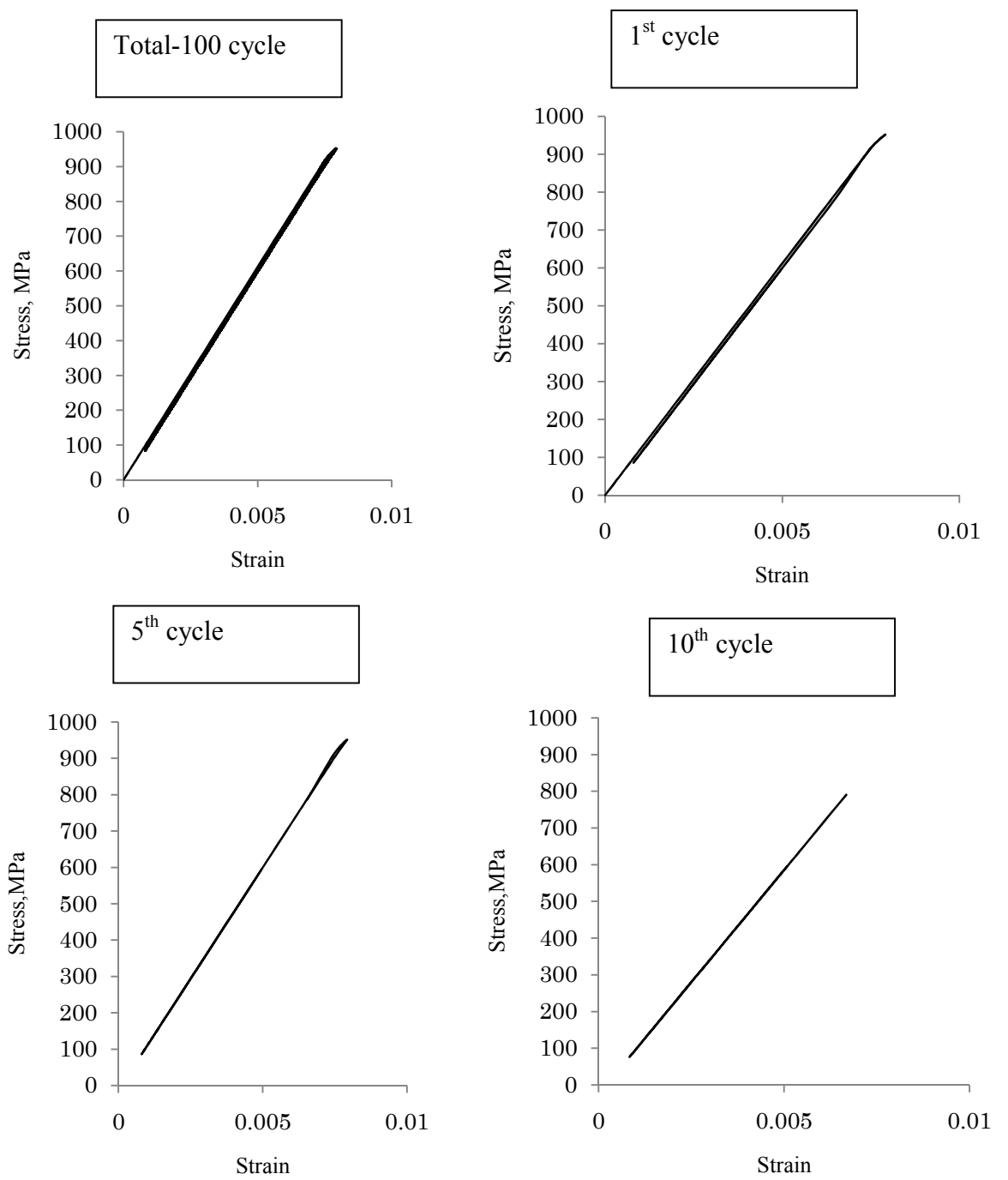


Fig. 2.14 Cyclic stress strain hysteresis at notch root under $R = 0.1$ at $\sigma_a = 260\text{MPa}$

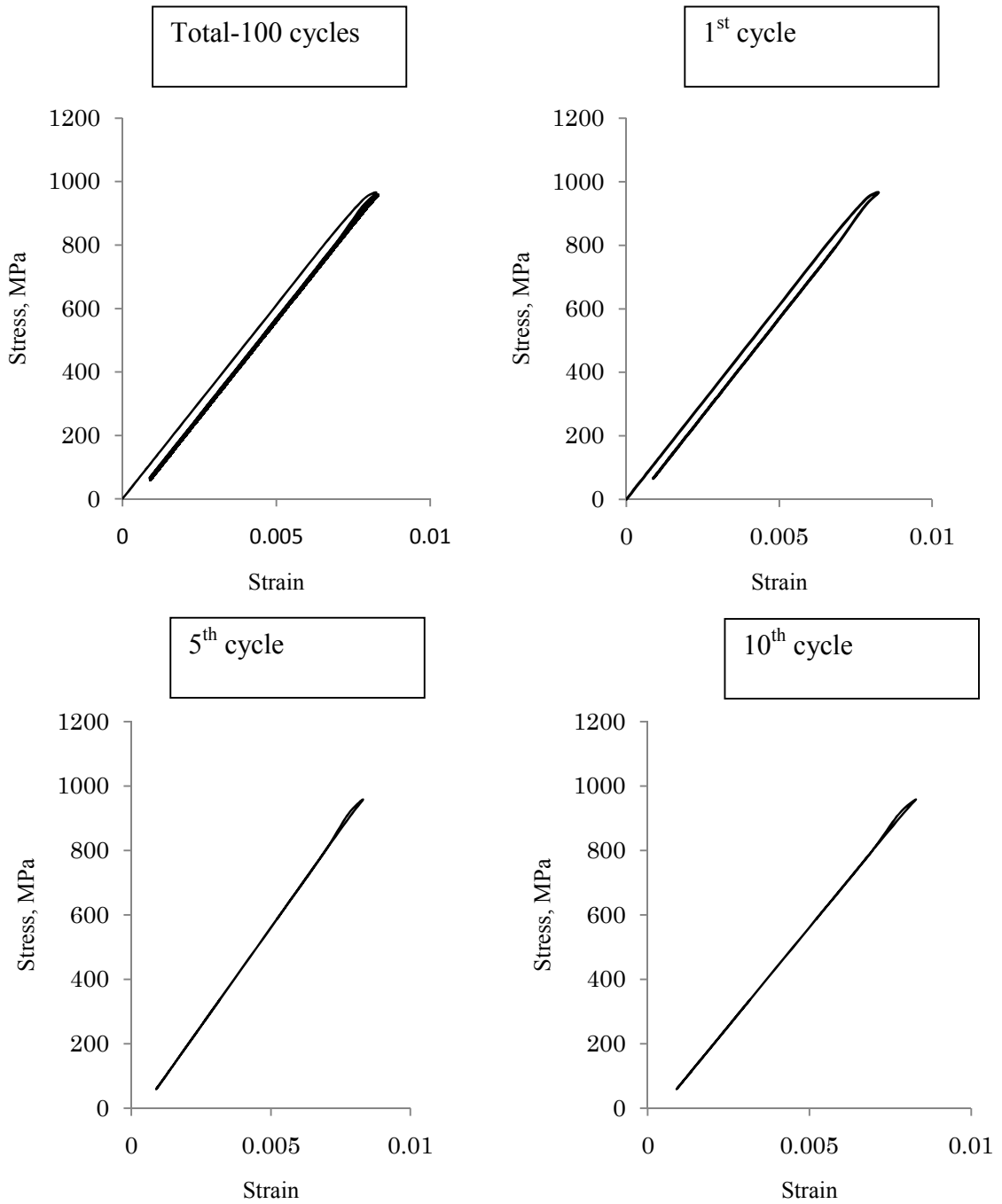


Fig. 2.15 Cyclic stress strain hysteresis at notch root under $R = 0.1$ at $\sigma_a = 280\text{MPa}$

2.3.4.3 Stress distribution at notch root for R=0.5

Contour plots of von Mises stress distribution induced by the cyclic loading at the notch root from FEA results are given in Fig. 2.16. These contour plots are taken at the maximum stress applied to the model. For all applied stress levels, von Mises stress was the highest at the notch root and decreased toward the center of the notch plane. When the applied stress amplitude is lower as $\sigma_a = 120\text{MPa}$, the highest von Mises stress values is lower than the yield strength and fully elastic deformation occurred at the notch root to notch center as shown in Fig. 2.16(a). But when stress amplitude is $\sigma_a = 160\text{MPa}$, von Mises stress at the notch root was higher than the yield stress but it decreased toward the notch center and elastic-plastic deformation behavior was obtained as shown in Fig. 2.16(b). When stress amplitude was higher as $\sigma_a = 200\text{MPa}$ in Fig. 2.16(c), von Mises stress value at the notch root and notch center was higher than the yield stress and fully plastic deformation behavior was observed. Fig. 2.17 shows the comparison of evolution of localized plastic strain at the notch root for three different stress amplitude levels.

2.3.4.4 Stress strain response hysteresis loop at notch root for R=0.5

Examples of stress-strain hysteresis at notch root during cyclic loading under R=0.5 estimated by the elastic-plastic FEA are shown in Fig.2.18. These stress-strains relationships were taken at the notch root of the comp 11 loading direction when maximum stress applied to the model. As found from the figure, when the nominal stress amplitude was in the lower range of 120 MPa, the stress-strain hysteresis was fully elastic. When the stress level was increased up to 160 MPa, plastic deformation was found at the first cycle and then the stress-strain response became linear elastic in

the following cycles. With further increasing the nominal stress amplitude up to 200 MPa, plastic deformation occurred at the first loading cycle and then small plastic deformation was repeated in a few cycles and finally the stress-strain response became linear elastic. It was also found from Fig. 2.18(c) that after localized plastic straining at notch root, the local mean stress decreased and the local stress ratio at notch root became low from the applied remote stress ratio of 0.5.

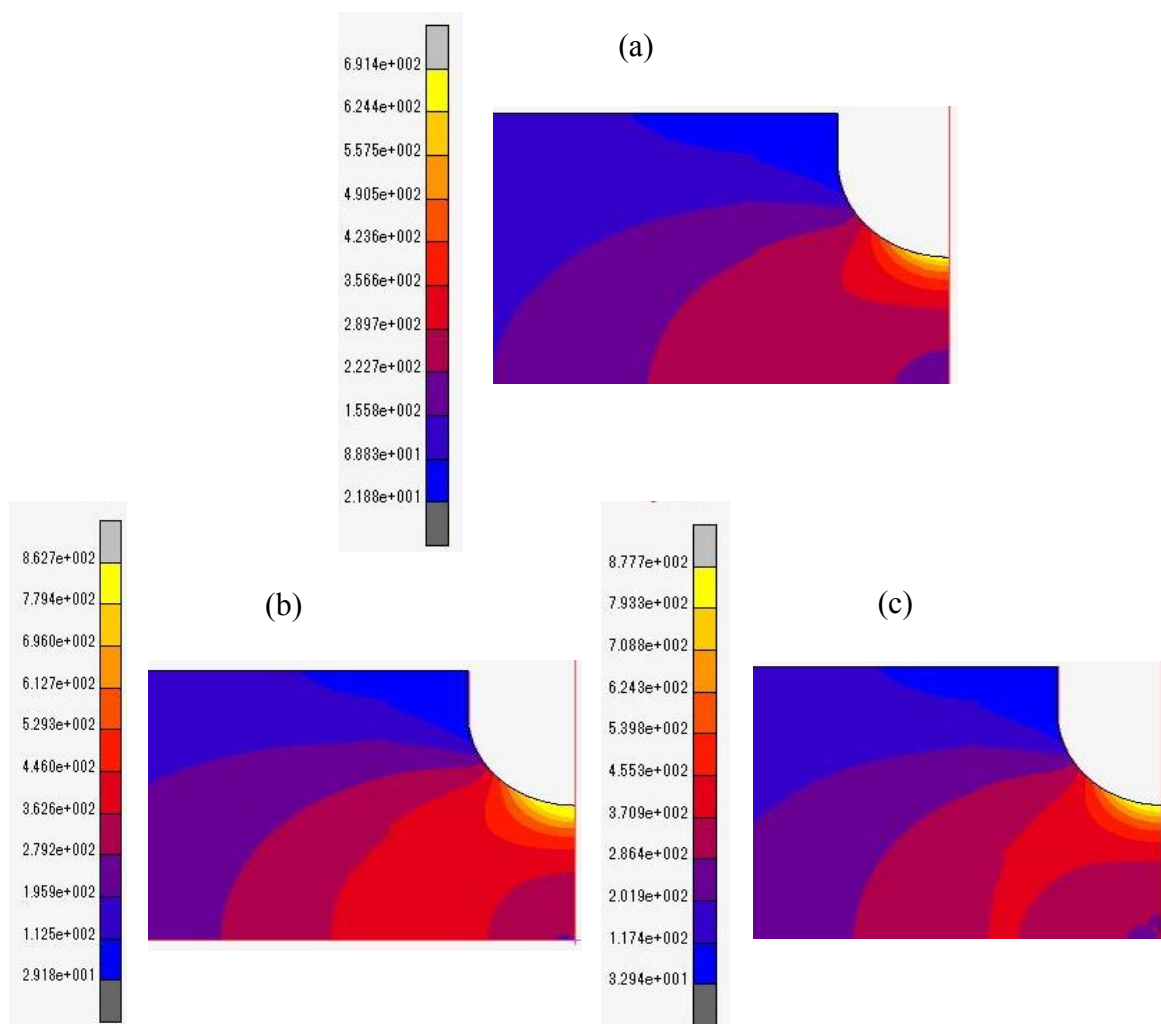


Fig. 2.16 Finite element analysis of notch specimen under load-controlled cyclic loading: von Mises stress distribution from notch root to notch center under $R = 0.5$:

(a) $\sigma_a = 120\text{MPa}$, (b) $\sigma_a = 160\text{MPa}$, (c) $\sigma_a = 200\text{MPa}$

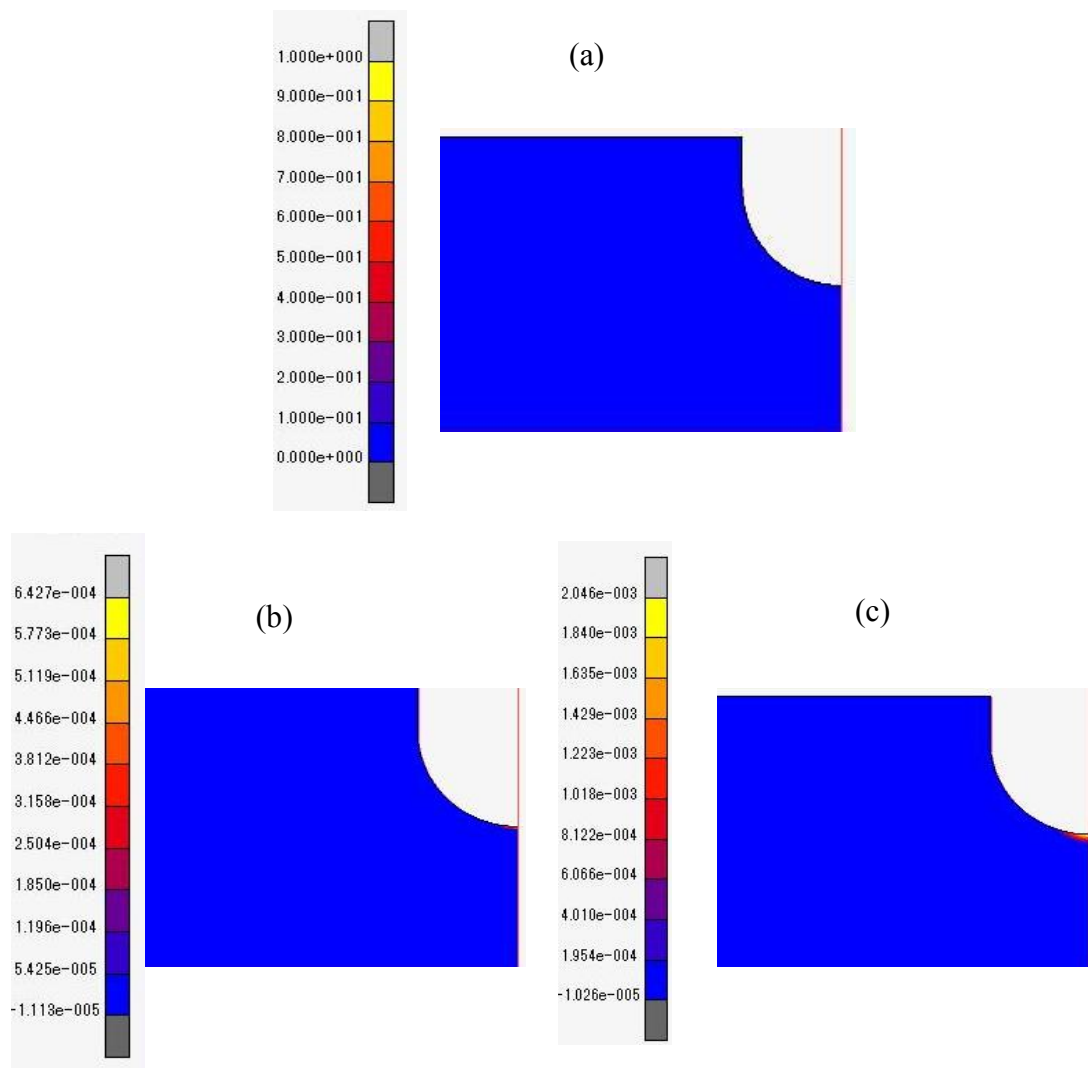
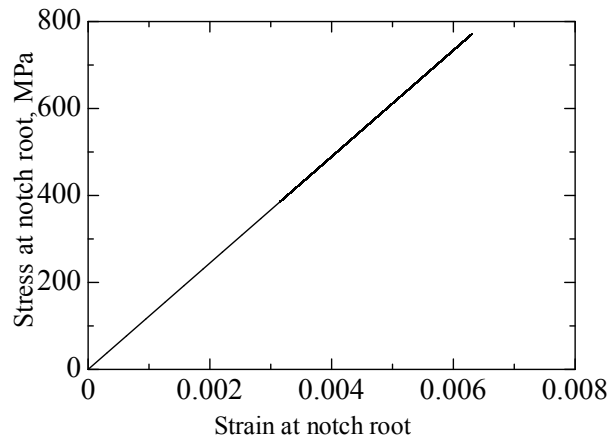


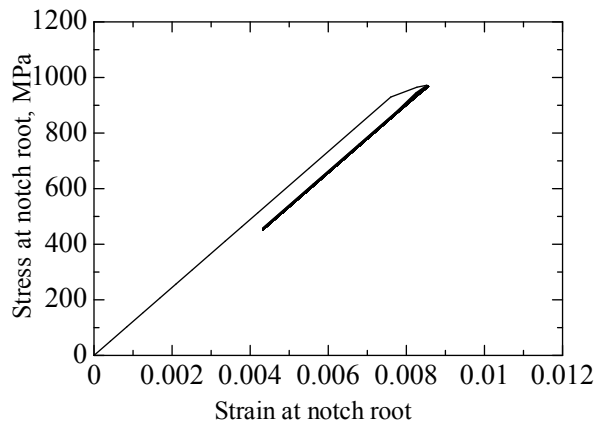
Fig. 2.17 Finite element analysis of notch specimen under load-controlled cyclic loading: plastic strain distribution from notch root to notch center under $R = 0.5$: (a) $\sigma_a = 120\text{MPa}$, (b) $\sigma_a = 160\text{MPa}$, (c) $\sigma_a = 200\text{MPa}$

Stress-strain curves at the notch root determined from the stress-strain analysis are presented from Fig. 2.19 to Fig. 2.21 for three stress amplitude levels 120MPa, 160MPa and 200MPa. In order to understand the total stress-strain history cycles and subsequent following cycles at notch root during cyclic loading, total cycles and each cycles behavior were taken out and also plotted as shown in figures.

(a)



(b)



(c)

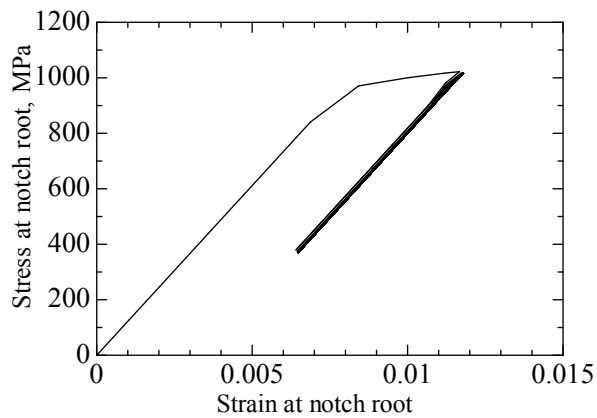


Fig. 2.18 Cyclic stress-strain hysteresis loops at notch root under the stress ratio of $R = 0.5$ (a) $\sigma_a = 120\text{MPa}$ (b) $\sigma_a = 160\text{MPa}$ (c) $\sigma_a = 200\text{MPa}$

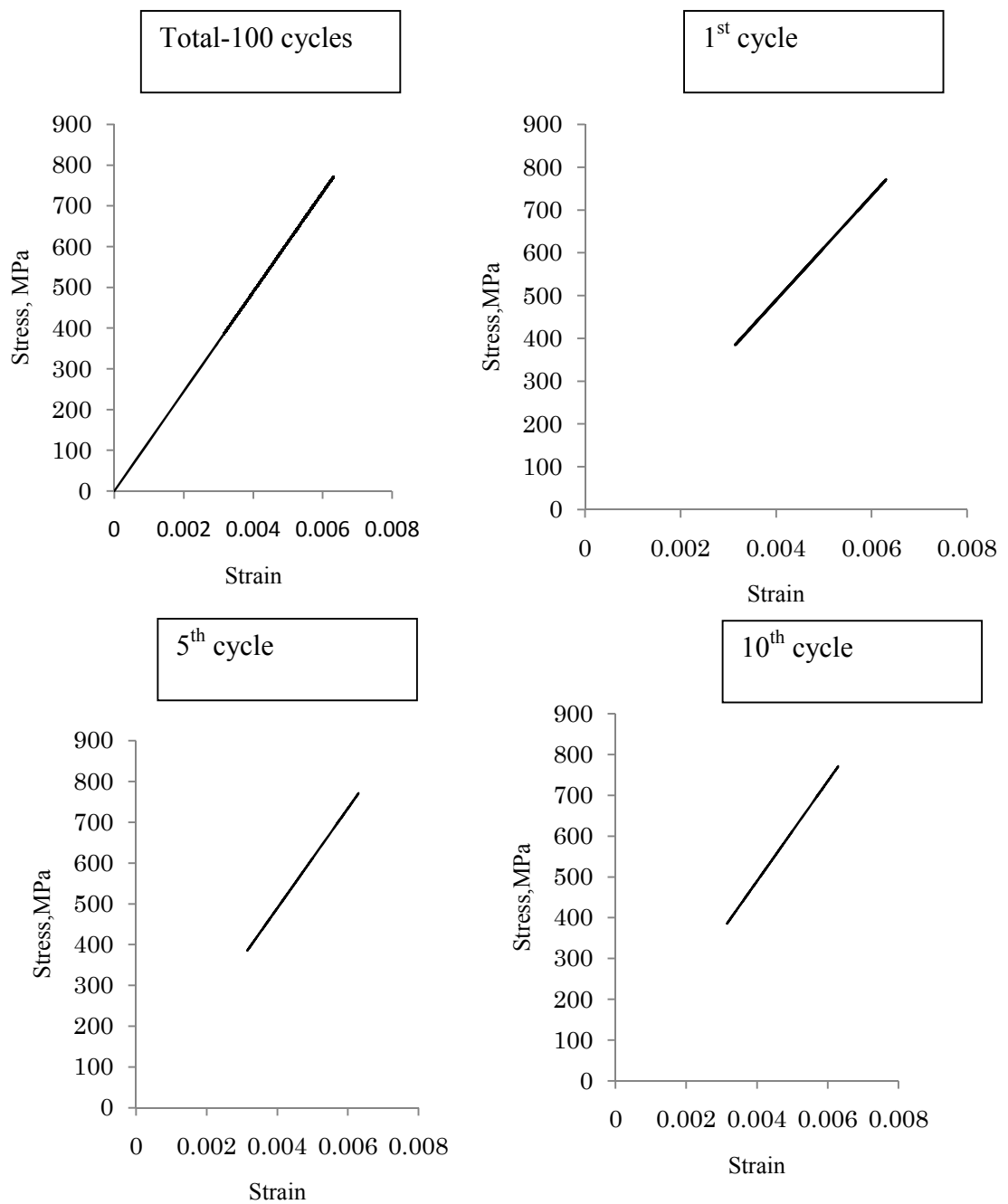


Fig. 2.19 Cyclic stress strain hysteresis at notch root under $R = 0.5$ at $\sigma_a = 120\text{MPa}$

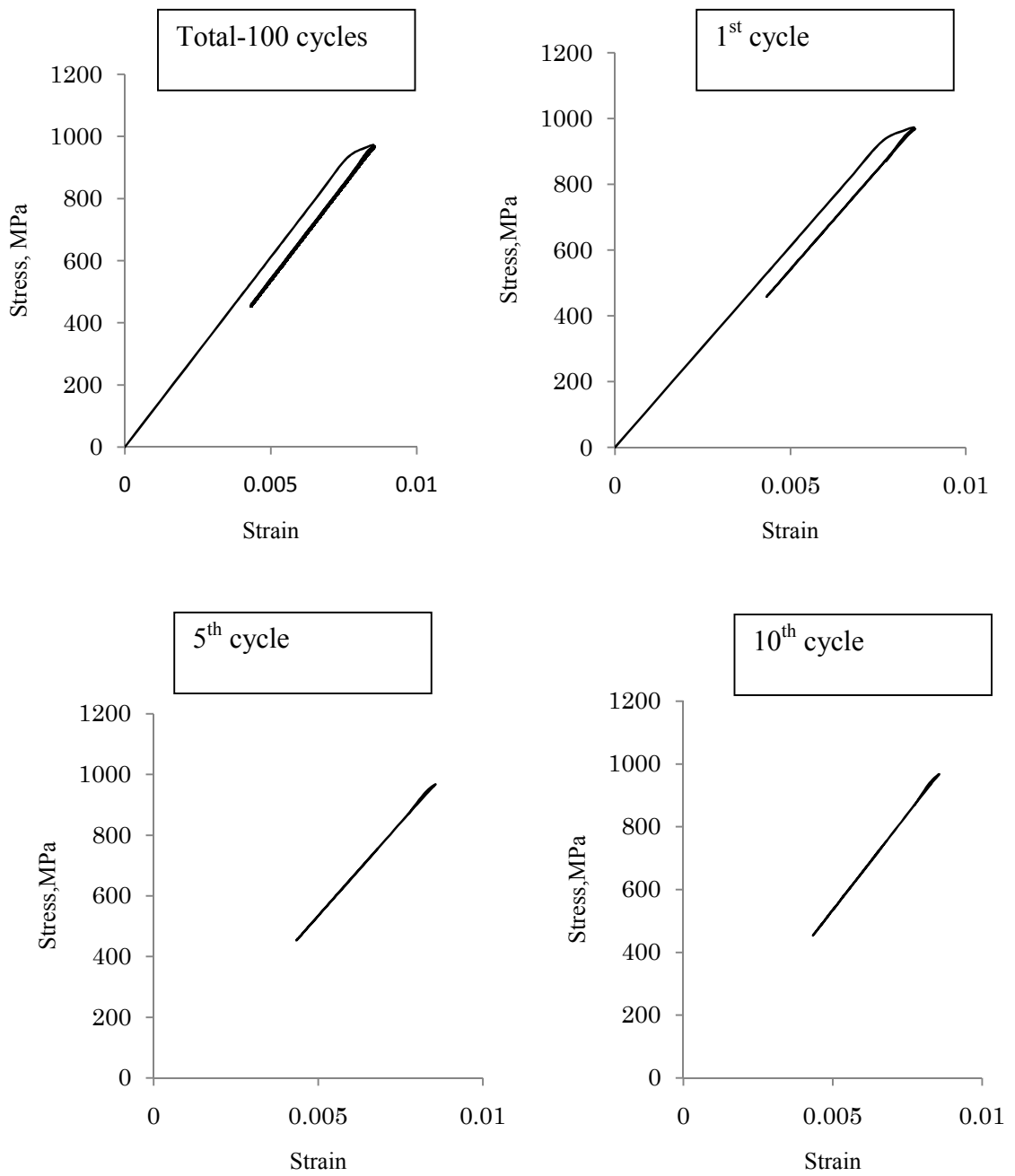


Fig. 2.20 Cyclic stress strain hysteresis at notch root under $R = 0.5$ at $\sigma_a = 160\text{MPa}$

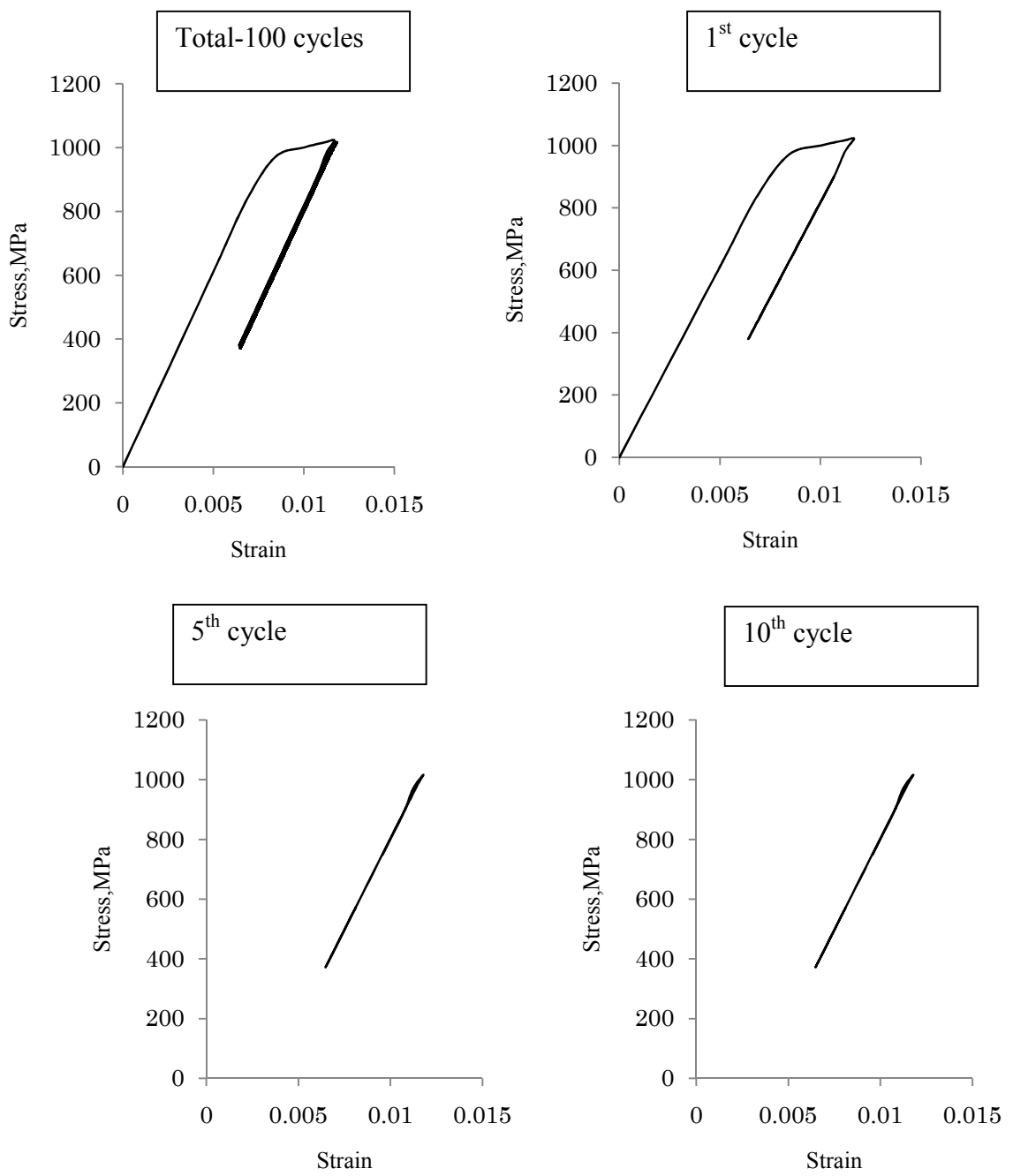


Fig. 2.21 Cyclic stress-strain hysteresis loops at notch root under the stress ratio of $R = 0.5$ at $\sigma_a = 200\text{MPa}$

2.4 Discussion

2.4.1 Critical nominal stress amplitude

As mentioned in the section 2.3.1, the S-N curve of the notched specimen was kinked at the critical nominal stress amplitude. The kinked points where the critical nominal stress amplitudes were 240 MPa and 170 MPa for $R=0.5$ and 0.1 , respectively, seemed to correspond to the development of a plastic zone size of about 0.06 mm regardless of the remote stress ratio, as seen from Figs. 2.8(b) and 2.9(b). Therefore, the nominal stress amplitude that induces the plastic deformation with the plastic zone size of about 0.06 mm would be the critical nominal stress amplitude. The plastic zone size of about 0.06 mm corresponded to the size of about 4 grains for the present material. Above the critical nominal stress amplitude, cyclic plastic deformation occurs in the initial several cycles, as seen in Fig. 2.12(c) and 2.18(c), while almost no cyclic plastic deformation occurs below the critical nominal stress amplitude as seen in Fig. 2.12(a) and 2.18(a).

2.4.2 Variation of local stress ratio at notch root

As mentioned in the section 2.4.1, the local stress ratio at the notch root is decreased with increasing applied nominal stress amplitude as shown in Fig. 2.22. The plastic deformation was formed near the notch root region at higher nominal stress amplitudes, as shown in Fig. 2.8(b) and 2.9(b). This local tensile plastic deformation at notch root will induce compressive residual stress at the notch root in the following cycles due to elastic constraint of the surrounding elastic body. This will be a main mechanism for the change of local stress ratio at the notch root from the remote stress ratio. This is when the nominal stress amplitude is high, the large plastic zone at the

notch root is formed and then the local stress ratio at the notch root is decreased. This can be also confirmed by the local stress ratio distribution near the notch root region, as shown in Fig. 2.23 and 2.24. This distribution almost corresponds to the plastic strain distribution shown in Fig. 2.8(b) and 2.9(b).

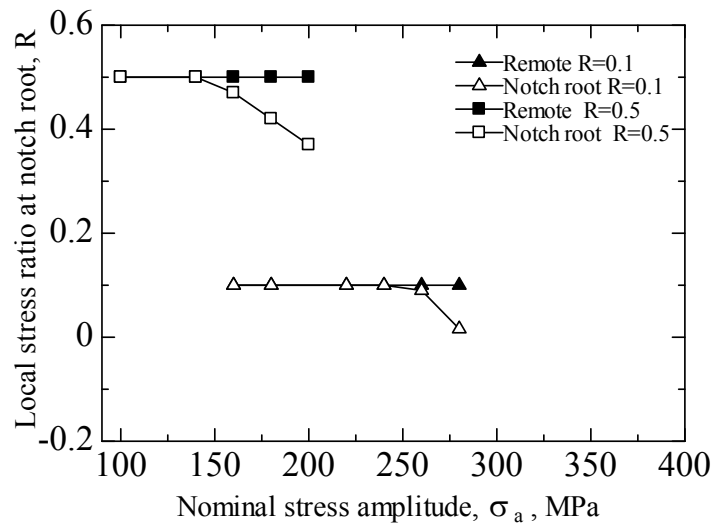


Fig. 2.22 Relationship between local stress ratio at notch root and applied nominal stress

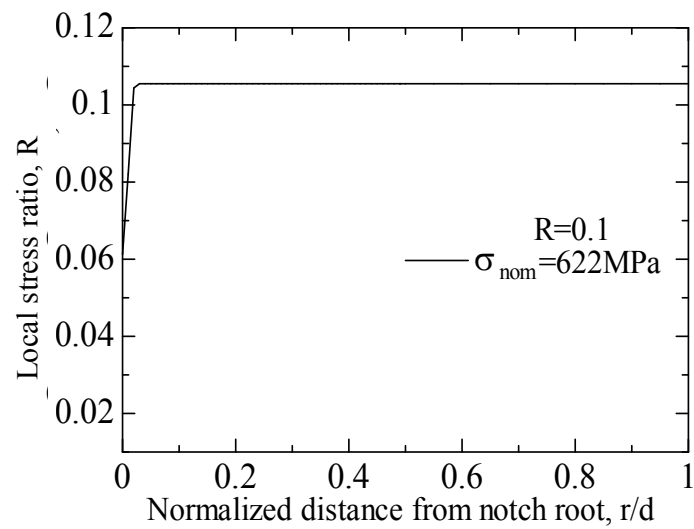


Fig. 2.23 Relationship between local stress ratio and distance from notch root under the remote stress ratio of 0.1

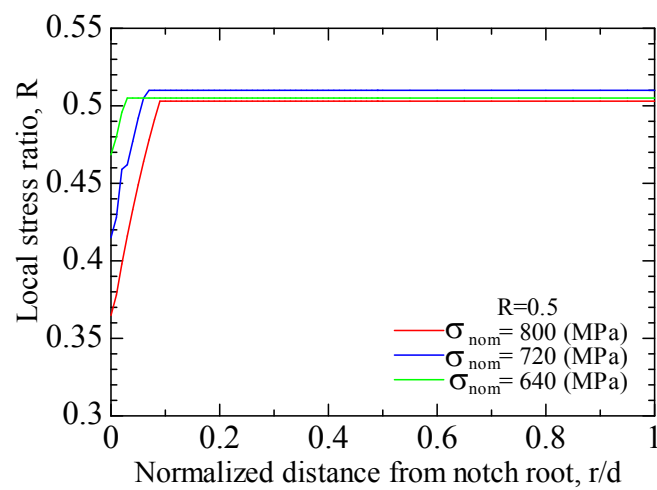


Fig. 2.24 Relationship between local stress ratio and distance from notch root under the remote stress ratio of 0.5

2.5 Conclusions

Notch fatigue behavior of Ti-6Al-4V titanium alloy has been investigated under load-controlled high cycle fatigue tests to investigate the effect of local stress ratio variation at the notch root in the high cycle fatigue regime and in the transition region between the high and low cycle fatigue regimes. The elastic-plastic FEA was also carried out to investigate the local stress ratio variation at the notch root. The main conclusions obtained are summarized as follows:

- (1) The obtained S-N curve for the notched specimen is kinked at certain nominal stress amplitude due to development of plastic deformation at the notch root. The kinked point of the S-N curve, which is called the critical nominal stress amplitude in this study.
- (2) With increasing nominal stress amplitude, the local stress ratio at the notch root decreased even under keeping the remote applied stress ratio constant. When the plastic deformation is developed locally at notch root, the residual compressive stress would be induced due to the elastic constraint of surrounding elastic body. This will be a main mechanism for variation of local stress ratio at the notch root.

References

- [1] N. E. Dowling, Mechanical behavior of materials^{2nd}, Prentice-Hall New Jersey (1999)
- [2] A. J. Mc Evily, Metal Failures: Mechanisms, Analysis, Prevention, John Wiley & Sons Inc. New York (2002)
- [3] L. P. Borrego, L. M. Abreu, J. M. Costa, J. M. Ferreira, Analysis of Low Cycle Fatigue In Almgisi Aluminum Alloys, Eng Fail Anal 11 (2004) 715-725
- [4] A. Ince, G.A. Glinka, Modification of Morrow and Smith-Watson-Topper Mean Stress Correction Model, Fatigue Fract Eng Mater Struct 34 (2011) 854-867
- [5] A. T. Brammer, J. B. Jordon, P. G. Allison, Barkey M. E. Strain-Controlled Low-Cycle Fatigue Properties Of Extruded 6061-T6 Aluminum Alloy, J Mater Eng Perform 22 (2013) 1348-1350
- [6] H. Neuber, Theory of Stress Concentration for Shear Strained Prismatic Bodies with Arbitrary Nonlinear Stress Strain Law, JApplMech 2 (1969) 544-551
- [7] G. Glinka, Calculation of Inelastic Notch-Tip Strain-Stress Histories Under Cyclic Loading, EngFractMech 22 (1985) 839-854
- [8] J. Morrow, Fatigue Properties of Metals, Fatigue Design Handbook, Warrendale (1968)
- [9] K. Walker, The Effect of Stress Ratio During Crack Propagation and Fatigue For 2024-T3 and 7075-T6 Aluminum, ASTM 462 (1970) 1-14
- [10] K. N. Smith, P. Watson, T. H. Topper, A Stress-Strain Function for The Fatigue of Metals, J. Mater 5 (1970) 767-778

- [11] M. Knop, R. Jones, L. Molent, C. Wang, On The Glinka and Neuber Methods For Calculating Notch Tip Strains Under Cyclic Load Spectra, *Int J Fatigue* 22 (2000) 743-755
- [12] ASTM E606-92, Standard Practice for Strain-Controlled Fatigue Testing (1998)
- [13] W. D. Pilkey, Peterson's Stress Concentration Factors^{3rd}, John Wiley & Sons New York (2007)
- [14] ASTM E468-11, Standard Practice for Presentation of Constant Amplitude Fatigue Test Results for Metallic Materials (2001)
- [15] J. C. Grosskreutz, G. G. Shaw, Mechanisms of Fatigue in 1100-0 and 2024-T4 Aluminum Air Force Material Report, Air Force Materials Laboratory, Research and Technology Division, Air Force Systems Command, AFML-TR-65-127 (1965)
- [16] S. Khan, A. Vyshnevskyy, J. Mosler, Low Cycle Lifetime Assessment of Al2024 Alloy, *Int J Fatigue* (32) 20101270-1277
- [17] Mentat II Users Guide, Marc Analysis Research Corporation, USA (2013)
- [18] G. Pluvinage, Notch Effects in Fatigue and Fracture, NATO Science Series 11 (2001)1-22
- [19] F. C. Campbell, Fatigue and Fracture-Understanding The Basics, ASM International (2012)
- [20] M. R. Bache, M. Tasleem, Fatigue Life Prediction Techniques for Notch Geometries in Titanium Alloy, *Int J Fatigue* 21 (1999) 187-197
- [21] R. Wang, L. Youtang, A. Huping, Low Cycle Fatigue Behaviors of TI-6AL-4V Controlled by Strain and Stress, *Key Eng*525-526(2013) 441-444

- [22] A. S. Beranger, A. Feaugas, M. Clavel, Low Cycle Fatigue Behavior of an A + B Titanium Alloy: Ti6246, Mater Sci Eng A 172 (1993) 31-41
- [23] R. Ghajar, J. K. Alizadeh, N. Naserifar, Estimation of Cyclic Strain Hardening Exponent and Cyclic Strength Coefficient of Steel By Artificial Neural Networks. ASME International Mechanical Engineering Congress and Exposition Proceedings12 (2008) 639-648

CHAPTER – 3

NOTCH FATIGUE BEHAVIOR OF

TI-6AL-4V ALLOY UNDER

DISPLACEMENT-CONTROLLED LOW

CYCLE FATIGUE TESTS

Chapter-3

Notch Fatigue Behavior of Ti-6Al-4V Alloy under Displacement-Controlled

Low Cycle Fatigue Tests

3.1. Introduction

The wide range fatigue behavior of smooth specimen has been commonly presented by using a total strain-life curve which includes elastic strain-life curve in high cycle fatigue regime and plastic strain-life curve in low cycle fatigue regime [1, 2]. The transition region between them where both elastic strain and plastic strain significantly influence fatigue life, is typically in the range of 10^2 to 10^5 cycles. When only the high cycle regime is concerned, the stress-life curve is used instead of the elastic strain-life curve. For the notched specimen, the stress strain concentration at the notch root and the localized plastic deformation near the notch tip are known to take place, which lead to fatigue crack nucleation at notch root. Several studies have been conducted for predicting the crack nucleation life at notch root, such as Neuber [3], Glinka [4] and SWT models [5].

For low cycle fatigue of smooth specimen, it has been known that strain-life curves are identical regardless of the applied stress ratio (mean stress) in the high

strain amplitude region [6, 7] while separated strain-life curves depending on the applied stress ratio are observed in the low strain amplitude region [7]. The mean stress at high strain amplitudes in low cycle fatigue region has been also reported to become zero (that is the stress ratio of -1) during fatigue cycle [8, 9]. To take account of the mean stress effect on low cycle fatigue behavior, various prediction methods, such as Morrow [10], Walker [11] and SWT [12] models have been proposed and successfully applied to the various specimen geometries, loading modes and materials. However, the stress ratio (mean stress) variation during fatigue loading at various strain amplitudes has not yet been clarified in detail.

For low cycle fatigue of notched specimen, it has been reported that the local mean stress at notch root decreases during cyclic loading under a constant remote stress ratio and becomes zero (that is the stress ratio of -1) [13, 14]. However, in the transition region between low cycle and high cycle fatigue regions, the local stress ratio variation at notch root at various strain amplitudes have not yet been clarified in detail. The most of research works have assumed that the local stress-strain state is stable and the mean stress (that is, the stress ratio) at notch root is also constant during fatigue loading. These assumptions will be satisfied in the high cycle fatigue region with small amount of local plastic deformation at the notch root. But in the transition region between low cycle and high cycle fatigue regions, it is not sure whether the mean stress and the stress ratio can be assumed to be constant during fatigue loading under a constant remote stress ratio. It is important to clarify the local stress ratio variation behavior at notch root during fatigue loading and its effect on fatigue life prediction for fatigue design of structural components with notch.

In the previous chapter, the load-controlled high-cycle fatigue tests of Ti-6Al-4V titanium alloy notched specimens were carried out to investigate the variation of local stress ratio at notch root and its effect on notch fatigue behavior in high cycle fatigue region. From the results, the kinking behavior of S-N curve at the critical nominal stress amplitude was found. At the nominal stress amplitudes higher than the critical nominal stress amplitude the variation of local stress ratio at the notch root was found during cyclic loading and its effect on the S-N curve behavior of notched specimen was clarified.

In the present chapter, notch fatigue behavior in the transition region between high and low cycle fatigue regions has been investigated by carrying out displacement-controlled low cycle fatigue tests of the Ti-6Al-4V alloy notched specimen, combined with the results in the previous chapter under load-controlled high cycle fatigue tests. The elastic-plastic finite element analysis of notched specimen under cyclic loading has been also carried out to investigate the local mean stress ratio variation at notch root depending on the applied nominal strain amplitude as well as stress-strain states during cyclic loading in detail. Based on the results of experiments and finite element analysis, mechanisms of local stress ratio variation have been discussed. Fatigue life predictions method with taking into account of the local stress ratio variation have been also performed for the whole range of the low cycle and high cycle fatigue regions including the transition region.

3.2. Experiments and FEM analysis

3.2.1. Material and specimens

The material, chemical composition, mechanical properties and specimen information are same as shown in previous Chapter-3.

3.2.2. Displacement-controlled fatigue strength test for low cycle fatigue region

Displacement-controlled fatigue tests of the smooth and notched specimens in the low cycle region were performed at room temperature using the same fatigue machine as used for the load-controlled fatigue tests according to the ASTM E606-92 [15]. A triangular waveform of loading with strain ratios of $R = -1$ for smooth specimen and 0.1 for notched specimen and a strain rate of 0.1% per second was used in the displacement-controlled fatigue tests. Five levels of strain amplitudes ranged from 0.6% to 1.3% under the strain ratio of $R = -1$ were applied to the smooth specimen and seven levels of strain amplitudes ranged from 0.4% to 1.4% under the strain ratio of $R=0.1$ were applied to the notched specimen. Each specimen was subjected to a constant cyclic strain until failure of the specimen which was defined by the 25% drop of maximum load during the test. The clip gage with gage length of 11.5 mm was mounted onto the notched specimen across the notch to monitor and control the displacement during testing. The calibration of the clip gage was made by using a micrometer and the controller of the test machine. Since the gage part includes both notch and smooth parts of the notched specimen, the nominal strain amplitude of the notched specimen is defined as: the range of displacement measured is normalized by the original gage length, which gives the nominal strain range, and then the nominal strain amplitude is obtained as the half of the nominal strain range. During the test, the

load and the displacement were continually monitored and recorded at proper intervals by using computer with a data collecting software. The monitored displacement was converted into the nominal strain amplitude in the computer. After the low cycle fatigue tests, all fracture surfaces were observed in detail by an SEM.

The cyclic stress-strain curve of the present material, which was needed in the finite element analysis (FEA), was obtained by the displacement-controlled cyclic loading test of the smooth specimen according to the incremental step test method [16, 17]. Detail of the test method can be found in previous chapter.

3.2.3 Finite element analysis

The elastic-plastic FEA was performed on the notched specimen under the displacement controlled conditions to investigate the stress-strain states, plastic deformation behavior and local stress ratio at notch root. Detail of the finite element analysis method can be found in the previous chapter.

3.3. Results

3.3.1 Fatigue strength test results in low cycle fatigue region

The low cycle fatigue test result for the smooth specimen under the displacement-controlled condition with fully reversed loading ($R = -1$) is shown in Fig 3.1. The relationship between strain amplitude and number of cycles to failure (S-N curve) for the present Ti-6Al-4V alloy was in the range of the reported S-N curves obtained by the low cycle fatigue tests [18, 19]. The present S-N curve can be expressed by the Coffin-Manson equation as [20, 21]:

$$\varepsilon_a = \frac{\sigma'_f}{E} (N_f)^b + \varepsilon'_f (N_f)^c \quad (3.1)$$

where N_f is the number of cycles to failure and not the reversals to failure, and σ'_f , ε'_f , b and c are the fatigue strength coefficient, the fatigue ductility coefficient, the fatigue strength exponent and the fatigue ductility exponent, respectively. The low cycle fatigue properties determined based on the y-intercepts and slope of log-log linear fitting lines are listed in Table 3.1. This result was used in the life prediction based on the FEA in the later section.

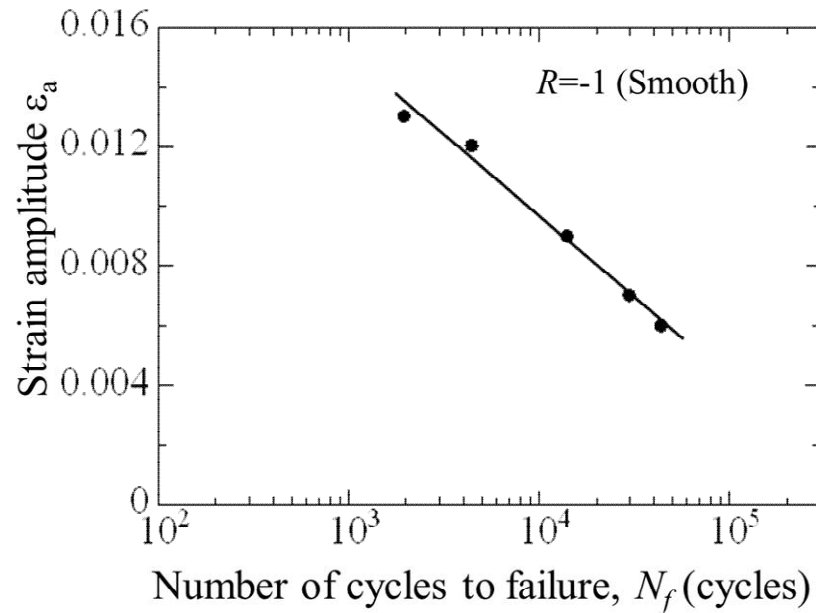


Fig. 3.1 S-N curves in the low cycle fatigue region of the smooth specimens at $R = -1$ for Ti-6Al-4V alloy

Table 3.1 Low cycle fatigue properties of the Ti-6Al-4V alloy

| | |
|--|--------|
| Fatigue strength coefficient, σ'_f | 2011 |
| Fatigue strength exponent, b | -0.071 |
| Fatigue ductility coefficient, ϵ'_f | 0.147 |
| Fatigue ductility exponent, c | -0.121 |

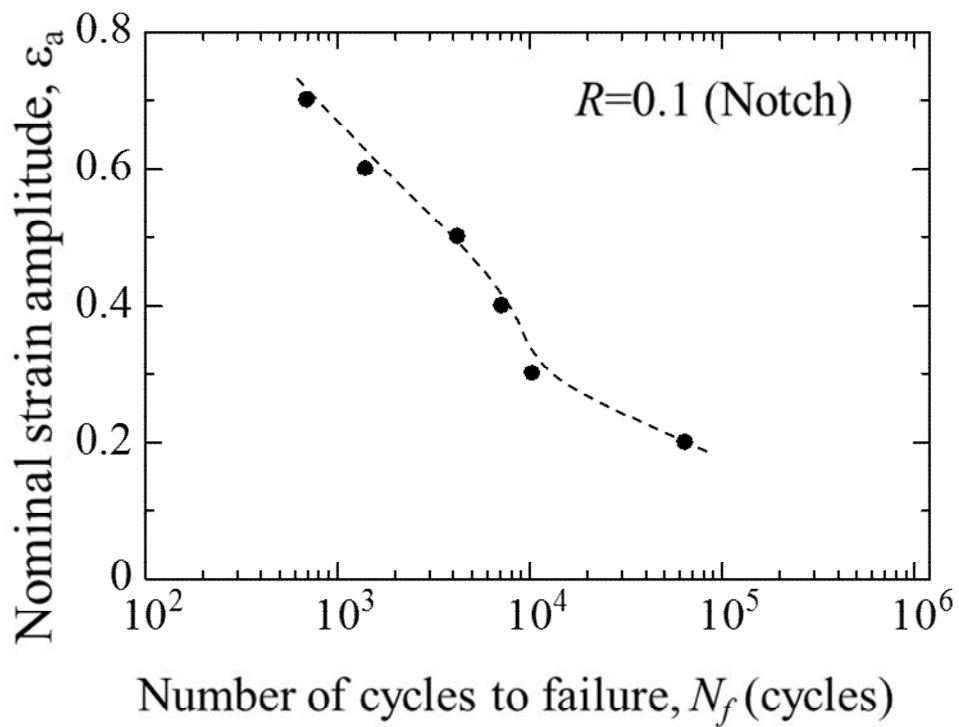


Fig. 3.2 S-N curves in the low cycle fatigue region of the notched specimens at $R = 0.1$ for Ti-6Al-4V alloy

Fig. 3.2 shows the result of the displacement-controlled low cycle fatigue tests for the notched specimen under $R = 0.1$. As seen from the figure, the S-N curve was not smooth and deflected at low nominal strain amplitudes. The cyclic stress strain hysteresis loops for the notched specimen under $R = 0.1$ at small and large nominal strain amplitudes are shown in Fig. 3.3. As seen from the figure, the difference of stress strain curve between loading and unloading cycles, that is hysteresis loop, is not significant while it becomes detectable with increasing nominal strain amplitude. This less significant hysteresis loop for the nominal strain and stress relationship in the notched specimen results from that, the large stress and strain are induced only at notch root, but this stress and strain concentration at notch root does not significantly influence the nominal stress and strain relationship.

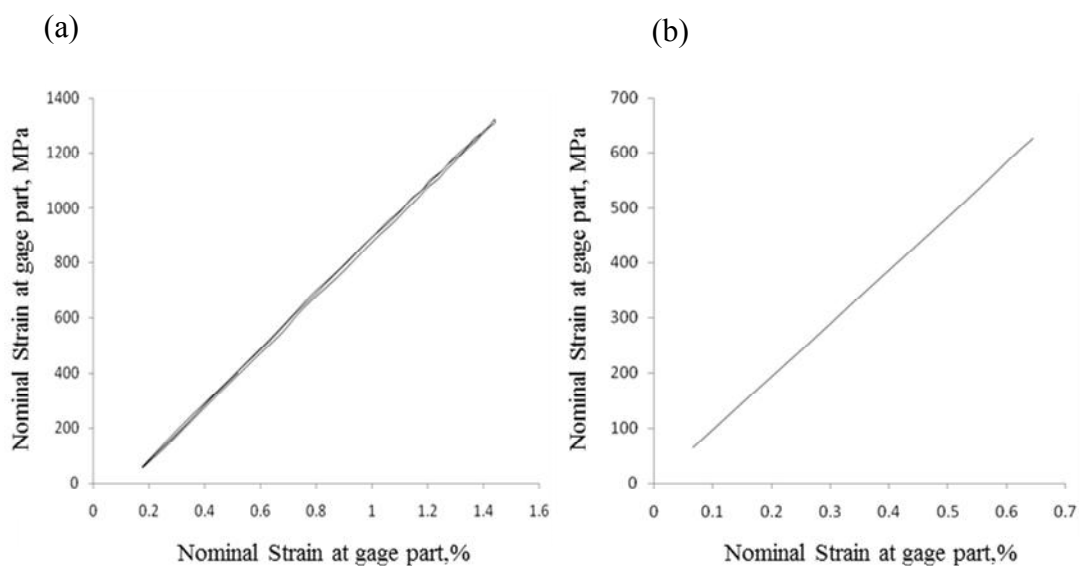


Fig. 3.3 Cyclic stress-strain hysteresis loops obtained by the low cycle fatigue test for the Ti-6Al-4V alloy under $R = 0.1$: (a) $\epsilon_a = 0.3\%$, (b) $\epsilon_a = 0.7\%$

3.3.2. Fracture surface observations

Examples of overall fracture surface observations for the notched specimen tested under $R = 0.1$ are shown in Fig. 3.4. As seen from the figure, a single fatigue crack nucleated at the nominal strain (stress) amplitudes lower than the kinked point. With increasing the nominal strain amplitude, the transition behavior from single to multiple fatigue crack nucleation could be observed as seen from Fig. 3.4(b, c). With further increasing the nominal strain amplitude, multiple fatigue cracks were nucleated. This change of crack nucleation behavior from single to multiple cracks will result from the extension of plastic deformation region at notch root. It was revealed that multiple fatigue cracks were nucleated at higher stress level than the kinked point, while only single fatigue crack was nucleated at lower stress level than the kinked point.

From the detailed observations of the crack nucleation sites at higher magnifications, it was confirmed that there was no internal or subsurface crack nucleation from inclusions or precipitates.

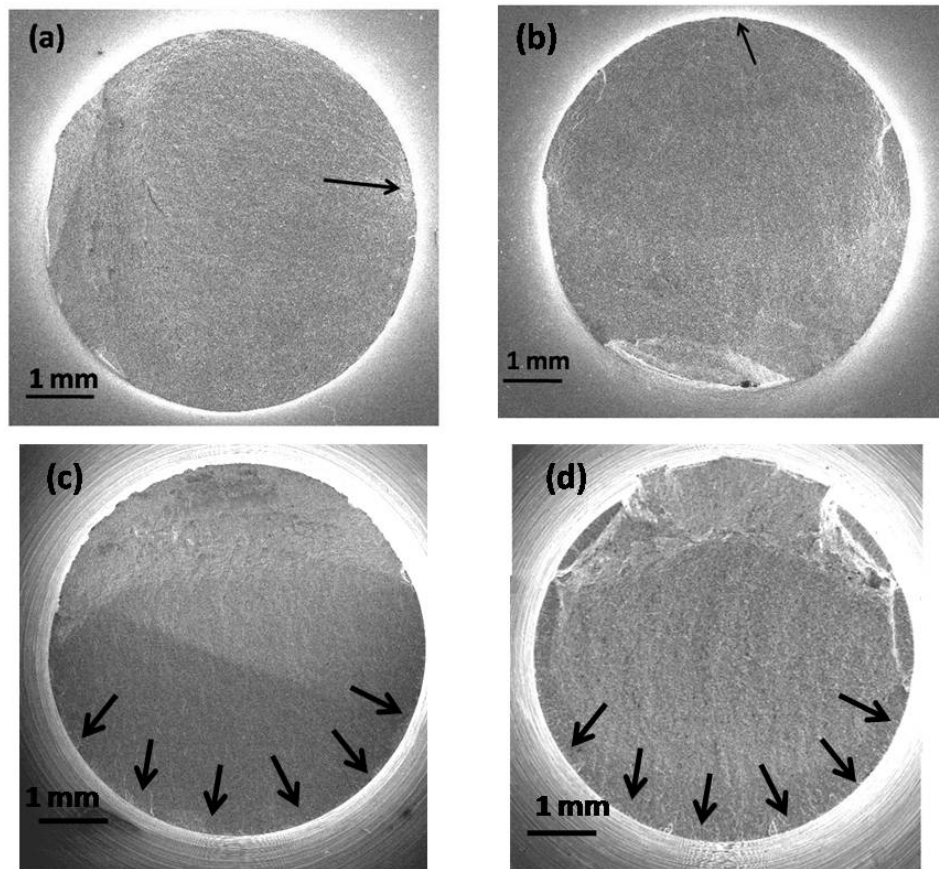


Fig. 3.4 Fatigue fracture surfaces of the notched specimens tested under $R = 0.1$:
(a) High cycle fatigue region: $\sigma_a = 180\text{MPa}$, $N_f = 4,376,196$ cycles, (b) Transition region: $\sigma_a = 280\text{MPa}$, $N_f = 44,756$ cycles, (c) Transition region: $\epsilon_a = 0.4\%$, $N_f = 64,425$ cycles, (d) Low cycle fatigue region: $\epsilon_a = 0.7\%$, $N_f = 697$ cycles

3.3.3. Stress distribution at the notch root under displacement-controlled condition for $R = 0.1$ in elastic-plastic FEA of notched specimen

From the elastic-plastic FEA results of the notched specimen under displacement-controlled condition (in low cycle fatigue region) with $R = 0.1$, the graphical representation and contour plots of the von Mises stress distributions along the notch section at the maximum load of the first cycle are shown in Fig. 3.5 and Fig. 3.7. The corresponding plastic strain distributions are also shown in Fig. 3.6 and Fig. 3.8. It is found from Fig.3.8 that the plastic deformation is limited near notch tip region at the nominal strain amplitude of 0.2%, while the plastic deformation is fully developed whole notch section at the nominal strain amplitudes higher than 0.2%.

The cyclic stress-strain responses of the element at the notch tip for various nominal strain amplitudes are shown in Fig. 3.9. These stress-strains relationships were taken at the notch root of the comp 11 loading direction when maximum stress applied to the model. As seen from Fig. 3.9(a), at the nominal strain amplitude of 0.2%, a plastic deformation is induced in the first cycle, then a small plastic deformation is repeated in the following several cycles, and subsequently a stabilized linear stress-strain response is achieved. This behavior is similar to that observed under load-controlled condition at nominal stress amplitudes higher than the kinked point. When the nominal strain amplitudes are increased up to 0.5% and 0.7%, while the initial plastic deformation in the first cycle due to plastic deformation in the notch section is similar to that at the nominal strain amplitude of 0.2%, the following cyclic stress-strain responses are non-linear and show obvious hysteresis loops, as seen from Fig. 3.9(b) and (c). It should be noted from the figure that the local stress ratio at notch root decreases and attains -1, while the applied remote stress ratio is kept to 0.1.

In order to understand the total stress-strain history cycles and subsequent following cycles at notch root during cyclic loading, total cycles and each cycles behavior was taken out and also plotted as shown in Fig. 3.10 to Fig. 3.12 for three nominal strain amplitude levels 0.2%, 0.5% and 0.7% .

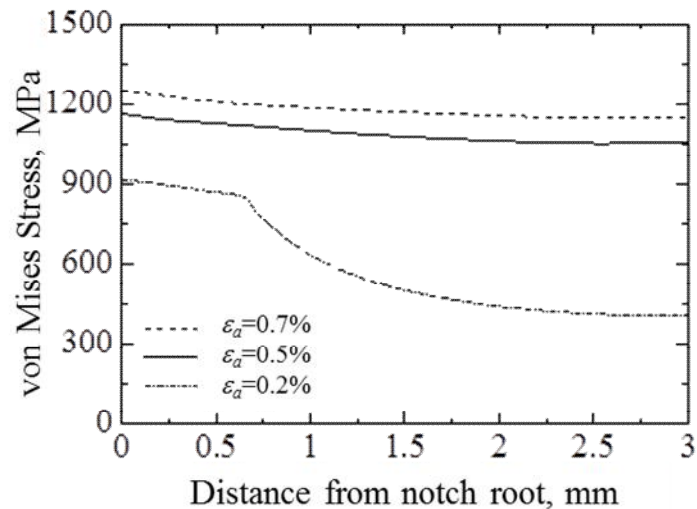


Fig. 3.5 The von Mises stress distribution near notch root in the first cycle under $R = 0.1$ in low cycle fatigue region

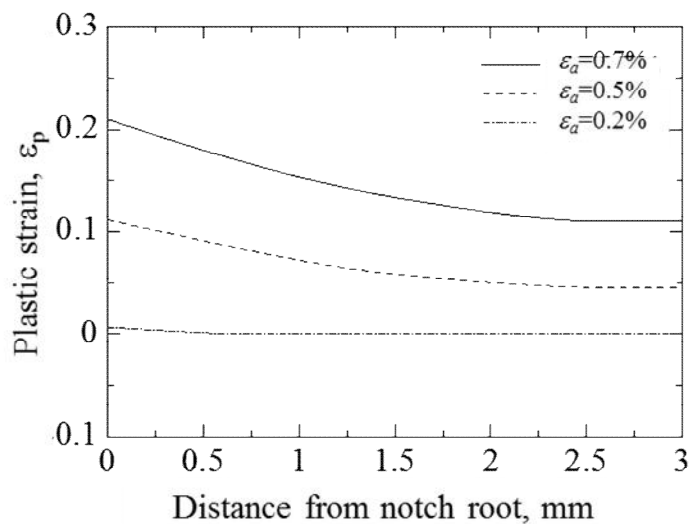


Fig. 3.6 The corresponding plastic strain distribution near notch root region in the first cycle under $R = 0.1$ in low cycle fatigue region

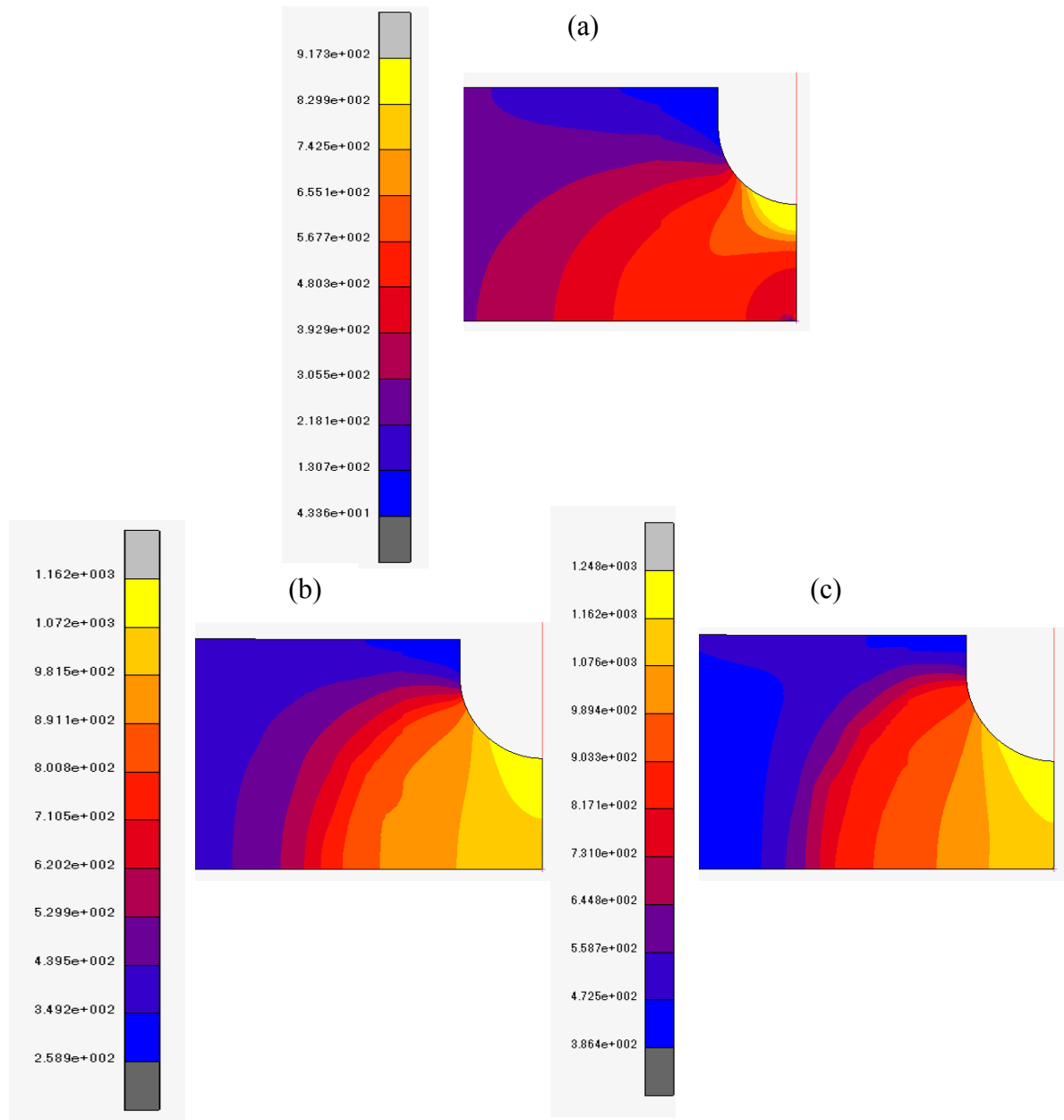


Fig. 3.7 Finite element analysis of notch specimen under displacement-controlled cyclic loading: von Mises stress distribution from notch root to notch center under $R = 0.1$: (a) $\epsilon_a = 0.2\%$, (b) $\epsilon_a = 0.5\%$, (c) $\epsilon_a = 0.7\%$

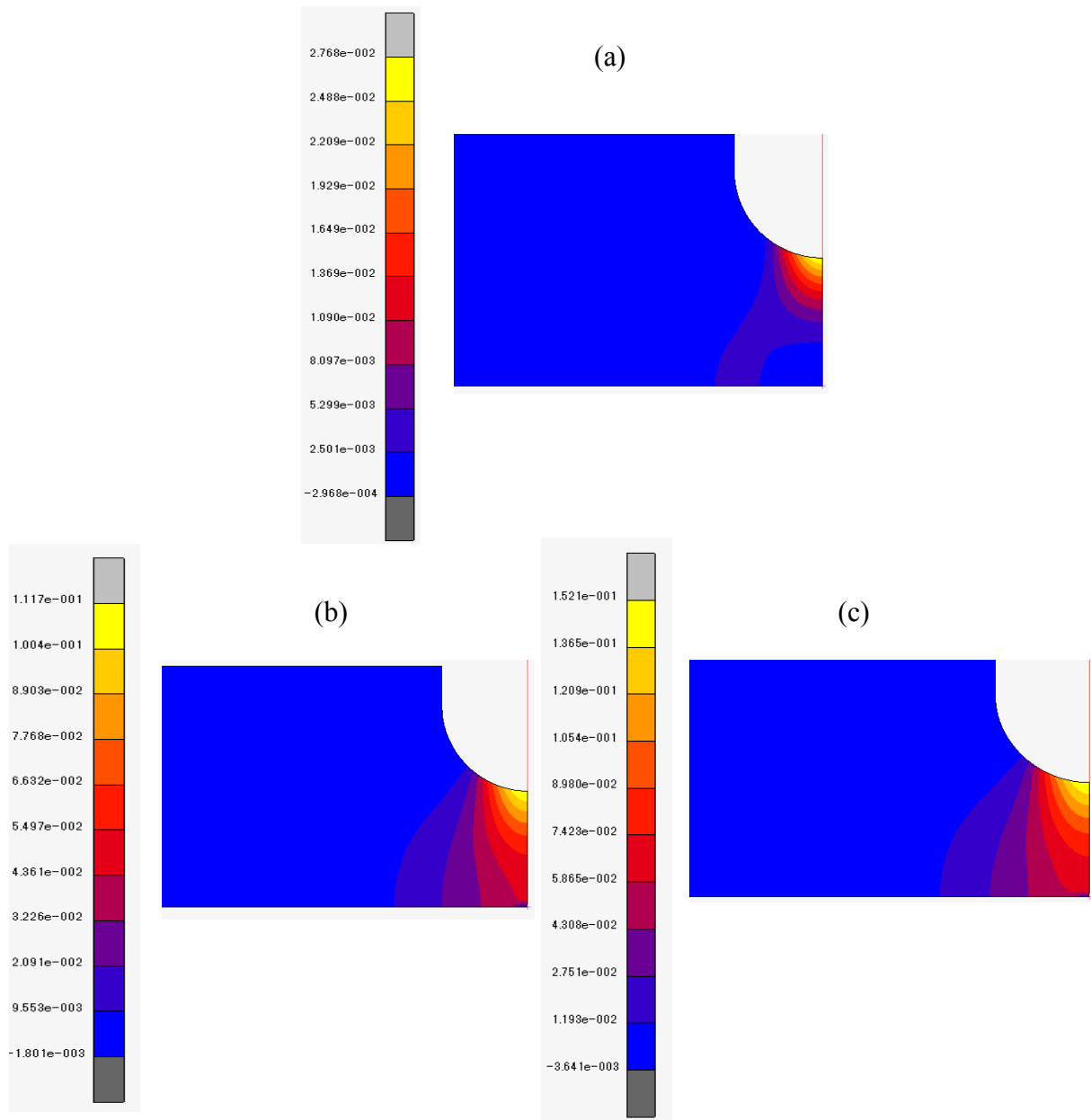


Fig. 3.8 Finite element analysis of notch specimen under displacement-controlled cyclic loading: plastic strain distribution from notch root to notch center under $R = 0.1$: (a) $\varepsilon_a = 0.2\%$, (b) $\varepsilon_a = 0.5\%$, (c) $\varepsilon_a = 0.7\%$

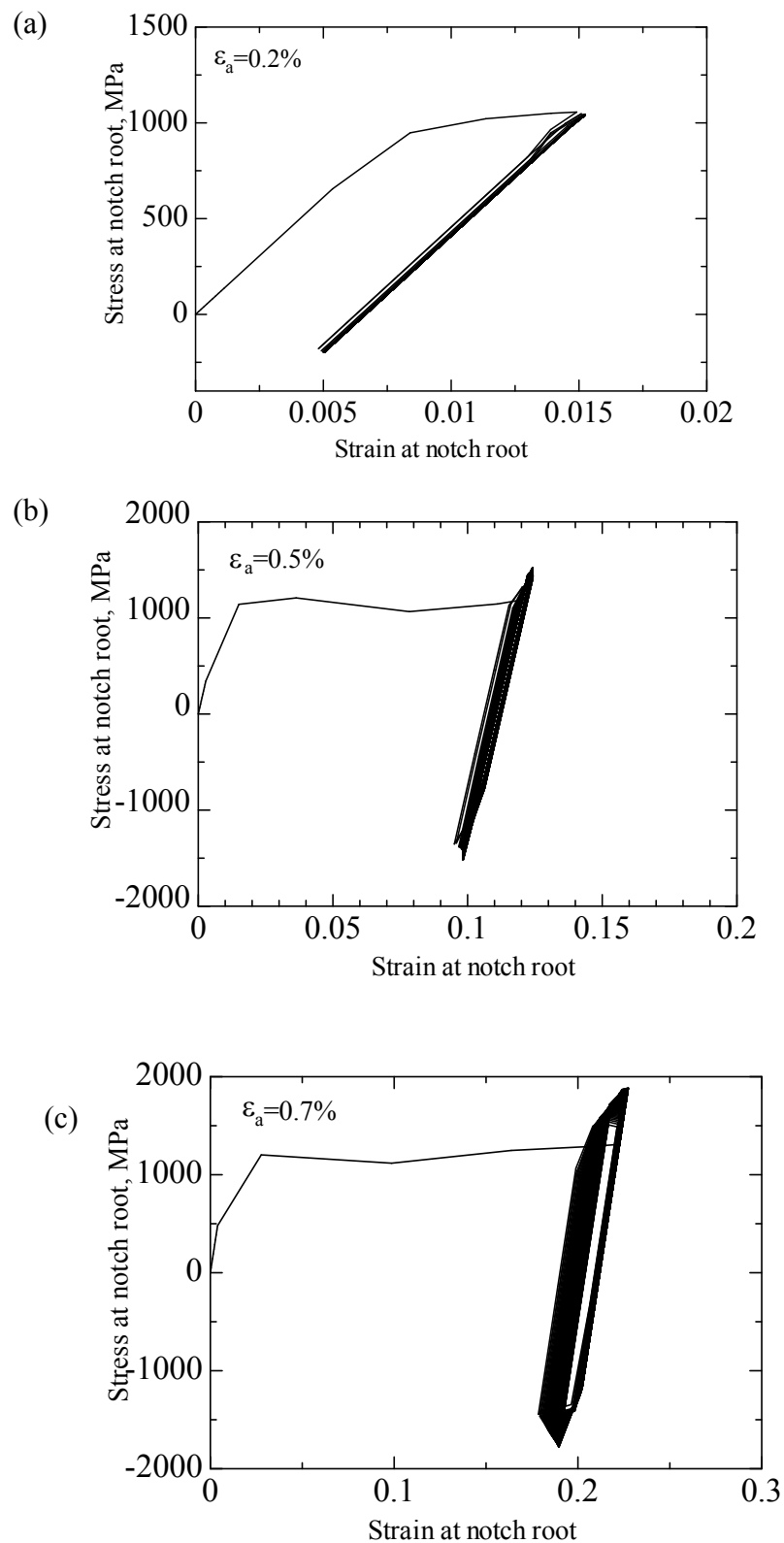


Fig. 3.9 Cyclic stress-strain hysteresis at notch root under $R = 0.1$ in low cycle fatigue region: (a) $\epsilon_a = 0.2\%$, (b) $\epsilon_a = 0.5\%$, (c) $\epsilon_a = 0.7\%$

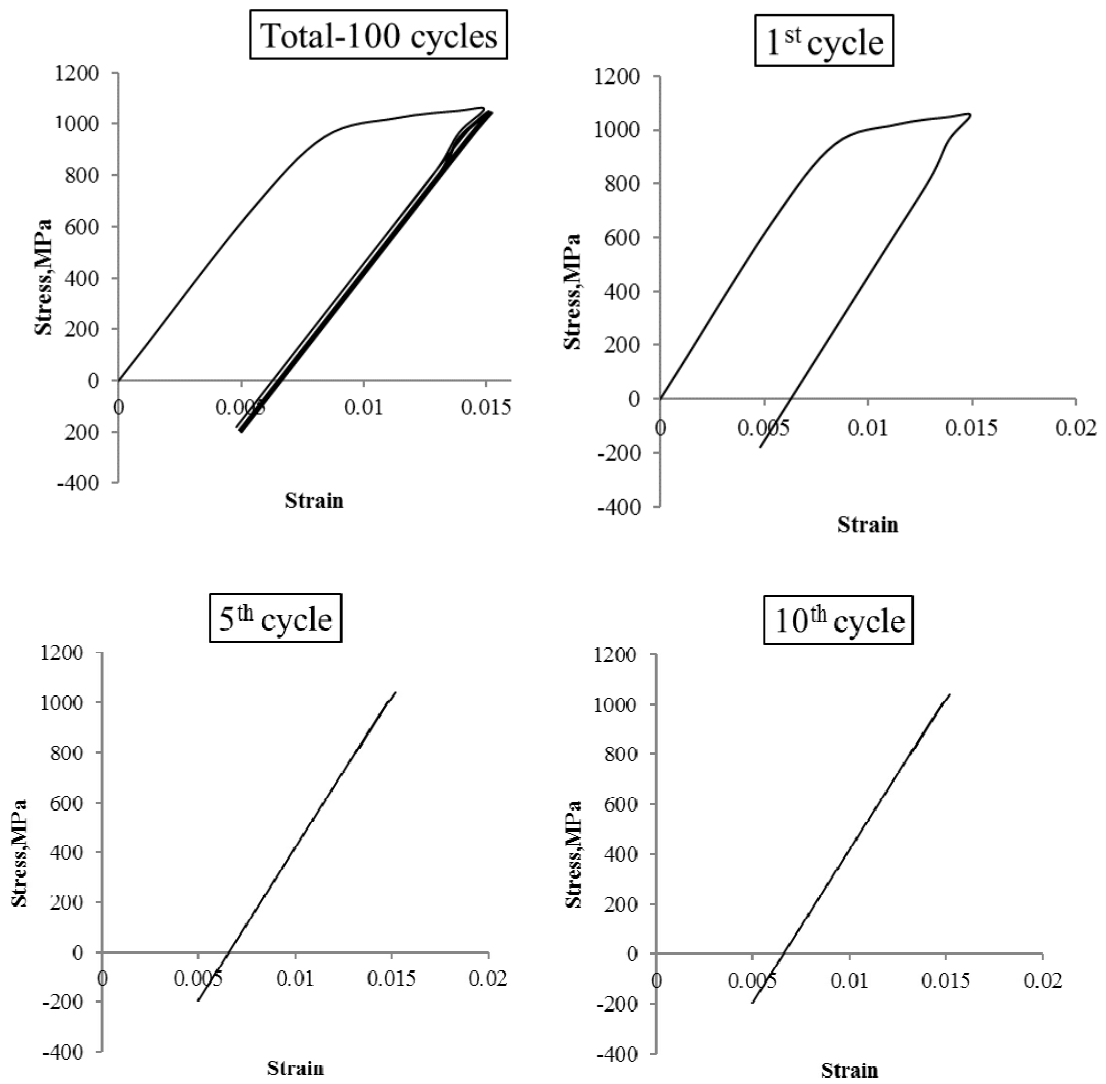


Fig. 3.10 Cyclic stress strain hysteresis at notch root under $R = 0.1$ in low cycle fatigue region at $\varepsilon_a = 0.2\%$

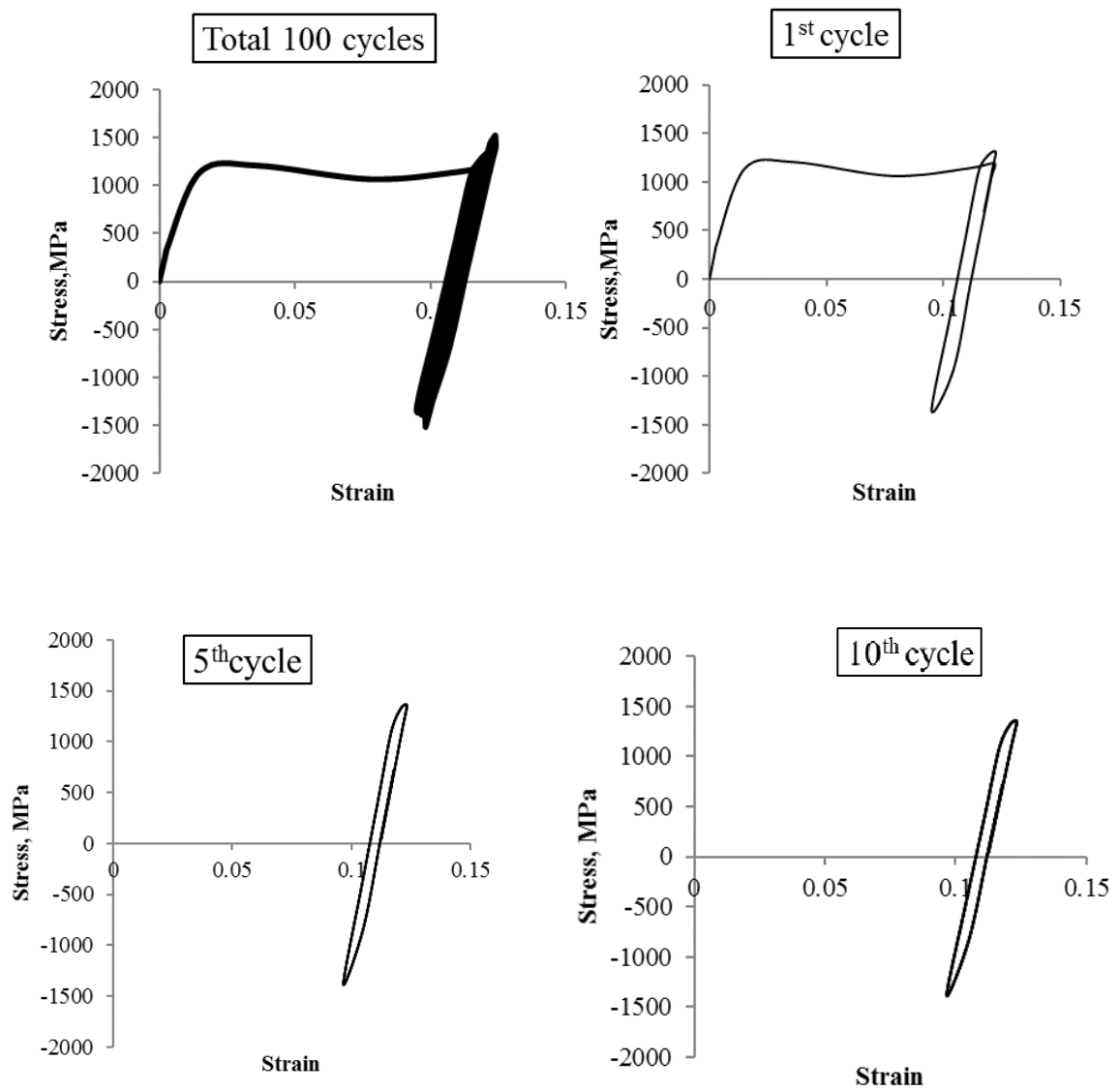


Fig. 3.11 Cyclic stress strain hysteresis at notch root under $R = 0.1$ in low cycle fatigue region at $\varepsilon_a = 0.5\%$

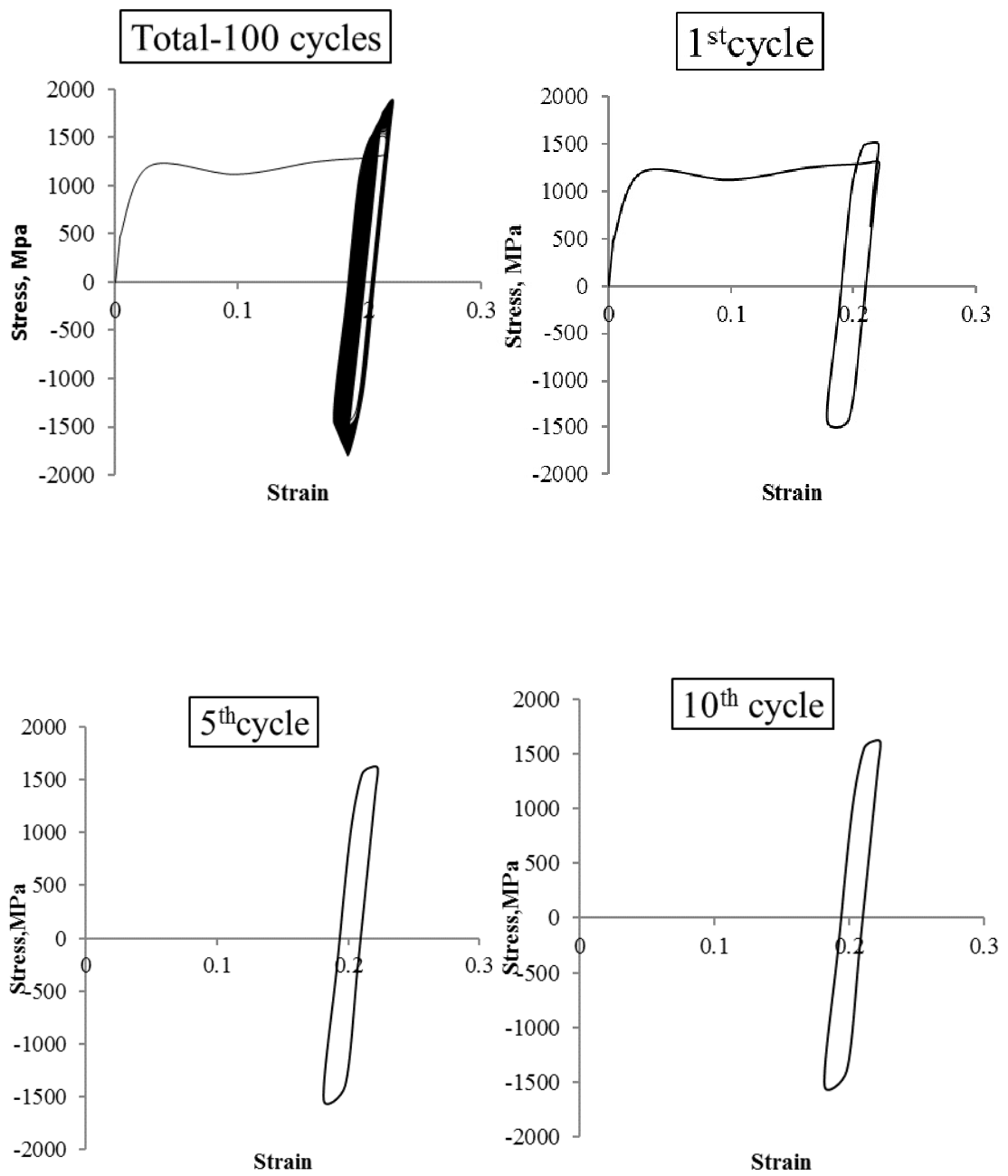


Fig. 3.12 Cyclic stress strain hysteresis at notch root under $R = 0.1$ in low cycle fatigue region at $\epsilon_a = 0.7\%$

The variation of local stress ratio at notch root stabilized during cyclic loading was investigated by the elastic-plastic FEA in the wide range of nominal strain amplitudes. From the results, the relationship between local stress ratio at notch root and applied nominal strain amplitude under the remote stress ratio of $R = 0.1$ is shown in Fig. 3.13. In the figure, the nominal stress amplitude under the load-controlled test is evaluated to the nominal strain amplitude by the half of gage length displacement divided by the gage length. This definition of nominal strain amplitude is consistent with that in the displacement-controlled fatigue experiment. As seen from the figure, the local stress ratio at notch root is the same as the remote stress ratio when the stress state at notch root is elastic. The local stress ratio decreases with developing the local plastic deformation at notch root and then reaches to $R = -1$ when the fully plastic deformation is achieved in the whole notch section as shown in Fig. 3.8(b) and (c).

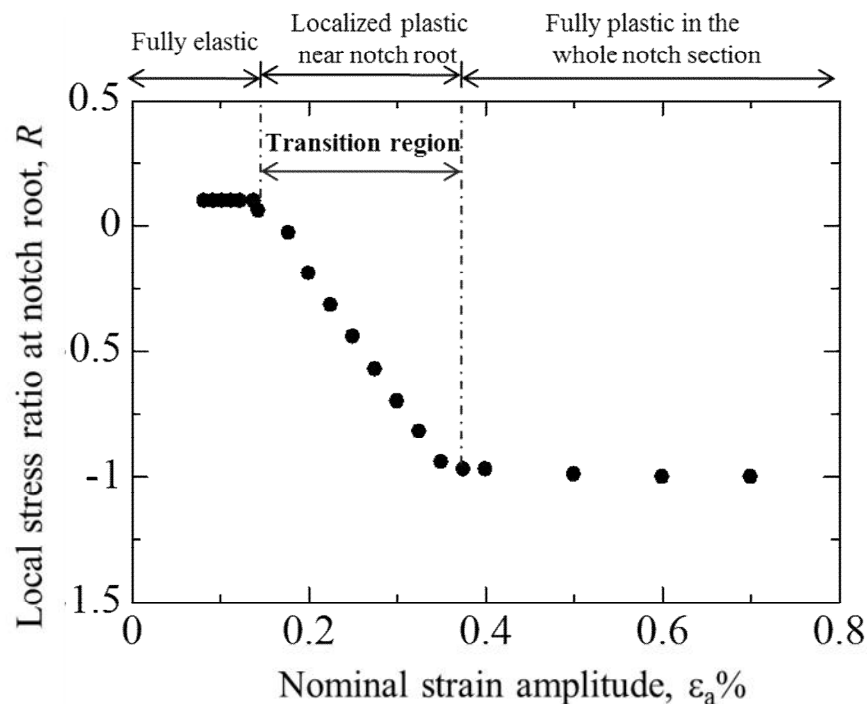


Fig. 3.13 Relationship between local stress ratio at notch root and applied nominal strain amplitude under the remote stress ratio of 0.1

3.4. Discussion

3.4.1. Mechanism for local stress ratio variation at notch root

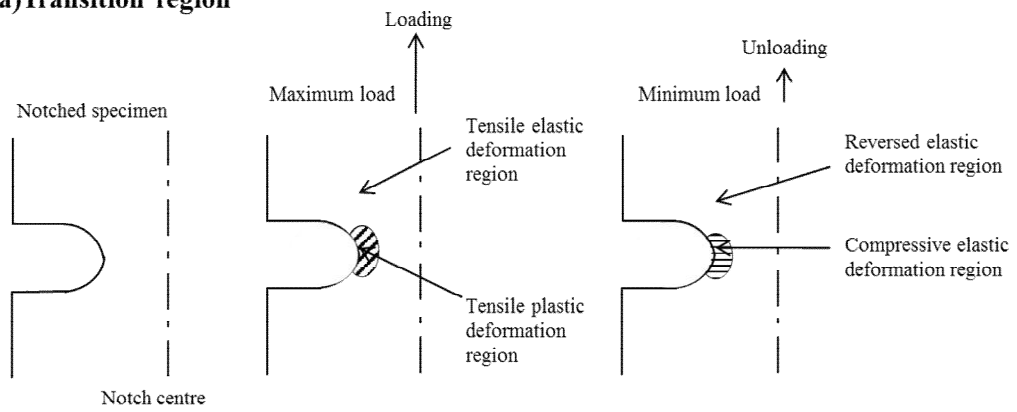
As mentioned in the section 3.3.5, the local stress ratio at notch root is decreased with increasing nominal stress and strain amplitudes in the transition region and reached to the local R -value of -1. To understand this variation behavior of local stress ratio, detailed elastic-plastic FEA was carried out for evaluating stress-strain variation during cyclic loading. Based on the FEA results, elastic-plastic deformation behavior during cyclic loading is schematically shown in Fig. 3.14. Since only elastic deformation with the same local stress ratio as the remote stress ratio is repeated in high cycle fatigue region, the schematic stress-strain response during cyclic loading in high cycle fatigue region is omitted. In case of nominal stress and strain amplitudes higher than the kinked point (in the transition region), the localized tensile plastic zone is formed near notch root region at the maximum load. After unloading to the minimum load, the compressive elastic deformation region is formed in the tensile plastic zone formed at the maximum load, as shown in Fig. 3.14(a). The volume expansion of the tensile plastic deformation region induces compressive stress due to the constraint by the surrounding elastic region with reversed elastic deformation during unloading cycle. This compressive stress reduces the mean stress and then the local stress ratio. This mechanism can be confirmed from Fig. 3.15, which shows the local stress ratio variation along the notch cross-section. As found from the figure, only plastically deformed near notch region shows the decreased local stress ratio and no variation of local stress ratio is seen in the elastic deformation region.

In case of low cycle fatigue region, the fully plastic deformation at the notch section is induced at the maximum load as shown in Fig. 3.15(b). After unloading to the minimum load, the compressive plastic deformation region is formed in the compressive elastic deformation region due to the significant constraint by the surrounding elastic region with reversed elastic deformation during unloading cycle. This mechanism is on the same line of the above mechanism in the transition region with a difference of magnitude of loading level. From the distribution of local stress ratio along the notch cross-section shown in Fig. 3.15(b), the compressive elastic deformation region shows the local stress ratios between 0.1 to -1, as same as in the transition region explained above. In the compressive deformation region, the local stress ratio becomes -1.

It is known that fatigue strength decreases with increasing stress ratio for the smooth specimen, as seen from previous chapter 2. Therefore, it would be expected that the change of local stress ratio at the notch root influences fatigue behavior and fatigue strength of the notched specimen.

To confirm the effect of local stress ratio on fatigue strength, the fatigue life of the notched specimen has been estimated by taking the local stress ratio variation at the notch root into consideration in the following section.

(a) Transition region



(b) Low cycle region

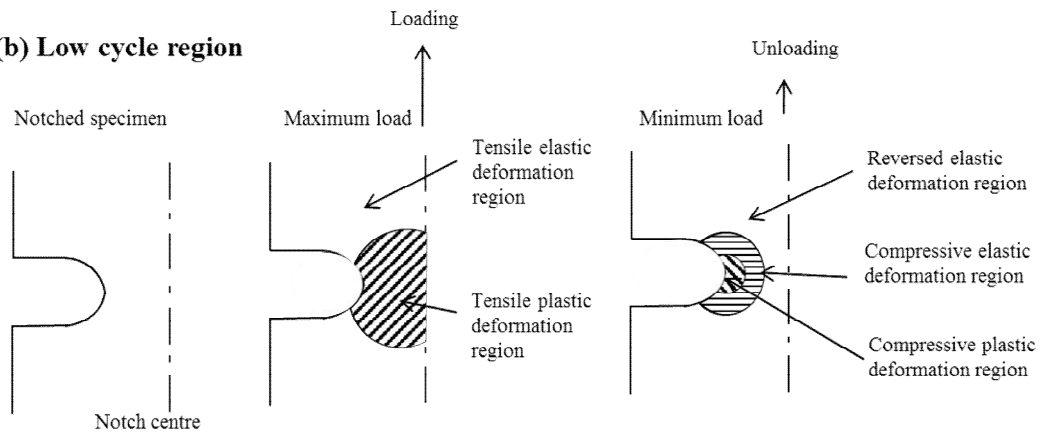


Fig. 3.14 A schematic explanation of the local mean stress or local stress ratio variation mechanism: (a) transition region (b) low cycle fatigue region

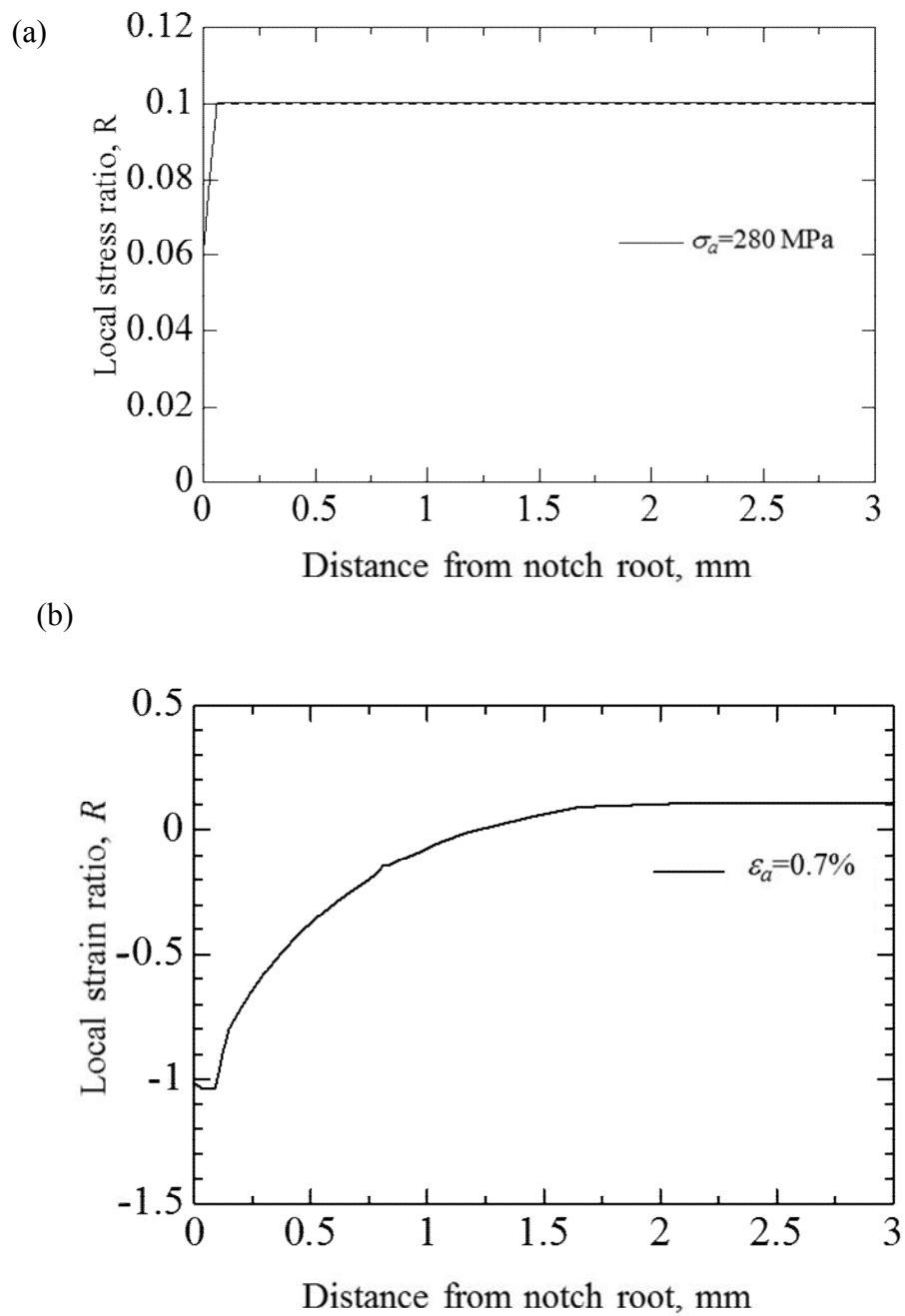


Fig. 3.15 Relationship between local stress ratio and distance from the notch root under the remote stress ratio of 0.1: (a) Transition region: $\sigma_a = 280 \text{ MPa}$
(b) Low cycle fatigue region : $\epsilon_a = 0.7\%$

3.4.2. Fatigue life predictions of the notched specimen

As discussed in the previous Chapter-2, the kinking behavior of S-N curve of notched specimens in high cycle fatigue region under the load-controlled fatigue tests and the local stress ratio variation at notch root above the kinking point have been discussed. By taking account the local stress ratio variation at notch root, fatigue life prediction should be carried out for notched specimen.

As can be seen from the previous chapter Fig. 2.4, the S-N curves in transition region between low and high cycle fatigue of the notched specimens under $R = 0.1$ is kinked at the critical nominal stress amplitude. In the present study, fatigue life prediction in wide range of fatigue from low cycle fatigue to high cycle fatigue including transition region has been carried out. The fatigue life has been estimated by two steps:

(1) At first, fatigue crack nucleation life is evaluated based on the SWT parameter combined with FEA.

(2) Fatigue propagation life has been estimated based on the fracture mechanics approach.

The detail of this prediction procedure has been explained as follow.

(1) Prediction 1: Taking the variation of local stress ratio at the notch root into consideration, the crack initiation life prediction is conducted based on the Smith-Waston-Topper (SWT) damage model [5]. However, the variation of local stress ratio was not significant in high cycle fatigue region and almost similar to the remote applied stress ratio. The crack propagation life prediction is also conducted based on

the linear elastic fracture mechanics. The total fatigue life N_f is obtained by the sum of crack initiation life, N_i and crack propagation life, N_p . The fatigue crack initiation life is predicted by combining the result of elastic-plastic FEA and SWT damage model. SWT mean stress parameter is given in the following equation.

$$\sqrt{\sigma_{\max} \varepsilon_a E} = f(N_f) \quad (3.2)$$

where σ_{\max} is given by $\sigma_{\max} = \sigma_m + \sigma_a$, σ_a is the stress amplitude and ε_a is the strain amplitude. This SWT parameter can be given by using the Coffin-Manson equation, Eq. (3.1), for taking account of the mean stress effect, as:

$$\sigma_{\max} \varepsilon_a = \frac{(\sigma'_f)^2}{E} (2N_f)^{2b} + \sigma'_f \varepsilon'_f (2N_f)^{b+c} \quad (3.3)$$

For each applied nominal stress level, σ_{\max} and ε_a are obtained from the FEA results which are varied with changing the local stress ratio at notch root. By combining the FEA results and the SWT parameter, the crack initiation lives for the notched specimens can be predicted by replacing N_f to N_i in Eq. (3.3).

The fatigue crack propagation life N_p is estimated by using the following Paris's equation [22],

$$\frac{da}{dN} = C(\Delta K)^m \quad (3.4)$$

where, da/dN is the crack growth rate, ΔK the stress intensity factor range, C and m the material constants. In the present study, the crack is assumed to be a surface elliptical crack with the crack depth a and length l ratio of 1. The stress intensity factor range for a surface elliptical crack is given as [23]:

$$\Delta K = 1.1215 \Delta \sigma \sqrt{\frac{\pi a}{Q}} \quad (3.5)$$

where $\Delta \sigma$ is the stress range, Q the shape factor for elliptical crack, which is given by [24]:

$$Q = 1 + 1.464 \left(\frac{a}{l} \right)^{1.65} \quad (3.6)$$

The crack propagation life N_p can be estimated by integrating the Paris's Eq. (3.4) combined with Eq. (3.5) with the integrating range from the initial crack depth a_i to the critical crack depth at fracture a_f . The initial crack depth is assumed to be the critical minimum crack depth when ΔK equals to ΔK_{th} as [25]:

$$a_i = \frac{1}{\pi} \left(\frac{\Delta K_{th}}{\Delta \sigma_w} \right)^2 \quad (3.7)$$

where $\Delta \sigma_w$ is the stress range at the fatigue limit and ΔK_{th} the threshold stress intensity factor range. In the prediction, dependency of ΔK_{th} on stress ratio was taken into consideration. The final crack depth is given by the following equation:

$$a_f = \frac{d_o}{2} - \sqrt{\frac{P}{\pi \sigma_B}} \quad (3.8)$$

where σ_B is the tensile strength obtained from the tensile test, P the applied maximum load and d_o is the gage section diameter of the specimen. Paris's law parameters c , m and the threshold stress intensity factor range ΔK_{th} for Ti-6Al-4V alloy were taken from the reference [26, 27]. Total fatigue life is obtained by the sum of the crack nucleation life and the crack propagation life.

In the transition and low cycle fatigue regions, where the local stress ratio at notch root is varied from the remote local stress ratio, fatigue life prediction has been carried out based on the SWT parameter combined with FEA, details of which has been explained as follow.

(2) Prediction 2: For this prediction, it is found that above the critical nominal stress amplitude in transition region and increasing nominal strain amplitude in low cycle fatigue region, transition behavior of fatigue fracture occurs from single to multiple fatigue crack nucleation was observed near the notch root region as shown in Fig. 3.4. The fatigue life is predicted by combining the results of elastic-plastic FEA and SWT damage model with taking the local stress ratio variation into consideration. The number of cycles required for crack propagation is neglected in this Prediction 2 due to the presence of multiple crack initiation at the notch root in the notch fatigued specimens tested at nominal stress amplitudes higher than the kinked point. The maximum nominal stress σ_{max} and the nominal strain amplitude ϵ_a are estimated based on the elastic-plastic FEA results at the stable state of stress-strain relation after several cycles and put into Eq.(3.3), where the local stress ratio is changed from the remote stress ratio, as seen from previous chapter Fig. 2.12(c). The maximum nominal stress is given by the average value of axial stress along the notch section at the maximum load and the nominal strain amplitude is given by the average value of axial strain amplitude along the notch section.

3.4.3 Comparison of the predicted lives and experimental results

The predicted fatigue lives for the notched specimens under $R = 0.1$ and the experimental results are compared in Fig. 3.16. As can be seen from the figures, the fatigue lives predicted by “Prediction 1” are in good agreement with the experiment in high cycle fatigue region under the kinked point. The fatigue lives predicted by “Prediction 2” are also in good agreement with the experimental results in both transition region with the local stress ratio variation and low cycle fatigue region with

the local stress ratio of -1. From the foregoing results, it is found that by taking account of the local stress ratio variation at notch root, fatigue lives in low cycle fatigue as well as transition region can be successfully predicted. In Fig. 3.16, the nominal strain amplitude - fatigue life (S-N) curve under the remote stress ratio of -1 is also shown, where the local stress ratio at notch root is also -1. The predicted S-N curve is in good agreement with the experimental results tested under the remote stress ratio of -1 in high cycle fatigue region. As found from the figure, in fatigue design of notched components, if the low cycle fatigue life including the transition region is predicted by assuming the stress ratio of -1, the predicted lives would be not in safety side in the transition region.

From the foregoing results, it would be concluded as: the SWT parameter is useful to predict the fatigue life of notched specimen in low cycle fatigue region and transition region between low cycle and high cycle fatigue regions, where the local stress ratio variation is taken into account. On the other hand, crack nucleation life prediction based on SWT parameter combined with crack propagation life prediction based on fracture mechanics approach is useful in high cycle fatigue region. Without taking account the local stress variation at notch root, the fatigue life prediction will be not safety side in transition region.

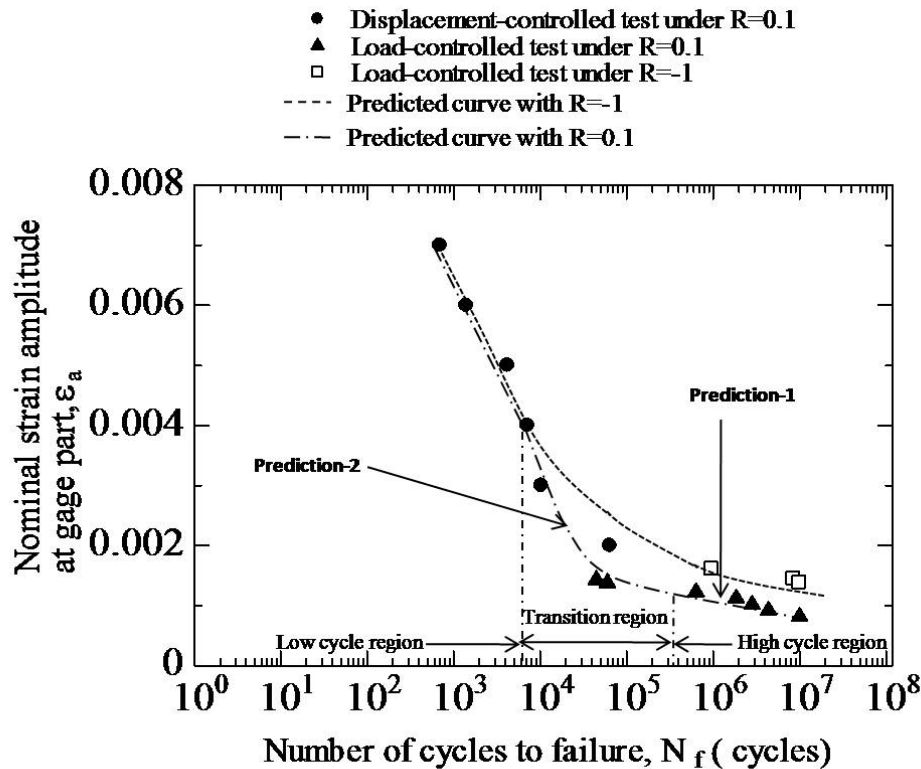


Fig. 3.16 Comparison between experimental and predicted fatigue lives for the notched specimen under remote stress ratio of 0.1 for the wide range of fatigue from low cycle to high cycle

3.5 Conclusions

Notch fatigue behavior in transition region between low cycle fatigue and high cycle fatigue regions has been investigated by combining the results under displacement-controlled low cycle fatigue tests in the present chapter and those under load-controlled high cycle fatigue tests in the previous chapter. The elastic-plastic stress and strain states and local stress ratio variation at the notch root under cyclic loading in low fatigue and transition regions have been investigated by carrying out

the elastic-plastic finite element analysis. The main conclusions are summarized as follows:

(1) The S-N curve obtained by the displacement-controlled low cycle fatigue test was not smooth and deflected in the lower nominal strain amplitude region, where the local stress ratio was varied depending on the applied nominal strain amplitude.

(2) Based on the elastic-plastic FEA results, the local stress ratio in high cycle fatigue region is constant and equal to the remote stress ratio. The local stress ratio varied at the kinked point and decreases with increasing nominal strain amplitude in transition region. The local stress ratio reaches -1 in low cycle fatigue region.

(4) The constraint due to the reversed elastic deformation during unloading is speculated to be the main mechanism to induce the compressive stress and vary the mean stress and local stress ratio.

(5) The fatigue life in wide range from low cycle fatigue and high cycle fatigue including transition region can be successfully predicted by taking account of local stress ratio variation at notch root based on the SWT parameter combined with elastic-plastic FEA under cyclic loading.

References

- [1] N. E. Dowling, Mechanical Behavior of Materials 2nd, Prentice-Hall New Jersey (1999)
- [2] A. J. McEvily, Metal Failures: Mechanisms, Analysis, Prevention. John Wiley & Sons Inc. New York (2002)
- [3] H. Neuber, Theory of Stress Concentration for Shear Strained Prismatic Bodies With Arbitrary Nonlinear Stress Strain Law, J Appl Mech 28 (1969) 544-551
- [4] G. Glinka, Calculation of Inelastic Notch-Tip Strain-Stress Histories Under Cyclic Loading, Eng Fract Mech 22 (1985) 839-854
- [5] K. N. Smith, P. Watson, T. H. Toppe, A Stress-Strain Function for The Fatigue Of Metals, J. Mater 5 (1970) 767-778
- [3] L. P. Borrego, L. M. Abreu, J. M. Costa, J. M. Ferreira, Analysis of Low Cycle Fatigue In AlMgSi Aluminum Alloys, Eng Fail Anal 11 (2004) 715-725
- [6] A. Ince, G. A. Glinka, Modification of Morrow and Smith-Watson-Topper Mean Stress Correction Models, Fatigue Fract Eng Mater Struct 34 (2011) 854-867
- [7] S. K. Koh, R. I. Stephens, Mean Stress Effects On Low Cycle Fatigue For A High Strength Steel, Fatigue Fract Engng Mater Struct 14 (1991) 413-428
- [8] S. Begum, D. L. Chen, Effect of Strain Ratio and Strain Rate on Low Cycle Fatigue Behavior of AZ31 Wrought Magnesium Alloy, Mater Sci Eng A 517 (2009) 334-343

- [9] H. Hao, D. Ye, C. Y. Chen, Strain Ratio Effects on Low-Cycle Fatigue Behavior and Deformation Microstructure of 2124-T851 Aluminum Alloy, *Mat Sci Eng A* 605 (2014) 151-159
- [10] J. Morrow, *Fatigue Properties of Metals*, Fatigue Design Handbook, Warrendale (1968)
- [11] K. Walker, The Effect of Stress Ratio During Crack Propagation and Fatigue For 2024-T3 and 7075-T6 Aluminum, *ASTM STP* 462 (1970) 1-14.
- [12] K. N. Smith, P. Watson, T. H. Topper, A Stress-Strain Function For The Fatigue Of Metals, *J. Mater* 5 (1970) 767-778
- [13] C-H Wang, L.R.F Rose, Transition and Steady-State Deformation at Notch Root Under Cyclic Loading, *Mech Mater* 30 (1998) 229-241
- [14] M. Knop, R. Jones, L. Molent, C. Wang, On the Glinka and Neuber Methods for Calculating Notch Tip Strains Under Cyclic Load Spectra, *Int J Fatigue*, 22 (2000) 743-755
- [15] ASTM E606-92, Standard Practice for Strain-Controlled Fatigue Testing, (1998)
- [16] S. Suresh, *Fatigue of Materials 2nd*, Cambridge University Press (1998)
- [17] A. J. Nachtigall, Cyclic Stress-Strain Curve Determination For D6AC Steel By Three Methods, Technical Report, NASA TM-73815, E-9402, Nachtigall Lewis Research Center Cleveland, Ohio United States (1977)
- [18] T. Akahori, M. Niinomi, K. Fukunaga, An Investigation of The Effect of Fatigue Deformation on The Residual Mechanical Properties of Ti-6Al-4V ELI, *Metall Mater Trans A* 31(8) (2000) 1937-1948

- [19] A. S. Beranger, X. Feaugas, M. Clavel, Low Cycle Fatigue Behaviors of An A + β Titanium Alloy: Ti6246, *Mat Sci Eng A*, 172 (1993) 31-41
- [20] L. F. Coffin, A Study of The Effects of Cyclic Thermal Stresses on A Ductile Metal. *Trans ASME* 76 (1954) 931-950
- [21] S. S. Manson, Behavior of Materials Under Conditions of Thermal Stress, NASA Report 1170 Supersedes NASA TN 2933 (1954)
- [22] P. Paris, F. Erdogan, A Critical Analysis of Crack Propagation Laws, *Transactions of the American Society of Mechanical Engineers. J Basic Eng* 85 (1963) 528-534
- [23] Y. Murakami, *Stress Intensity Factors Handbook*, Pergamon Press (1987)
- [24] J. G. Merkle, A Review of Some of The Existing Stress-Intensity Factor Solutions For Part-Through Surface Cracks, U.S. Atomic Energy Commission ORNL-TM-3983 (1973)
- [25] M. H. El Haddad, K. N. Smith, T. H. Topper, Fatigue Crack Propagation of Short Cracks, *J Eng Mater Technol* 101(1979) 42-46
- [26] R. O. Ritchie, D. L. Davidson, B. L. Boyce, J. P. Campbell, O. Roder, High-Cycle Fatigue of Ti-6Al-4V. *Fatigue Fract Engng Mater Struct* 22 (1999) 621-631
- [27] R. K. Nalla, B. L. Boyce, J. P. Campbell, J. O. Peters, R. O. Ritchie, Influence of Microstructure on High-Cycle Fatigue of Ti-6Al-4V: Biomdal vs. Lamellar Structures, *Metall Mater Trans A* 33 (2002) 899-918

CHAPTER – 4

NOTCH FATIGUE BEHAVIOR OF A2024-

T4 ALLOY IN HIGH CYCLE FATIGUE,

TRANSITION AND LOW CYCLE

FATIGUE REGIONS

Chapter-4

Notch Fatigue Behavior of A2024-T4 Alloy in High Cycle Fatigue, Transition and Low Cycle Fatigue Regions

4.1 Introduction

In the previous chapters, notch fatigue behavior of Ti-6Al-4V alloy was investigated by combining the load-controlled high cycle fatigue test and displacement-controlled low cycle fatigue tests as well as the elastic-plastic finite element analysis. The results revealed that the local stress ratio in high cycle fatigue region is constant and the same as the applied remote stress ratio. The local stress ratio varied at the nominal strain amplitudes higher than the kinked point due to plastic deformation developed at notch root. The local stress ratio decreased with increasing the nominal strain amplitude and then reached to -1 in low cycle fatigue region. The region with variation of local stress ratio from the remote stress ratio to -1 can be defined as the transition region. The wide range of fatigue life from low cycle to high cycle including transition region could be successfully predicted by taking account the local stress ratio variation at notch root based on the SWT parameter combined with elastic-plastic finite element analysis under cyclic loading.

However, the detail of local stress ratio variation and its effect on notch fatigue behavior of different materials have not yet been clarified. Generally speaking, the

aluminum alloy has different mechanical properties, such as Young's modulus, lower yield stress and lower tensile strength compared to the titanium alloy used in the previous chapters. Therefore, in the present chapter, A2024-T4 alloy was selected for a material with different mechanical properties to compare notch fatigue behavior of the Ti-6Al-4V alloy especially in the transition region of S-N curve. Based on the elastic-plastic finite element analysis and the load-controlled high cycle fatigue test results, notch fatigue behavior of the A2024-T4 alloy as well as the material dependence of local stress ratio variation were discussed.

Table 4.1 Chemical composition of the A2024-T4 alloy used

| Si | Fe | Cu | Mn | Mg | Cr | Zn | Ti | Al |
|------|------|-----|------|-----|------|------|------|---------|
| 0.11 | 0.24 | 4.5 | 0.57 | 1.5 | 0.04 | 0.02 | 0.01 | Balance |

Table 4.2 Mechanical properties of the A2024-T4 alloy used

| | |
|-------------------------------|----------|
| Young's modulus, E | 73.3 GPa |
| 0.2% Proof stress, σ_y | 458 MPa |
| Tensile strength, σ_u | 601 MPa |
| Elongation at break | 14% |
| Hardening coefficient, K | 844 MPa |
| Hardening exponent, n | 0.112 |

4.2 Experiments and FEM analysis

4.2.1 Material and specimens

A2024-T4 alloy was used for the present investigation. The chemical composition and mechanical properties of the A2024-T4 alloy are shown in Tables 4.1 and 4.2, respectively. The microstructure of the A2024-T4 alloy is also shown in Fig. 4.1. The average grain size measured by the line intersect method (ASTM E112) was 109 μm .

Figure 4.2 shows shapes and dimensions of the smooth and notched specimens used. Both the smooth and notched specimens were designed according to ASTM-E606 [1]. The notched specimen had a U-shaped circumferential notch with a notch root radius of 2 mm and a depth of 3 mm. Elastic stress concentration factor of the notch was 1.55 [2].

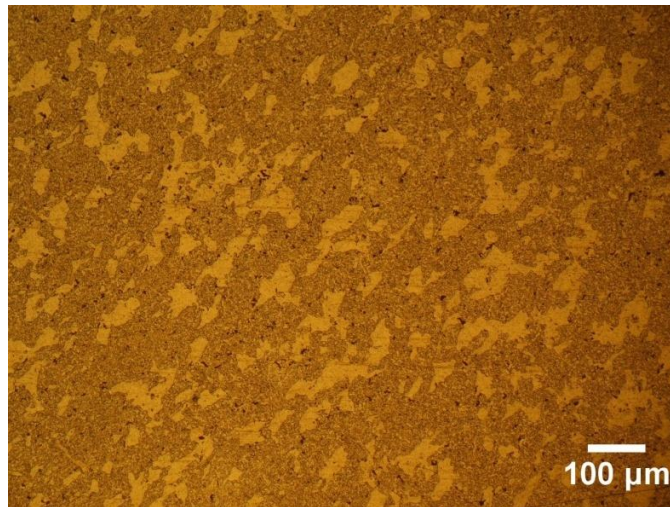


Fig. 4.1 Microstructure of the A2024-T4 alloy used

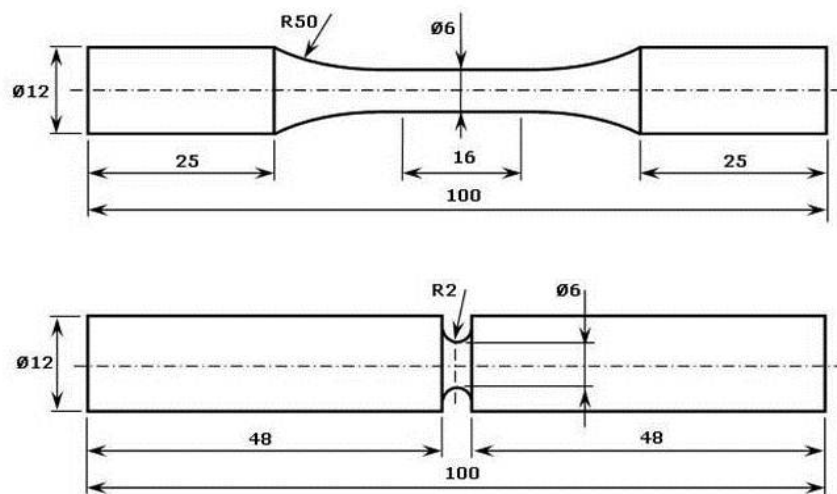


Fig. 4.2 Shape and dimensions of the smooth and notched specimens (in mm)

4.2.2 Tensile test

A tensile test of the smooth specimen was performed at a displacement rate of 0.5mm/min by using an Instron-type tensile test machine with a capacity of 50 kN to obtain mechanical properties, which were used for the finite element analysis (FEA).

4.2.3 Load-controlled fatigue strength test

Conventional load-controlled fatigue strength tests to obtain S-N curves were carried out at a frequency of 20 Hz under a sinusoidal wave form with different stress ratios (R) of 0.1 and 0.5 by using a servo-hydraulic fatigue testing machine with a load capacity of 50 kN. Loading alignment was carefully adjusted before conducting the tests according to ASTM E606. The numbers of smooth specimens tested were 10 and 7 for $R=0.1$ and 0.5, respectively. To obtain the fatigue limit according to ASTM E468-11, the staircase method [3, 4] was applied to the fatigue test of smooth specimen under $R = 0.1$ using 20 specimens. Those of notched specimens were 13 for both $R = 0.1$ and 0.5. All tests were performed in laboratory air at room temperature. Fracture surfaces of the specimens were examined in detail by using a scanning electron microscope (SEM).

4.2.4 Strain-controlled fatigue strength test

Low cycle fatigue tests of the smooth specimens were performed under fully reversed loading to obtain an S-N curve in the low cycle fatigue regime. The test range of applied strain amplitude was from 0.6% to 1.1% under a triangular wave form with a strain rate of 0.1% per second. Each specimen was subjected to a constant cyclic strain until failure of the specimen, which was defined by the 25% drop of maximum load during the test.

4.2.5 Cyclic stress-strain curve

To obtain a cyclic stress-strain curve of the present material, which was used in the FEA, strain-controlled tests were performed for the smooth specimen. The specimen was subjected to fully reversed loading with triangular wave form according to a standard incremental step test method [5, 6] in a servo-hydraulic fatigue testing machine with a load capacity of 50 kN. An extensometer with 13 mm gauge length was used for the strain-controlled test. In this method, the specimen was subjected to block loading with gradually increasing and decreasing strain amplitudes. Details of the block loading with the maximum strain amplitude of 1% were as follows: the starting strain amplitude was 0.4% and increased up to 1% with a strain increment step of 0.1% under a strain rate of 0.05% per second. The strain decreasing process was symmetrically reversed to the strain increasing process. After repeated few loading blocks, the stress-strain response was stabilized. By connecting the peak stresses at each hysteresis loops in the stabilized block, cyclic stress-strain curve was obtained.

4.2.6 Finite element analysis

The elastic-plastic FEA was performed on the notched specimen under the load-controlled conditions to investigate the stress-strain states, plastic deformation behavior and local stress ratio at notch root. Detail of the finite element analysis method can be found in the previous Chapter-2.

4.3. Results

4.3.1 Load-controlled fatigue strength tests of the smooth and notched specimens

Figure 4.3 shows relationships between nominal stress amplitude and number of cycles to failure for the smooth and notched specimens under two different R of 0.1 and 0.5. The nominal stress for the notched specimen was evaluated by the applied load divided by the minimum cross-sectional area at notch root. As seen from the figure, significant reduction of fatigue strength was observed in the notched specimen compared to the smooth specimen, which is commonly known as the effect of notch [7]. It is also well known that fatigue strength decreased with increasing stress ratio R (that is, mean stress σ_m) [8], where the relationship between mean stress and stress ratio is given as: $\sigma_m = (1+R)\sigma_{max}/2$, where σ_{max} is the maximum stress. In the higher stress and shorter life region for the notched specimen, the S-N curve is not smooth and kinked, which is similar phenomenon to the titanium alloy reported in previous chapters. The kinked point of the present A2024-T4 alloy was about 170 MP for $R = 0.1$ and 143 MPa for $R=0.5$. On the other hand, the kinking behavior was not clearly observed in the smooth specimens.

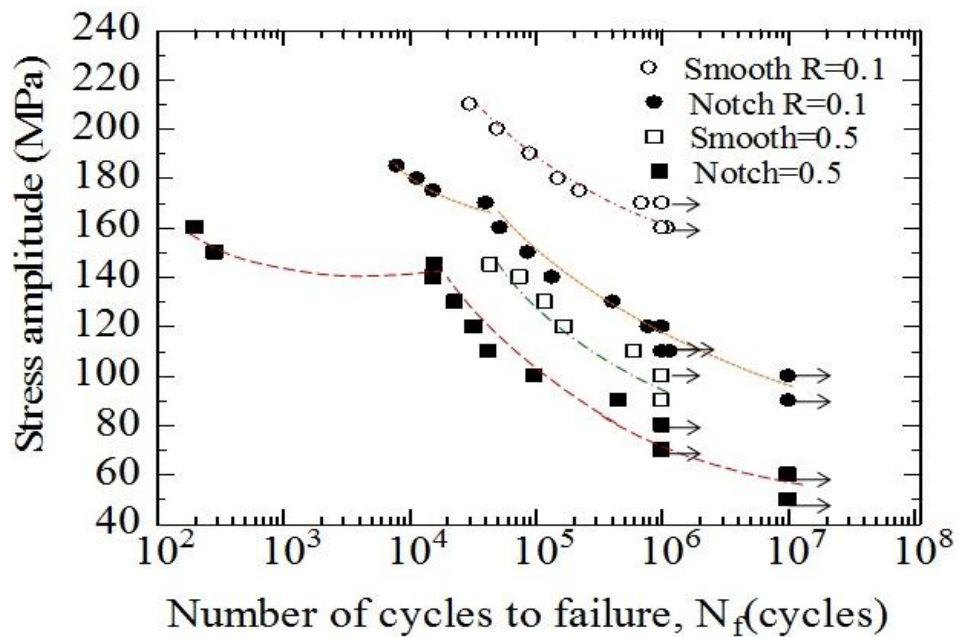


Fig. 4.3 S-N curves for the smooth and notched specimens of the A2024-T4 alloy

Overall fracture surface observations for the smooth and notched specimens tested under $R = 0.1$ are shown in Fig. 4.4. As seen from the figure, only single fatigue crack was nucleated for the smooth specimen regardless of applied stress level. For the notched specimen, multiple fatigue cracks were nucleated at higher stress level, while only single fatigue crack was nucleated at lower stress level. These observations suggest that multiple cracks are nucleated when plastic deformation at notch root develops, while single crack is nucleated under elastic deformation at notch root. Similar fracture surface characteristics were found for the case of $R = 0.5$, as shown in Fig. 4.5.

Grosskreutz et al. [9] reported that most of micro cracks were nucleated at constituent inclusions on the specimen surface in A2024 alloy. Moreover, damage in aluminum alloys was usually nucleated in large and brittle intermetallic particles or coarse precipitates, and sometimes also in smaller particles such as dispersoids or precipitates [10, 11]. However, in the present 2024 aluminum alloy, fatigue cracks were

nucleated only from the specimen surface and no inclusion or precipitates were observed at the crack nucleation sites. Therefore, slip band formation on the specimen surface, as proposed by Forsyth [12], will be a main mechanism for the present aluminum alloy.

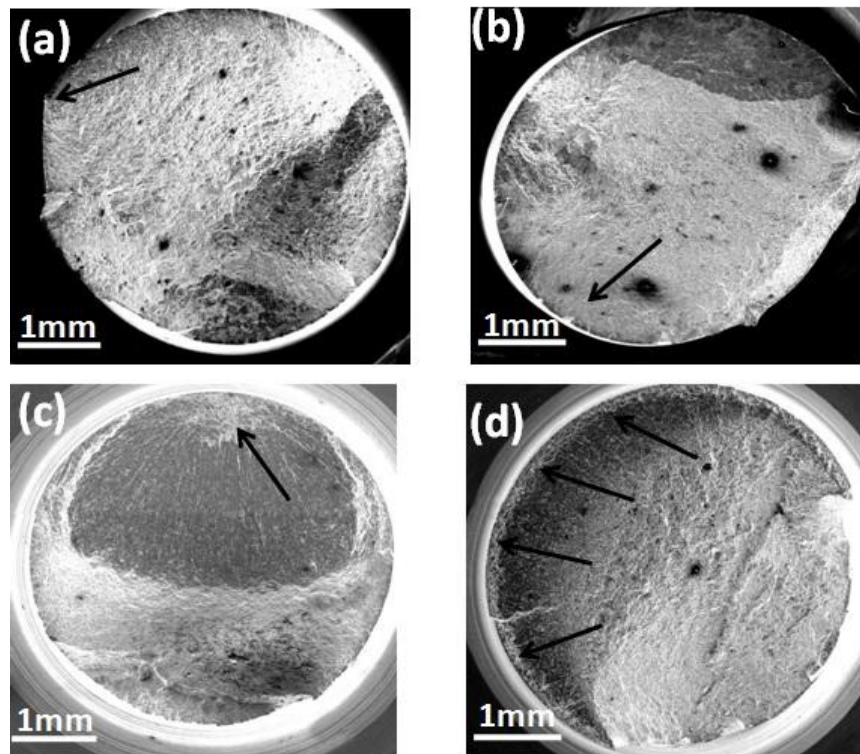


Fig. 4.4 Fatigue fracture surfaces of the smooth specimens tested at (a) $\sigma_a = 180$ MPa, $N_f = 150,235$ cycles (b) $\sigma_a = 200$ MPa, $N_f = 49,703$ cycles and the notched specimen tested at (c) $\sigma_a = 120$ MPa, $N_f = 780,000$ cycles (d) $\sigma_a = 180$ MPa, $N_f = 11,500$ cycles under $R = 0.1$

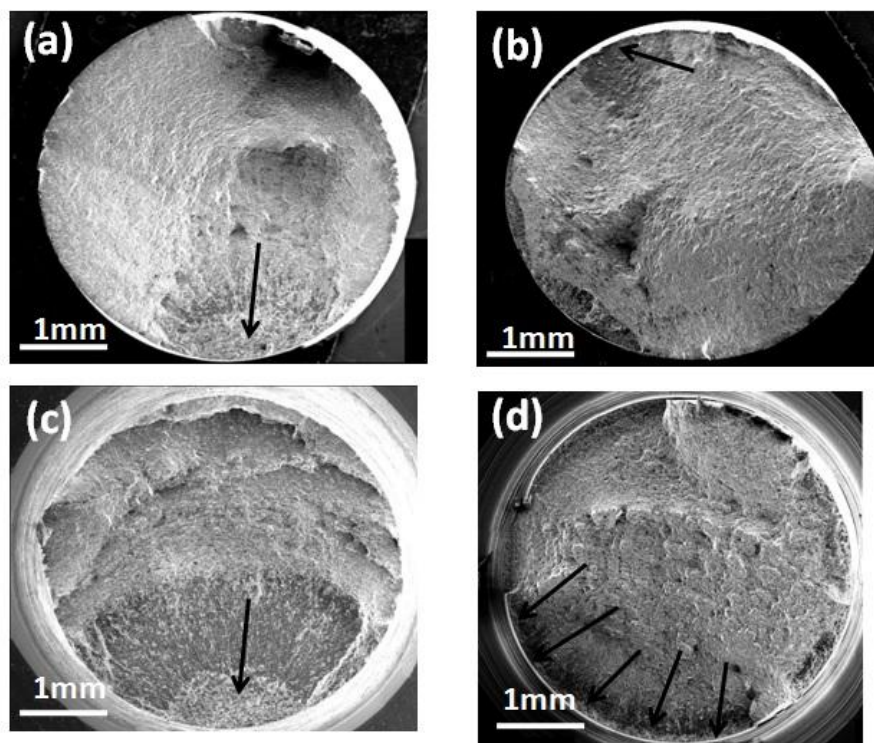


Fig. 4.5 Fatigue fracture surfaces of the smooth specimens tested at (a) $\sigma_a = 110$ MPa, $N_f = 601,495$ cycles (b) $\sigma_a = 120$ MPa, $N_f = 167,576$ cycles and the notched specimen tested with (c) $\sigma_a = 90$ MPa, $N_f = 458,014$ cycles (d) $\sigma_a = 145$ MPa, $N_f = 15,489$ cycles under $R = 0.5$

4.3.2 Cyclic stress-strain behavior

The cyclic stress-strain curve determined by using the incremental step method under a strain-controlled cyclic loading test is shown in Fig. 4.6. The relationship between cyclic strain amplitude $\Delta\varepsilon/2$ and cyclic stress amplitude $\Delta\sigma/2$ can be expressed in the following equation [13].

$$\Delta\varepsilon/2 = \Delta\sigma/2E + \left(\Delta\sigma/2K'\right)^{1/n'} \quad (4.1)$$

Where K' is the cyclic strength coefficient, n' is the cyclic strain hardening exponent and E is the Young's modulus. The cyclic properties determined from the figure are listed in Table 4.3. In Fig. 4.6, a stress-strain curve under the static tensile test of the same

material is also presented. As seen from the figure, the present material showed the cyclic hardening behavior, which is in accordance with the previous report [14]. The obtained cyclic stress-strain relationship was utilized in the FEA simulation under fatigue loading.

Table 4.3 Cyclic properties of the A2024-T4 alloy

| | |
|--|----------|
| Young's modulus, E | 73.3 GPa |
| Cyclic yield strength, σ'_y | 538 MPa |
| Cyclic strength coefficient, K' | 689 MPa |
| Cyclic strain hardening exponent, n' | 0.036 |

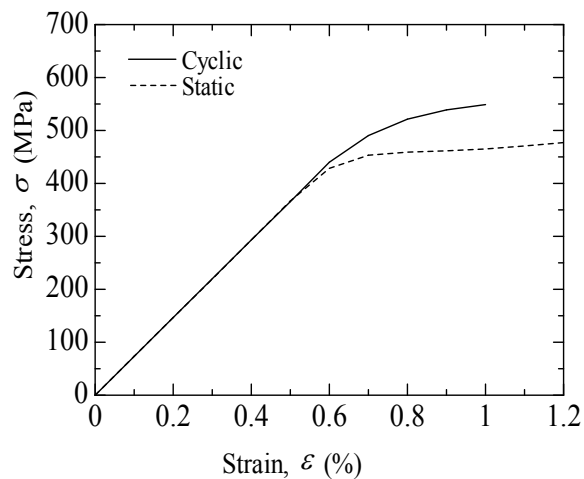


Fig. 4.6 Cyclic stress strain curve for the A2024-T4 alloy

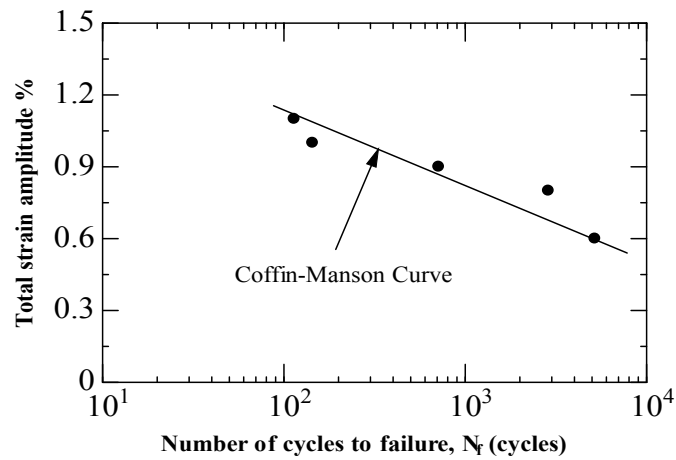


Fig. 4.7 S-N curve for low cycle fatigue of the A2024-T4 alloy

4.3.3 Strain-controlled fatigue test of the smooth specimen

The low cycle fatigue test result under fully reversed loading for the 2024-T4 aluminum alloy is shown in Fig.4.7. The relationship between total strain amplitude and number of cycles to failure can be presented by the Coffin-Manson equation [15, 16]:

$$\varepsilon_a = \frac{\sigma'_f}{E} (N_f)^b + \varepsilon'_f (N_f)^c \quad (4.2)$$

where N_f is the number of cycles to failure and not the reversals to failure, and σ'_f , ε'_f , b and c are the fatigue strength coefficient, the fatigue ductility coefficient, the fatigue strength exponent and the fatigue ductility exponent, respectively. The low cycle fatigue properties determined based on the y-intercepts and slope of log-log linear fitting lines are listed in Table 4.4. This result was used in the life prediction in the later section.

Table 4.4 Low cycle fatigue properties of the A2024-T4 alloy

| | |
|--|---------|
| Fatigue strength coefficient, σ'_f | 956 MPa |
| Fatigue strength exponent, b | -0.071 |
| Fatigue ductility coefficient, ϵ'_f | 0.081 |
| Fatigue ductility exponent, c | -0.69 |

4.3.4 Elastic-plastic FEA at notch root

From the results of elastic-plastic FEA of the notched specimen, the von Mises stress distributions at notch root for all applied stress levels at the maximum load of the first cycle are shown in Fig.4.8. The corresponding plastic strain distributions are also presented in the figure. As seen from the figure, the plastic strain is developed at notch root at higher nominal stress amplitudes than 140 MPa and 100 MPa for $R = 0.1$ and 0.5 , respectively.

4.3.4.1 Stress distribution at notch root for $R = 0.1$

Contour plots of von Mises stress distribution induced by the cyclic loading at the notch root from FEA results are given in Fig. 4.9. These contour plots are taken at the maximum stress applied to the model. For all applied stress levels, von Mises stress is the highest at the notch root and decreased toward the center of the notch plane. When the applied stress amplitude is lower as $\sigma_a = 90$ MPa, the highest von Mises stress values is lower than the yield strength and fully elastic deformation occurred at the notch root to notch center as shown in Fig. 4.9(a). But when stress amplitude is $\sigma_a = 140$ MPa, von Mises stress at the notch root were higher than the yield stress but it decreased toward the

notch center and elastic-plastic deformation behavior was obtained as shown in Fig. 4.9(b). When stress amplitude was higher as $\sigma_a = 180$ MPa in Fig. 4.9(c), von Mises stress value at the notch root and notch center was higher than the yield stress and fully plastic deformation behavior was observed. Fig. 4.10 show the comparison of evolution of localized plastic strain at the notch root for three different stress amplitude levels.

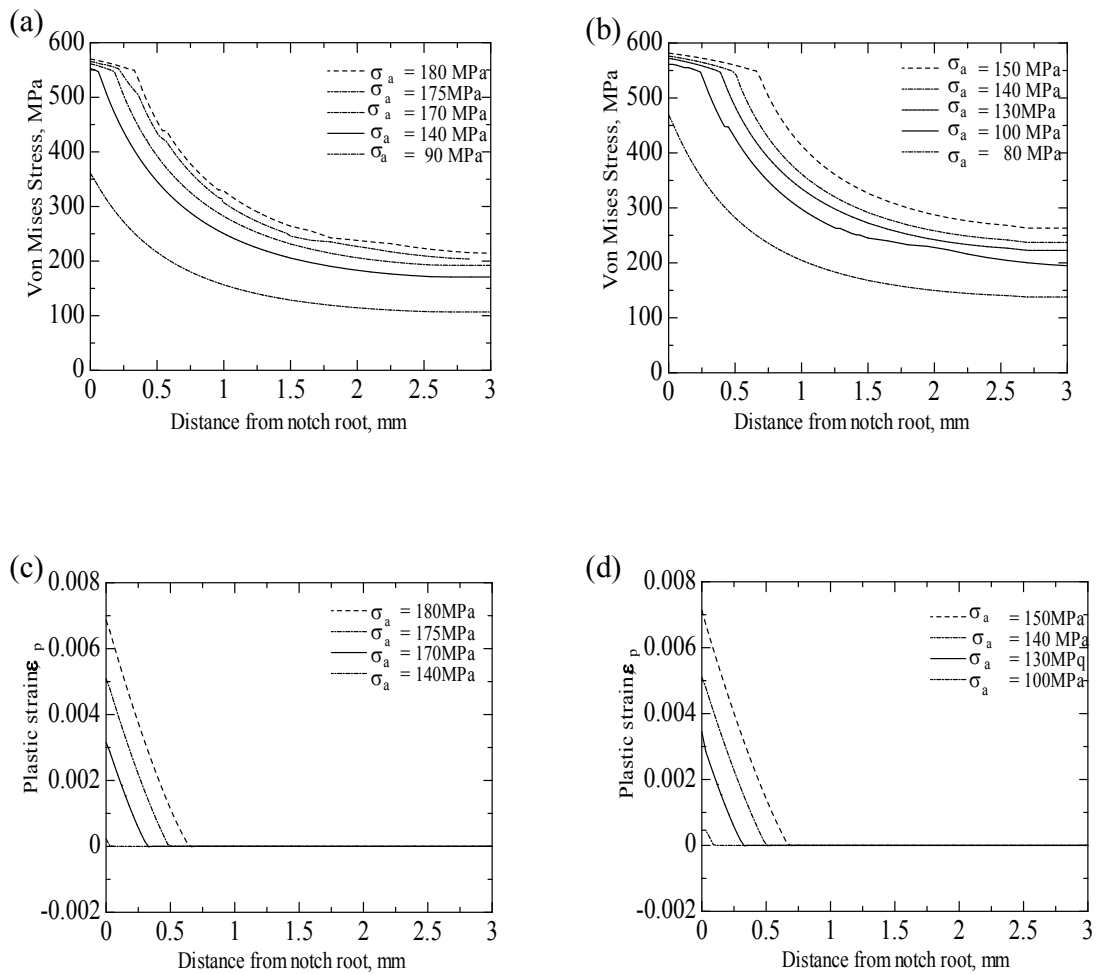


Fig. 4.8 The von Mises stress distribution near notch root in the first cycle; (a) $R = 0.1$, (b) $R = 0.5$ and the corresponding plastic strain distribution near notch root: (c) $R = 0.1$, (d) $R = 0.5$

4.3.4.2 Stress strain response hysteresis loop at notch root for $R = 0.1$

Examples of stress-strain hysteresis at notch root during cyclic loading under $R=0.1$ estimated by the elastic-plastic FEA are shown in Fig. 4.11. These stress-strains relationships were taken at the notch root of the comp 11 loading direction when maximum stress applied to the model. As found from the figure, when the nominal stress amplitude was in the lower range of 90 MPa, the stress-strain hysteresis was fully elastic. When the stress level was increased up to 150 MPa, plastic deformation was found at the first cycle and then the stress-strain response became linear elastic in the following cycles. With further increasing the nominal stress amplitude up to 180 MPa, significant plastic deformation occurred at the first loading cycle and then small plastic deformation was repeated in a few cycles and finally the stress-strain response became linear elastic. It was also found from Fig. 4. 11(c) that after large plastic straining at notch root, the local mean stress decreased and the local stress ratio at notch root became low from the applied remote stress ratio of 0.1.

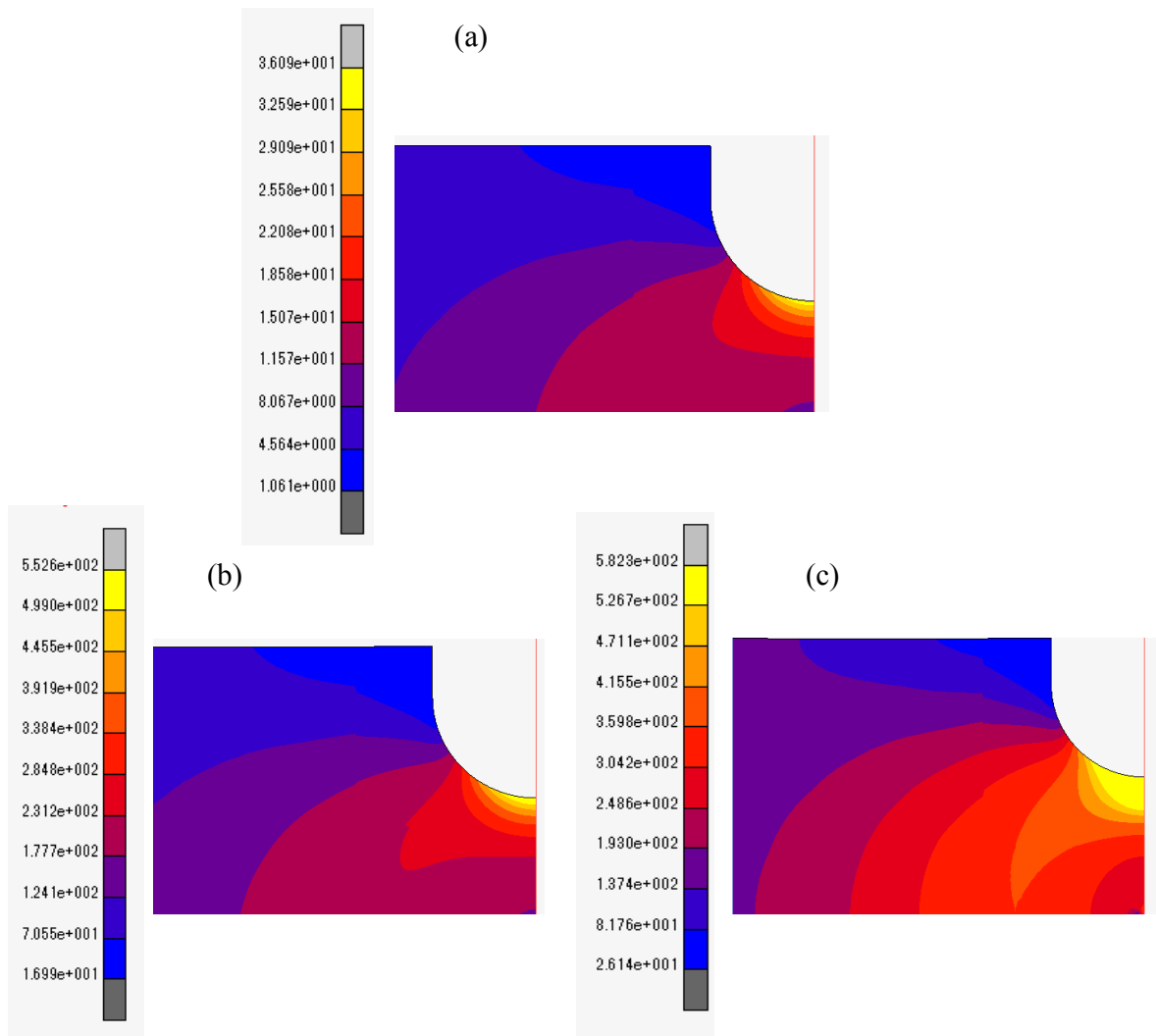


Fig. 4.9 Finite element analysis of notch specimen under load-controlled cyclic loading: von Mises stress distribution from notch root to notch center under $R = 0.1$: (a) $\sigma_a = 90$ MPa, (b) $\sigma_a = 140$ MPa, (c) $\sigma_a = 180$ MPa

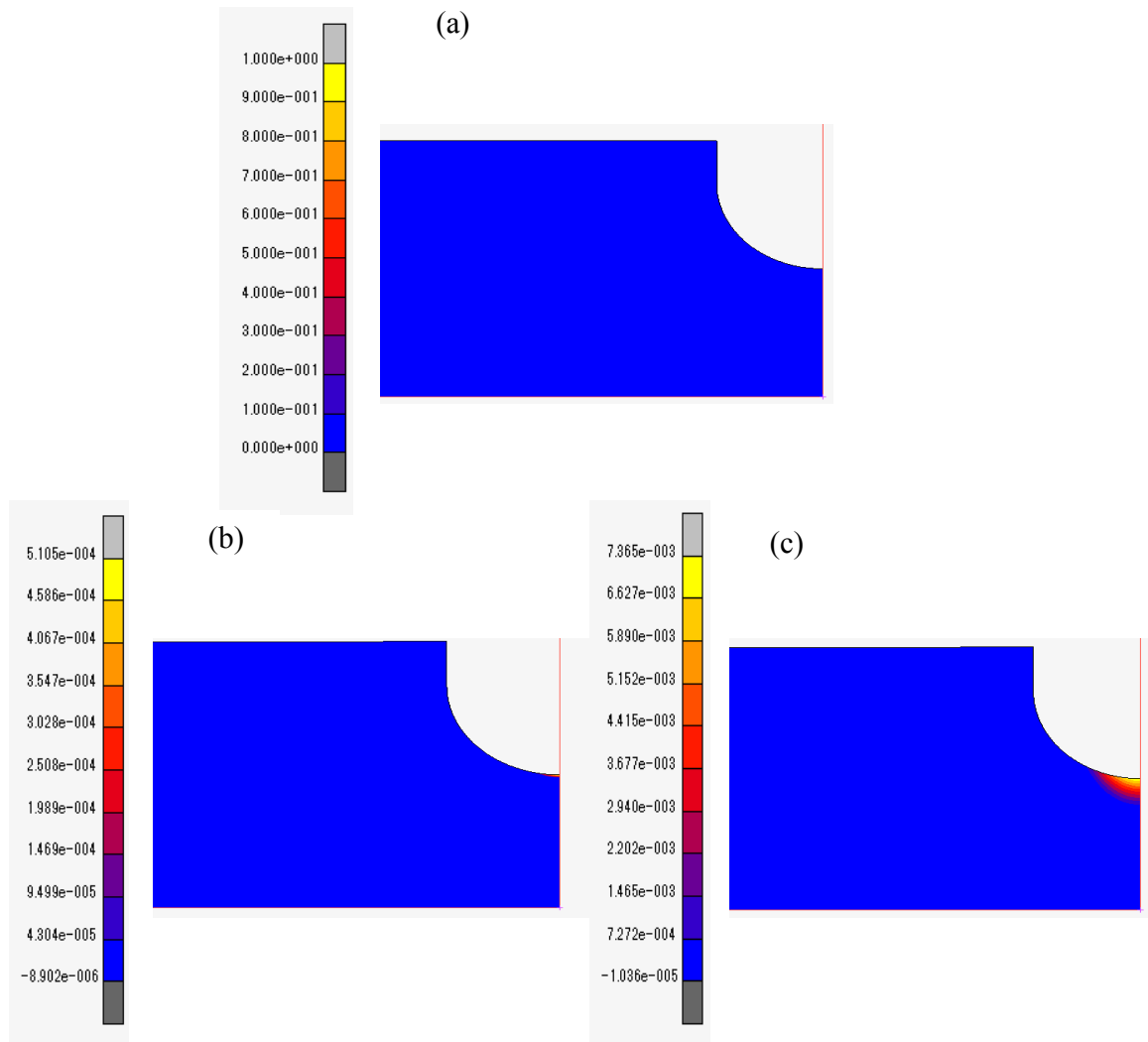


Fig. 4.10 Finite element analysis of notch specimen under load-controlled cyclic loading: plastic strain distribution from notch root to notch center under $R = 0.1$: (a) $\sigma_a = 90 \text{ MPa}$, (b) $\sigma_a = 140 \text{ MPa}$, (c) $\sigma_a = 180 \text{ MPa}$

Stress-strain curves at the notch root determined from the stress-strain analysis are presented from Fig. 4.12 to Fig. 4.14 for three stress amplitude levels 90 MPa, 140 MPa and 180 MPa. In order to understand the total stress-strain history cycles and subsequent following cycles at notch root during cyclic loading, total cycles and each cycles behavior was taken out and plotted as shown in Fig. 4.12 to 4.14.

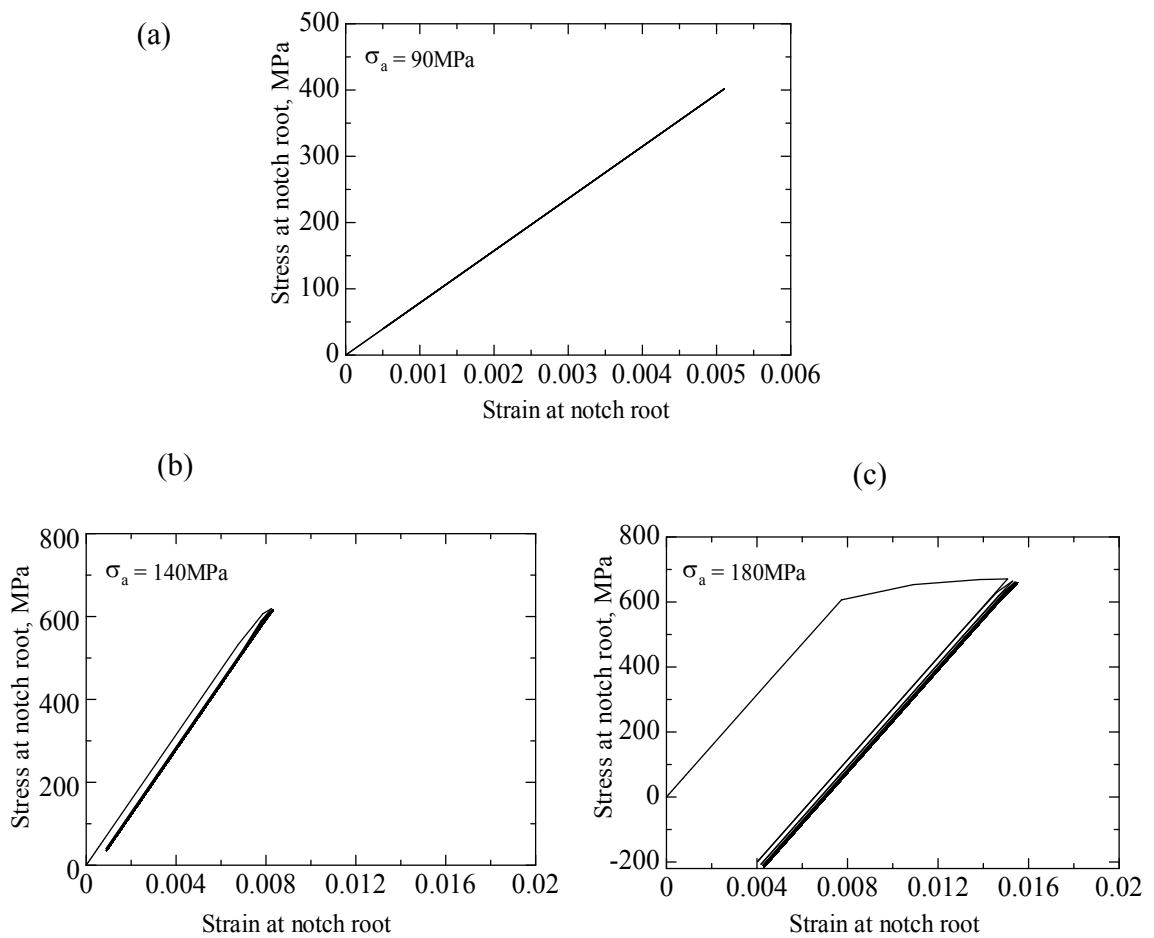


Fig. 4.11 Cyclic stress strain hysteresis at notch root under $R = 0.1$: (a) $\sigma_a = 90 \text{ MPa}$, (b) $\sigma_a = 140 \text{ MPa}$, (c) $\sigma_a = 180 \text{ MPa}$

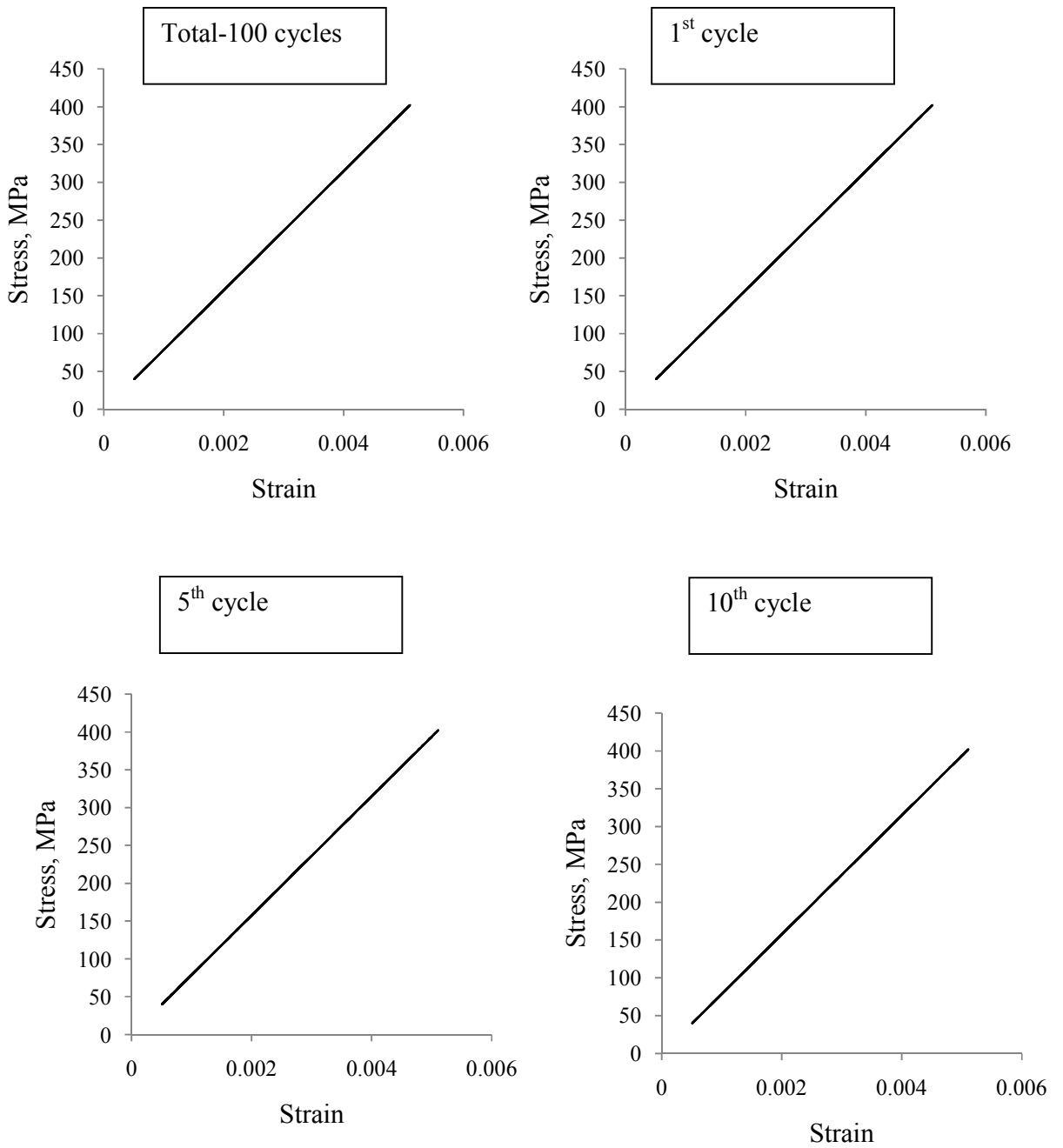


Fig. 4.12 Cyclic stress strain hysteresis at notch root under $R = 0.1$ at $\sigma_a = 90$ MPa

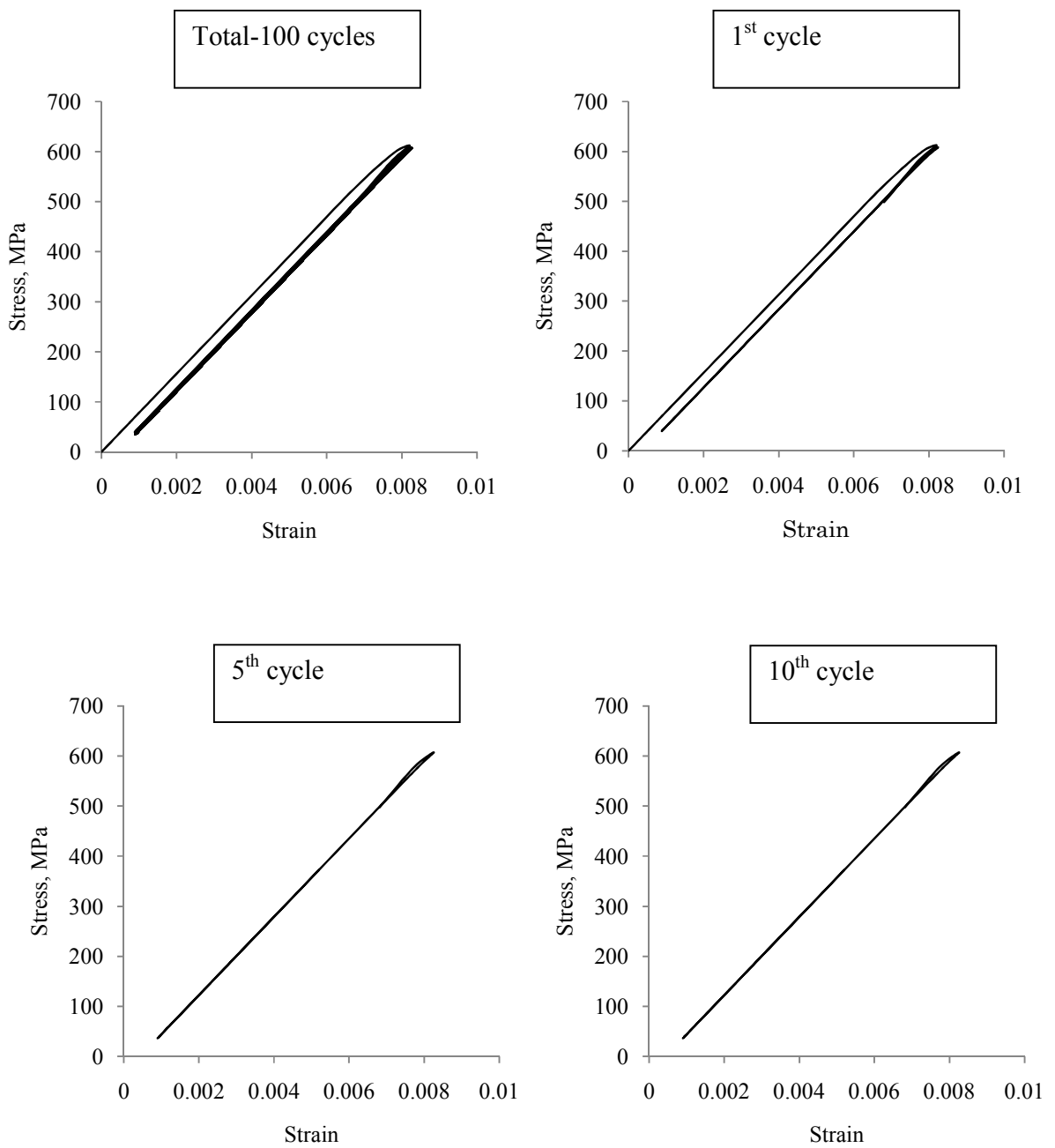


Fig. 4.13 Cyclic stress strain hysteresis at notch root under $R = 0.1$ at $\sigma_a = 140$ MPa

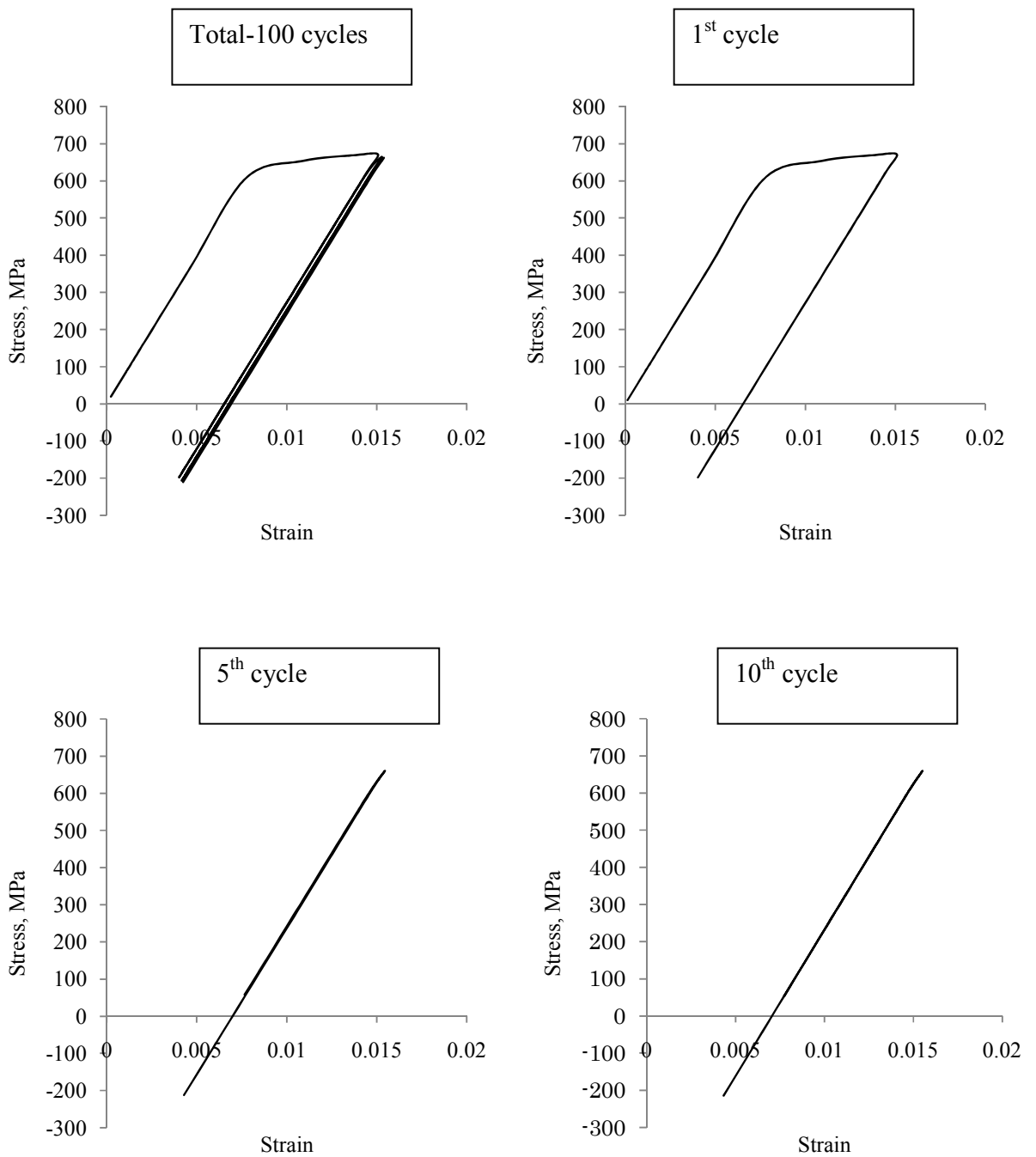


Fig. 4.14 Cyclic stress strain hysteresis at notch root under $R = 0.1$ at $\sigma_a = 180$ MPa

4.3.4.3 Stress distribution at notch root for $R = 0.5$

Distributions of von Mises stress induced by the cyclic loading at the notch root from FEA results are given in Fig. 4.15. These contour plots are taken at the maximum stress applied to the model. For all applied stress levels, von Mises stress is the highest at the notch root and decreased toward the center of the notch plane. When the applied stress amplitude is lower as $\sigma_a = 80$ MPa, the highest von Mises stress values is lower than the yield strength and fully elastic deformation occurred at the notch root to notch center as shown in Fig. 4.15(a). But when stress amplitude is $\sigma_a = 100$ MPa, von Mises stress at the notch root were higher than the yield stress but it decreased toward the notch center and elastic-plastic deformation behavior was obtained as shown in Fig. 4.15(b). When stress amplitude was higher as $\sigma_a = 150$ MPa in Fig. 4.15(c), von Mises stress value at the notch root and notch center was higher than the yield stress and fully plastic deformation behavior was observed. Fig. 4.16 show the comparison of evolution of localized plastic strain at the notch root for three different stress amplitude levels.

4.3.4.4 Stress strain response hysteresis loop at notch root for $R = 0.5$

Stress-strain curves at the notch root determined from the stress-strain analysis are presented in Fig. 4.17 for three stress amplitude levels 80 MPa, 100 MPa and 150 MPa. These stress-strains relationships were taken at the notch root of the comp 11 loading direction when maximum stress applied to the model. In all applied stress amplitude level, plastic deformation occurred only at first loading cycle, and thereafter the cyclic behavior corresponded to an elastic- shakedown response. Increase in plastic deformation with increase in applied stress amplitude is observed at the notch root as shown in the figure. To understand stress-strain behavior after first cycle, each cycle behaviors are taken out and plotted as shown in Fig. 4.18 to Fig. 4.20.

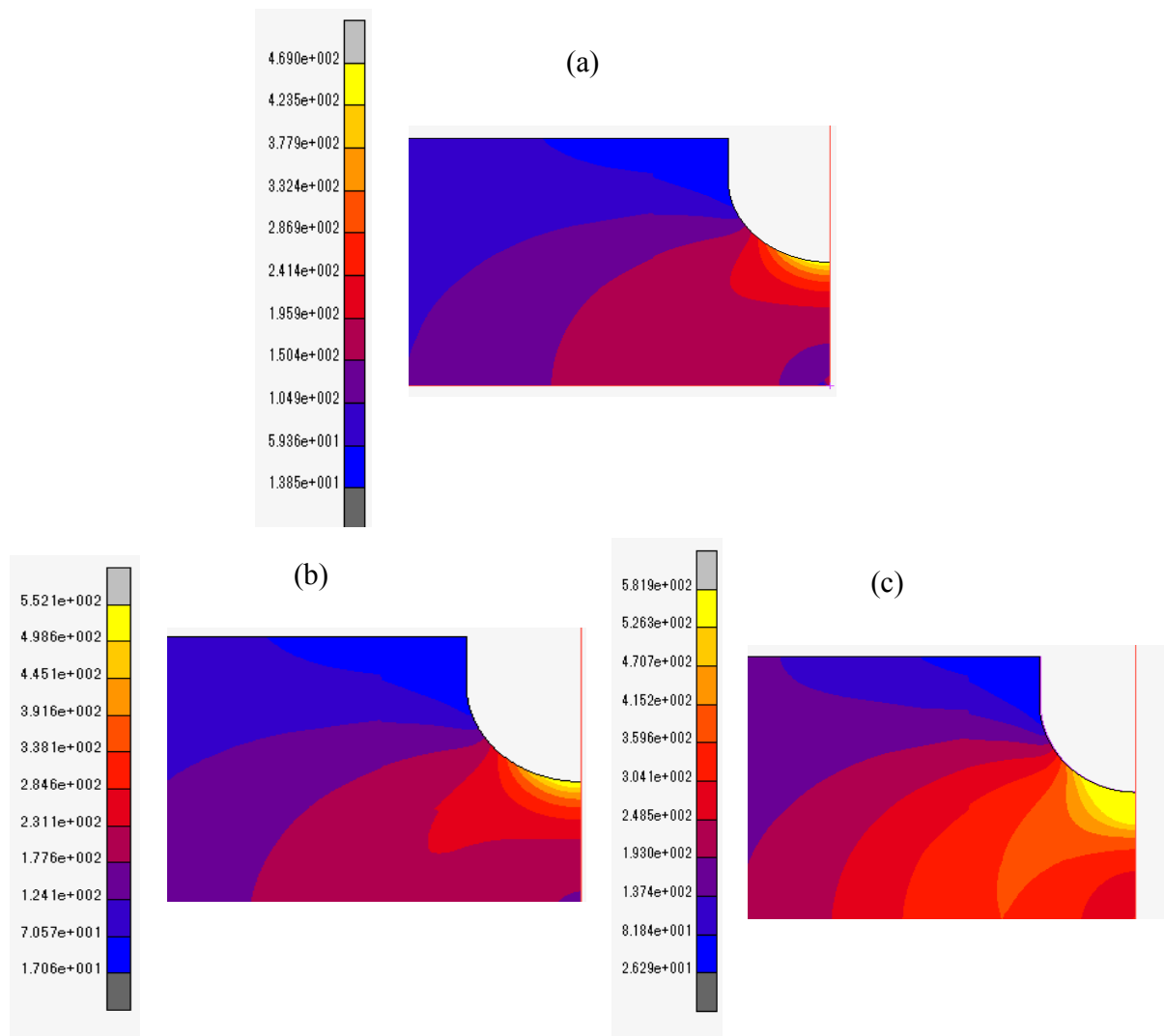


Fig. 4.15 Finite element analysis of notch specimen under load-controlled cyclic loading: von Mises stress distribution from notch root to notch center under $R = 0.5$:
 (a) $\sigma_a = 80$ MPa, (b) $\sigma_a = 100$ MPa, (c) $\sigma_a = 150$ MPa

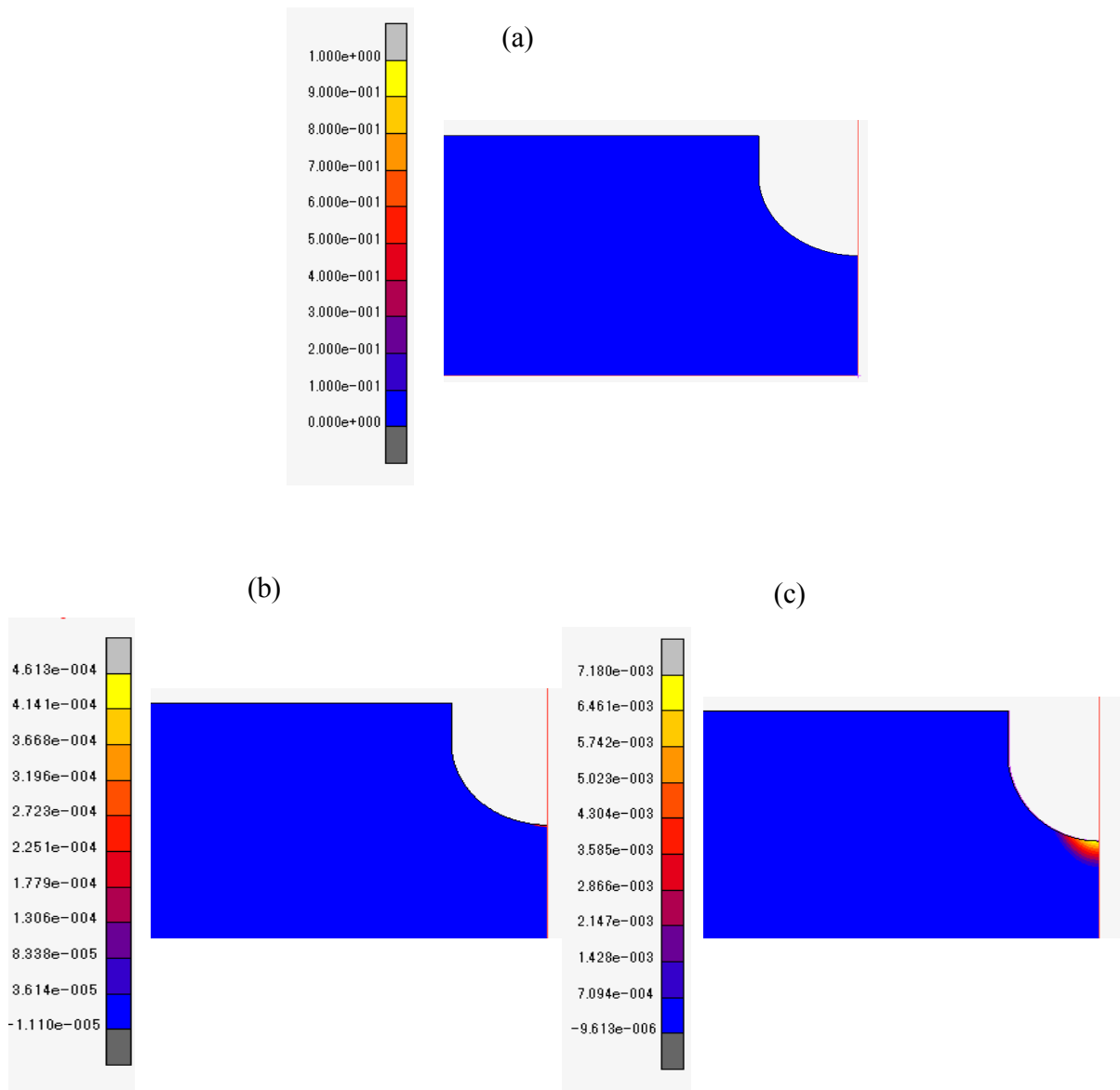


Fig.4.16 Finite element analysis of notch specimen under load-controlled cyclic loading: plastic strain distribution from notch root to notch center under $R = 0.5$: (a) $\sigma_a = 80$ MPa, (b) $\sigma_a = 100$ MPa, (c) $\sigma_a = 150$ MPa

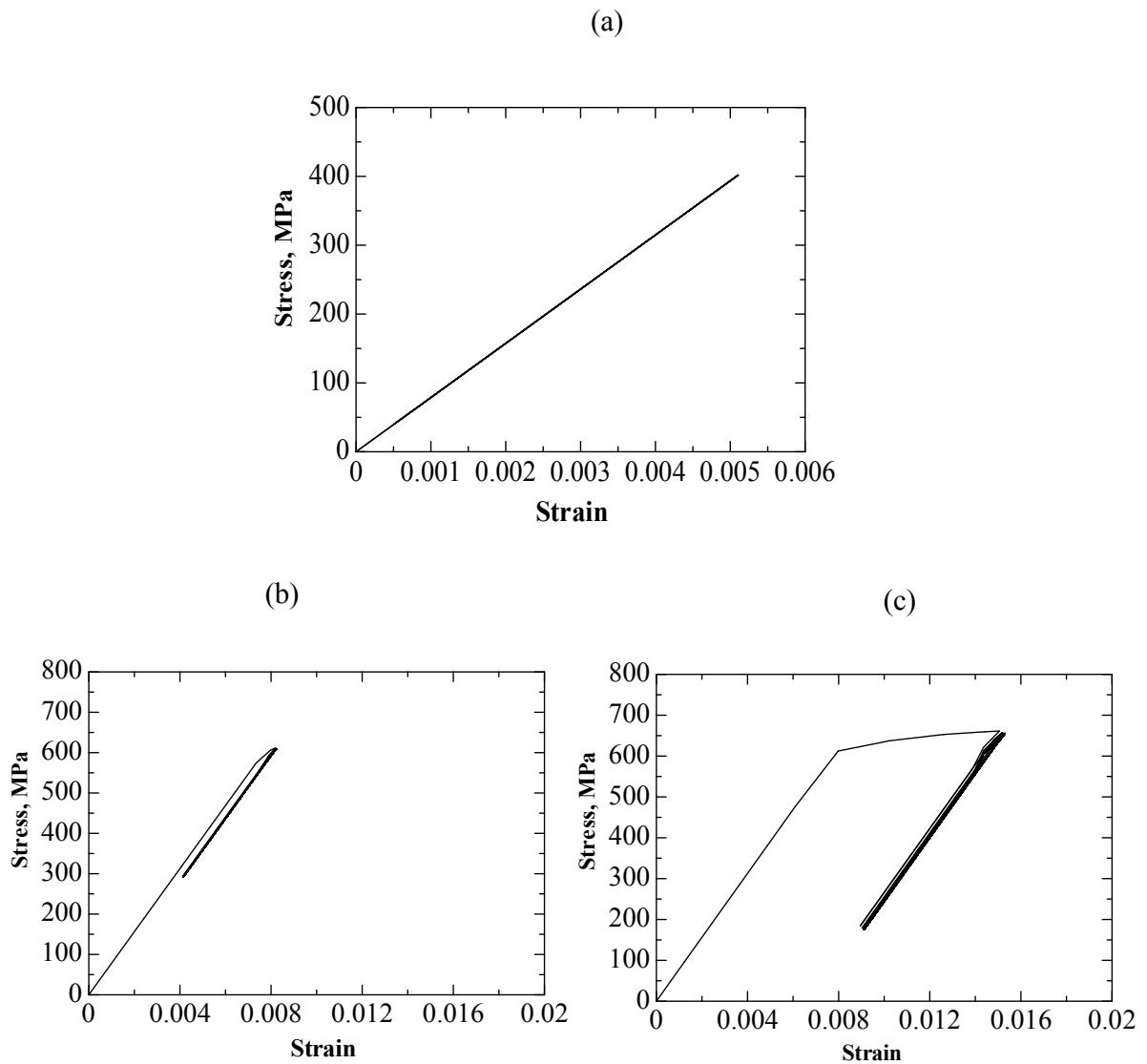


Fig. 4.17 Cyclic stress strain hysteresis at notch root under $R=0.5$: (a) $\sigma_a = 80$ MPa,
(b) $\sigma_a = 100$ MPa, (c) $\sigma_a = 150$ MPa

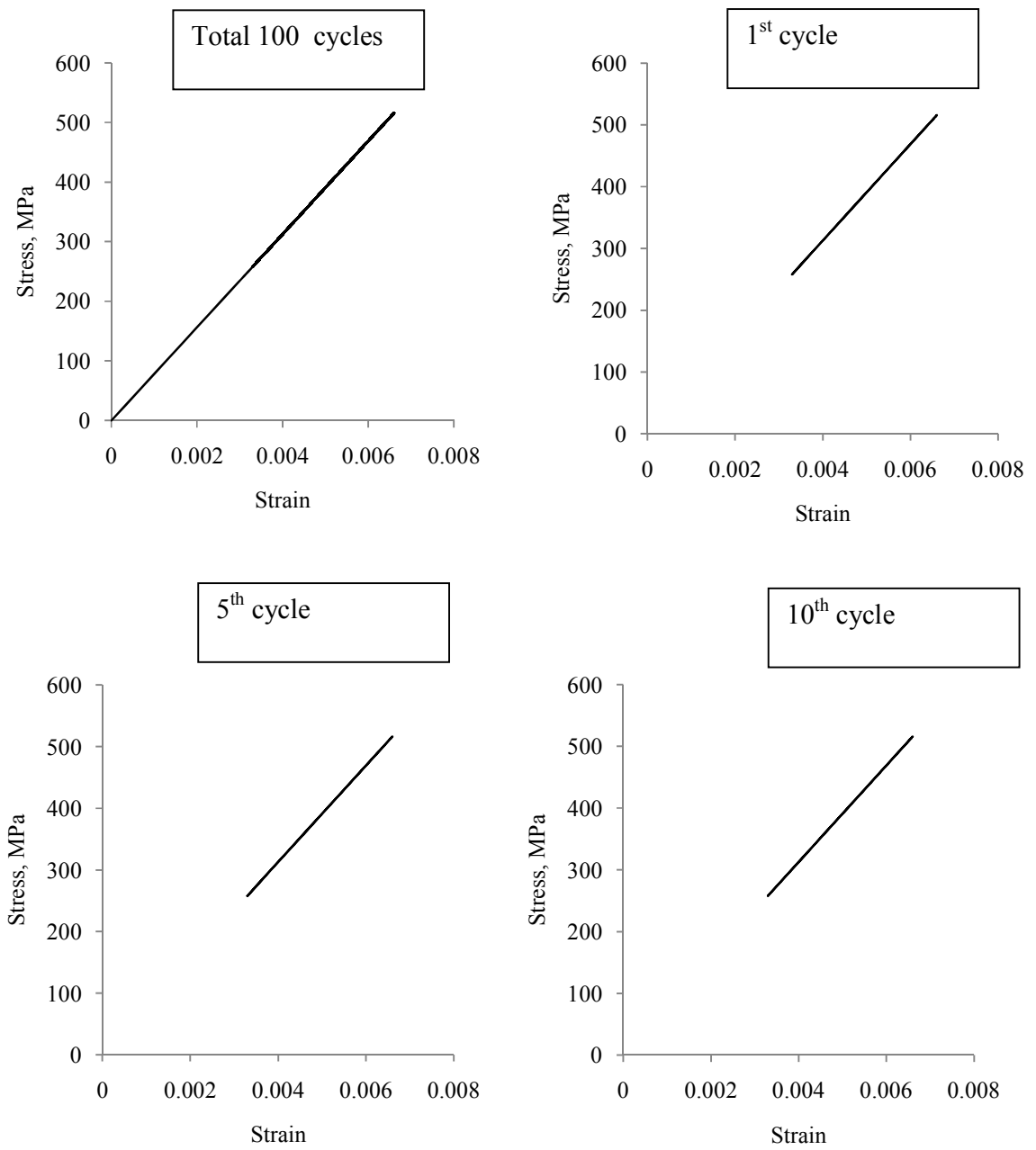


Fig. 4.18 Cyclic stress strain hysteresis at notch root under $R = 0.5$ at $\sigma_a = 80$ MPa

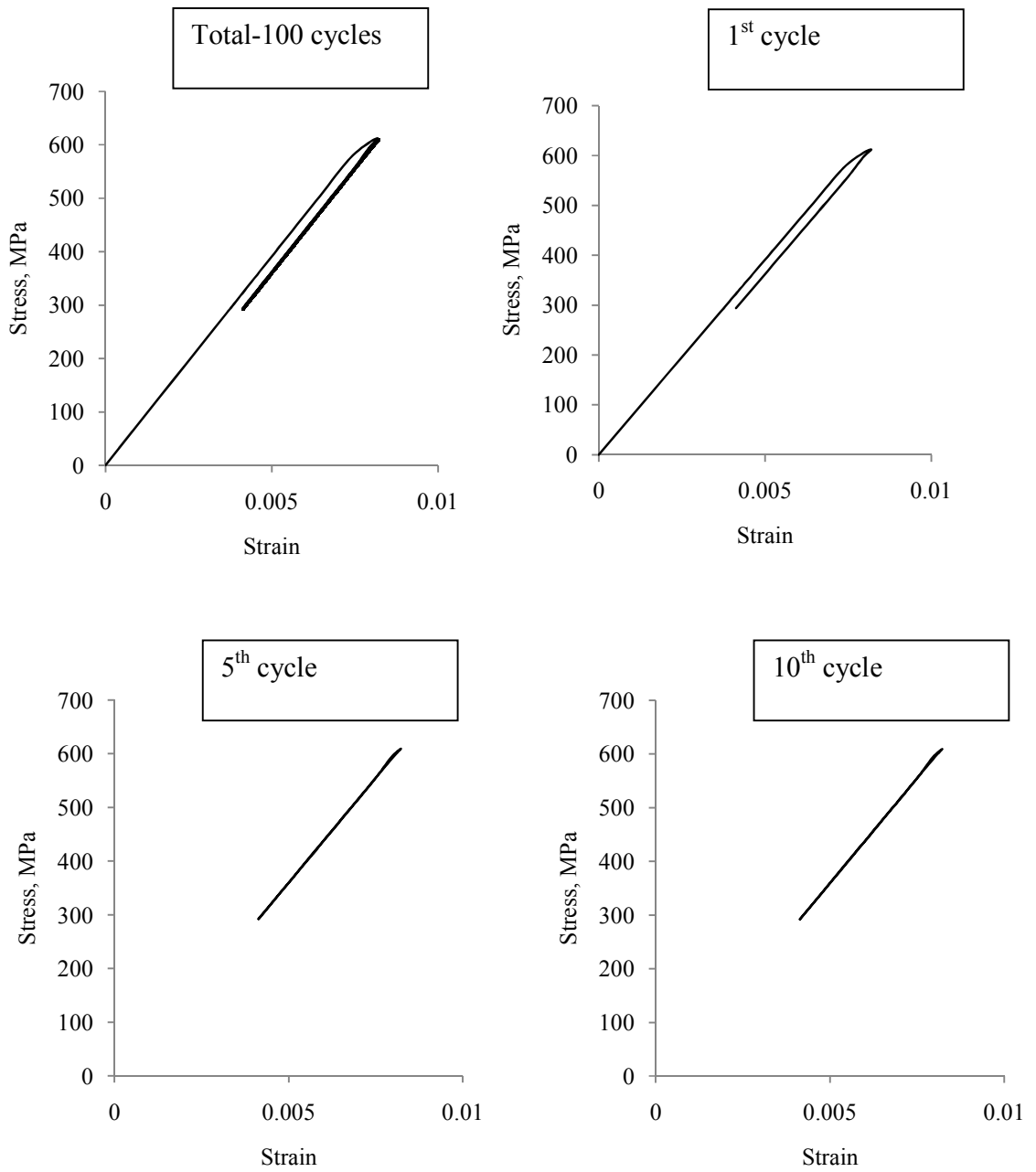


Fig. 4.19 Cyclic stress strain hysteresis at notch root under $R = 0.5$ at $\sigma_a = 100$ MPa

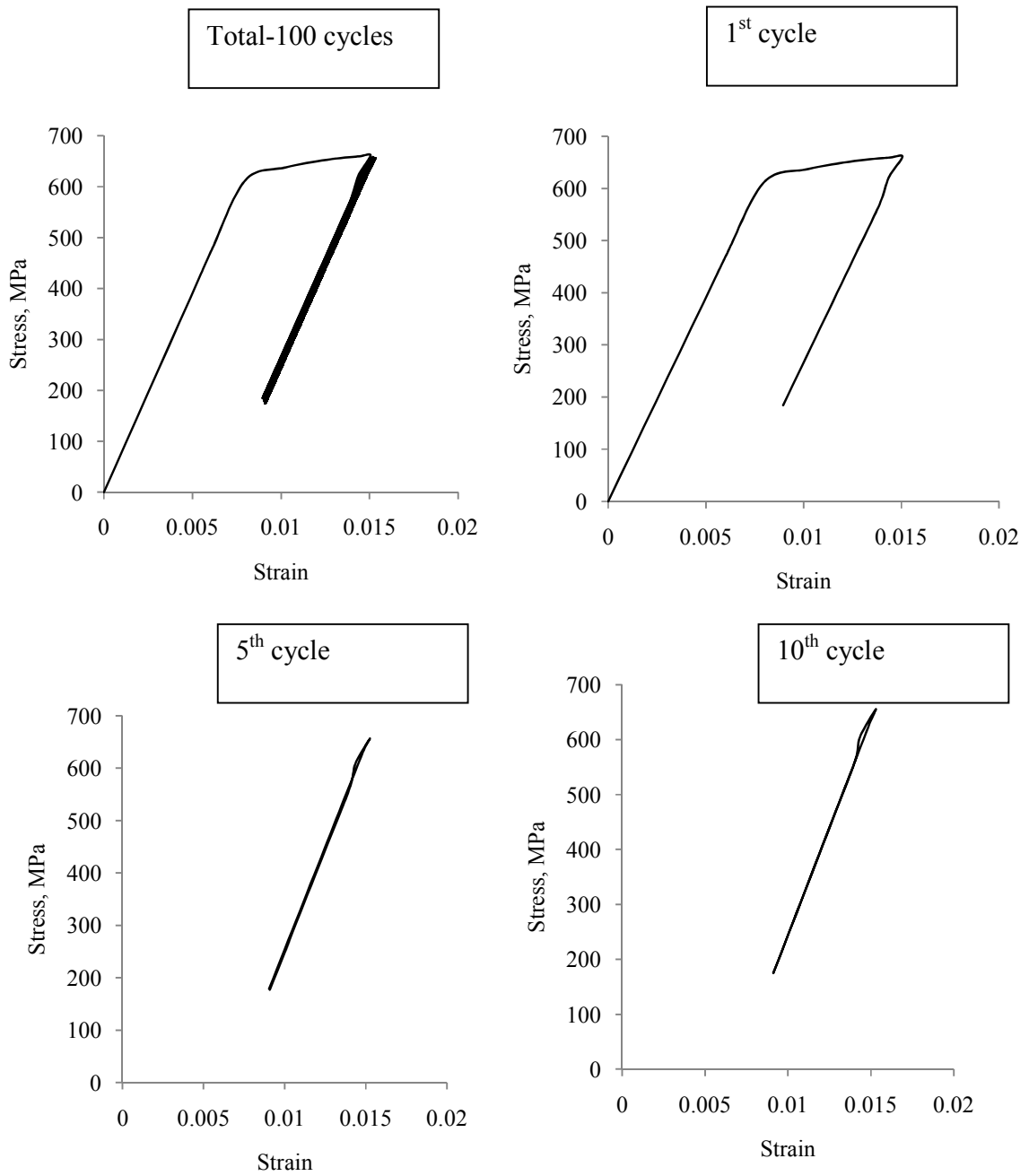


Fig. 4.20 Cyclic stress strain hysteresis at notch root under $R = 0.5$ at $\sigma_a = 150$ MPa

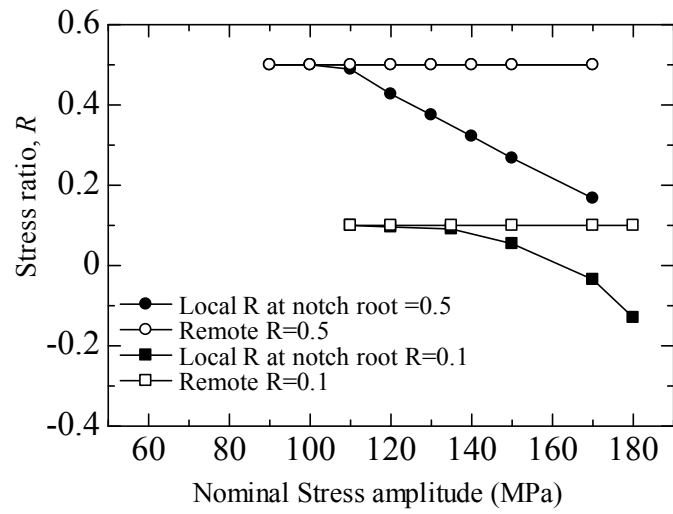


Fig. 4.21 Relationship between local stress ratio at notch root and applied nominal stress amplitude under the remote stress ratios of 0.1 and 0.5

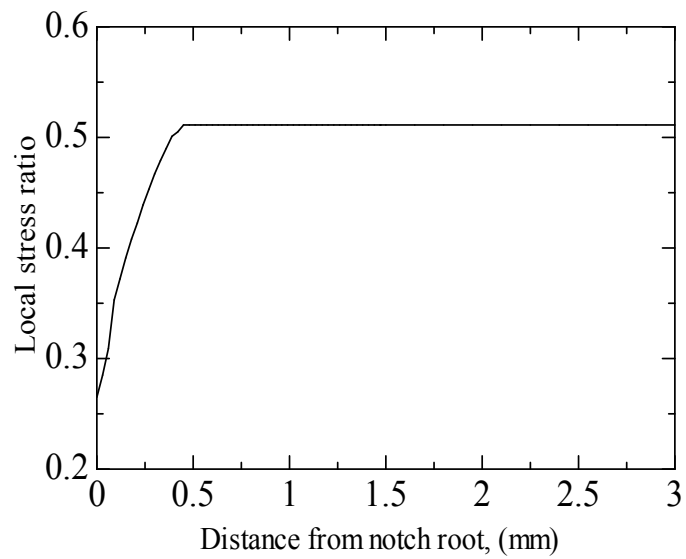


Fig. 4.22 Relationship between local stress ratio and distance from notch root at $\sigma_a = 150$ MPa under the remote stress ratio of 0.5

4.4. Discussion

4.4.1 Critical nominal stress amplitude

As mentioned in the section 4.3.1, the S-N curve of the notched specimen was kinked at the critical nominal stress amplitude. The kinked points, where the critical nominal stress amplitudes were 140 and 175 MPa for $R = 0.5$ and 0.1, respectively, seemed to correspond to the development of a plastic zone size of about 0.5 mm regardless of the remote stress ratio, as seen from Figs. 4.8(c) and (d). Therefore, the nominal stress amplitude that induces the plastic deformation with the plastic zone size of about 0.5 mm would be the critical nominal stress amplitude. The plastic zone size of about 0.5 mm corresponded to the size of about 5 grains for the present material. Above the critical nominal stress amplitude, cyclic plastic deformation occurs in the initial several cycles, as seen in Fig. 4.11(c), while almost no cyclic plastic deformation occurs below the critical nominal stress amplitude as seen in Fig. 4.11(a) and (b). The cyclic plastic deformation may cause the nucleation of multiple cracks, as seen in Fig. 4.4(d) and Fig. 4.5(d).

4.4.2 Variation of local stress ratio at notch root

From the results, relationships between stress ratio at notch root and applied nominal stress amplitude for $R = 0.1$ and 0.5 are shown in Fig. 4.21. As seen from the figure, even under the constant remote stress ratio, the local stress ratio at notch root significantly decreased with increasing applied nominal stress amplitude. The plastic deformation was formed near the notch root region at higher nominal stress amplitudes, as shown in Fig. 4.8(c) and (d). This local tensile plastic deformation at notch root will induce compressive residual stress at the notch root in the following cycles due to elastic

constraint of the surrounding elastic body. This will be a main mechanism for the change of local stress ratio at the notch root from the remote stress ratio. That is when the nominal stress amplitude is high, the large plastic zone at the notch root is formed and then the local stress ratio at the notch root is decreased. This can be also confirmed by the local stress ratio distribution near the notch root region, as shown in Fig. 4.22. This distribution almost corresponds to the plastic strain distribution shown in Fig. 4.16(b) and (c).

On the other hand, if the plastic zone increases with further increasing nominal stress amplitude and the elastic-plastic hysteresis can be created at the notch root, the local stress ratio at the notch root is speculated to approach to $R = -1$ as already discussed in previous chapter. The common explanation for this is as follows [17]: since the deformation in the plastic zone at the notch root is constrained by the gradient of plastic strain in the plastic zone and also by the deformation of the surrounding elastic region, then the cyclic deformation in the plastic zone at the notch root becomes under the fully reversed strain controlled condition. It is known that fatigue strength decreases with increasing stress ratio for the smooth specimen [5], as seen from Fig. 4.3. Therefore, it would be expected that the change of local stress ratio at the notch root influences fatigue behavior and fatigue strength of the notched specimen.

4.4.3 Comparison of S-N curve kinking behavior in A2024-T4 alloy and Ti-6Al-4V alloy

As mentioned above, the S-N curves of both aluminum alloy and titanium alloy notched specimen showed kinked behavior at the critical nominal stress amplitude under two different stress ratios. In order to compare the kinking behavior between two different materials, the critical nominal stress amplitude as well as the number of cycles to failure at the kinking point are listed in Table 4.5. In the table, the values for the Ti-6Al-4V alloy are also listed. As seen from the table, the critical nominal stress amplitudes normalized by the cyclic yield stress for both the materials were almost the same under each stress ratio. This means that the kinking behavior may be normalized dominantly by the cyclic yield stress. The number of cycles to failure at the kinked point was significantly different and those of the Ti-6Al-4V alloy were larger compared to A2024-T4 alloy, which may depend on each S-N curve as a material property.

For further understanding of kinking behavior, the plastic zone sizes at the critical nominal stress amplitudes of 170 MPa under $R = 0.1$ and 143 MPa under $R = 0.5$ were estimated based on the FEA results. The estimated sizes were almost 0.5 mm for both $R = 0.1$ and 0.5. Since the average grain size of the present A2024-T4 alloy was 109 μm , it was found that the plastic zone size of about 0.5mm corresponded to the size of about 4 grains for the present A2024-T4 alloy. For the Ti-6Al-4V alloy, the critical plastic zone size was about 0.06mm for both $R=0.1$ and 0.5, as indicated in Table 4.5. The similar correspondence between the plastic zone size at the kinked point and the size of about 4 grains has been found in the Ti-6Al-4V alloy with the same notch geometry. Therefore, it is speculated that the kinking behavior is induced when the plastic zone size increases up to about the size of 4 grains for both aluminum alloy and titanium alloy.

The local stress ratio at the notch root decreased with increasing applied nominal stress amplitude, as shown in Fig. 4.2.1. The similar variation of local stress ratio has been observed in the Ti-6Al-4V alloy. The mechanism of variation of local stress ratio of the notched specimen under a constant remote stress ratio has been discussed in the previous chapter as: the local tensile plastic deformation is formed at the notch root when the maximum load applied and then when the applied load relieves in unloading process, the compressive residual stress is induced in this local tensile plastic zone with volume expansion due to elastic constraint of the surrounding elastic body and then the mean stress becomes lower. The larger plastic zone at the notch root formed at higher nominal stress amplitudes results in more significant decrease of the mean stress at notch root. The decrease of mean stress is equivalent to the decrease of stress ratio.

To compare and discuss more about the variation of local stress ratio between Ti-6Al-4V alloy and A2024-T4 alloy, the relationship between local stress ratio and nominal stress amplitude normalized by cyclic yield stress under the remote stress ratio of 0.5 is shown in Fig. 4.23. As seen from the figure, the decrease of local stress ratio with increasing normalized nominal stress amplitude was significant in the A2024-T4 alloy compared to the Ti-6Al-4V alloy.

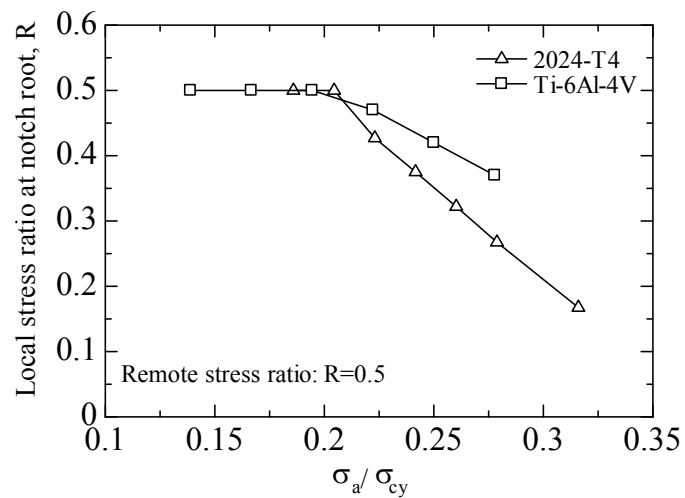


Fig. 4.23 Comparison of local stress ratio variation under the remote stress ratio of 0.5 for two different materials

The lower cyclic yield stress and the lower cyclic hardening coefficient with cyclic hardening behavior in the A2024-T4 alloy, which may induce more significant plastic deformation during fatigue loading, will contribute to the significant decrease of local stress ratio compared to the Ti-6Al-4V alloy with higher cyclic yield stress, higher cyclic hardening coefficient and cyclic softening behavior.

Table 4.5 Characteristics values at the kinked point

| | A2024-T4 alloy | | Ti-6Al-4V alloy | |
|--|-----------------|-------------------|-------------------|-----------------|
| | $R=0.1$ | $R=0.5$ | $R=0.1$ | $R=0.5$ |
| Critical nominal stress amplitude, σ_a [MPa] | 170 | 143 | 240 | 170 |
| Critical plastic zone size [μm] | 500 | 500 | 60 | 60 |
| Critical nominal stress amplitude normalized by cyclic yield stress σ_a/σ_{cy} | 0.32 | 0.27 | 0.33 | 0.24 |
| Number of cycles to failure [cycles] | 4×10^4 | 1.8×10^4 | 5.5×10^4 | 4×10^4 |

4.4.4 Fatigue life predictions of the notched specimen for A2024-T4 alloy

In the previous titanium alloy investigation, the kinking behavior of S-N curve of notched specimens in wide range of low cycle to high cycle fatigue region under the load and displacement-controlled fatigue tests have been discussed. The local stress ratio variations at notch root above the kinking points were also discussed. By taking account the local stress ratio variation at notch root, fatigue life prediction has been successfully carried out based on SWT parameter and elastic-plastic finite element analysis for Ti-6Al-4V alloy.

In this chapter, we would like to apply and confirm the effect of local stress ratio on fatigue strength of notched specimens for aluminum alloy, the fatigue life of the notched specimen has been estimated by taking the local stress ratio variation at the notch root into consideration in the following section.

As can be seen from Fig. 4.3, the S-N curves of the notched specimens under $R = 0.5$ and 0.1 are kinked at the critical nominal stress amplitude. In lower stress levels, fatigue fracture behavior seems to be elastic, while it seems to be elastic-plastic in the higher stress levels, as speculated from Figs. 4.8, 4.11 and 4.17. Therefore, two kinds of predictions have been attempted for aluminum alloy. In Prediction 1, the fatigue lives are predicted for the nominal stress amplitudes lower than the kinked point, where the variation of local stress ratio is taken into account. In Prediction 2, the fatigue lives are predicted for the nominal stress amplitudes higher than the kinked point, where the variation of local stress ratio is also taken into. The low cycle fatigue properties used in the FEA and the SWT life prediction are listed in Tables 4.3 and 4.4. The other material properties used in the fatigue crack propagation life prediction (Paris's law parameters c ,

m and the threshold stress intensity factor range ΔK_{th} for A2024-T alloy at $R=0.1$ and 0.5) have been referred from Ref. [18].

(1) Prediction 1: In high cycle fatigue region with no significant local stress ratio variation, the fatigue life has been estimated by two steps: (1) at first, fatigue crack nucleation life is evaluated based on the SWT parameter combined with FEA, and then (2) fatigue propagation life has been estimated based on the fracture mechanics approach. The detail of this prediction procedure has been explained as “Prediction 1” in the previous Chapter-3.

(2) Prediction 2: In this prediction, it is assumed that fatigue fracture occurs in low cycle fatigue manner near notch root region. The fatigue life is predicted by combining the results of elastic-plastic FEA and SWT damage model with taking the local stress ratio variation into consideration. The number of cycles required for crack propagation is neglected in this due to the presence of multiple crack initiation at the notch root in the notch fatigued specimens tested at nominal stress amplitudes higher than the kinked point. A detail of prediction method has been explained as “Prediction 2” in the previous Chapter-3.

4.4.5 Comparison of the predicted lives and experimental results

Figures 4.24 and 4.25 show the comparison between the experimental results and the predicted lives of the notched specimens for $R = 0.1$ and 0.5 , respectively. As can be seen from the figures, the predicted lives of Prediction 1 was in good agreement with the experimental results at the lower stress amplitudes, while the predicted lives were not in agreement with the experimental results at the stress amplitudes above the critical nominal stress amplitude at the kinked point.

At the stress amplitudes higher than the critical nominal stress amplitude, the predicted lives with Prediction 2 was in good agreement with the experimental results, while they gave the unsafe side of prediction at lower stress amplitudes below the critical nominal stress amplitude as found from Fig. 4.21. It is also found that by consideration of local stress ratio variation gives more accurate life predictions in notched specimens.

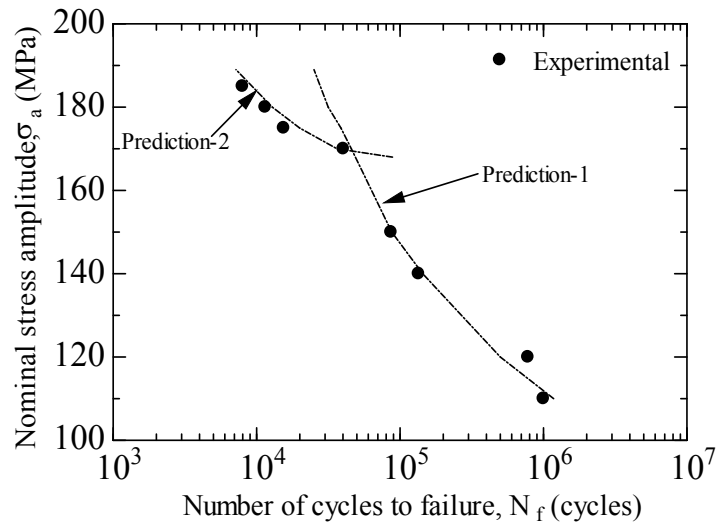


Fig. 4.24 Comparison between experimental and predicted fatigue lives for notched specimens under $R = 0.1$

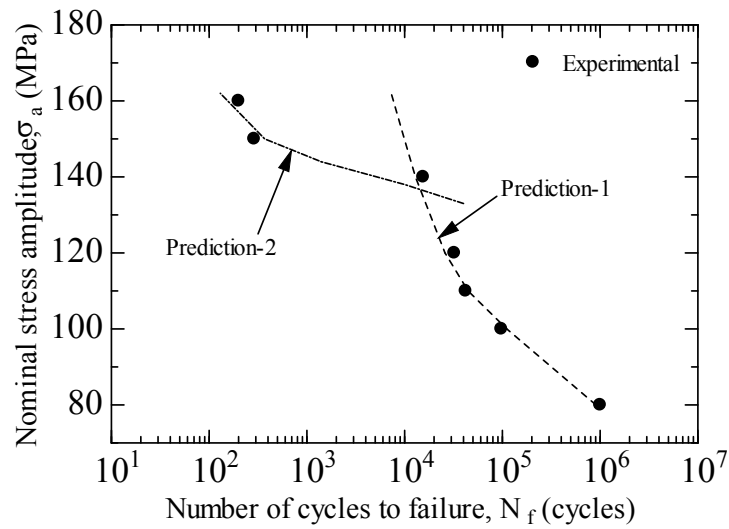


Fig. 4.25 Comparison between experimental and predicted fatigue lives for notched specimens under $R = 0.5$

In this study, elastic-plastic finite element analysis was also performed in low cycle fatigue region with the applied remote stress ratio of $R = 0.1$ and low cycle fatigue region to high cycle fatigue region with applied remote stress ratio of -1 . Based on the finite element analysis results, it can be observed that the local stress ratio significantly varied from the applied remote stress ratio of $R = 0.1$ and it continuously decreased in transition region and finally it reached to -1 in low cycle fatigue region at high strain amplitudes similar to the Ti-6Al-4V alloy results. However, the local stress ratio variation was not found in the applied remote stress ratio of $R = -1$ in wide range of fatigue region. Thus, fatigue lives are also predicted based on the finite element analysis results for both stress ratio and fatigue regimes. The predicted fatigue lives obtained from elastic-plastic finite element analysis with stress ratio of $R=0.1$ and -1 are shown in Fig 4.26. As can be seen in the figure, by taking account the local stress ratio variation at notch root in low cycle fatigue region as well as transition region and high cycle fatigue region, fatigue lives are successfully predicted for $R = 0.1$ and -1 .

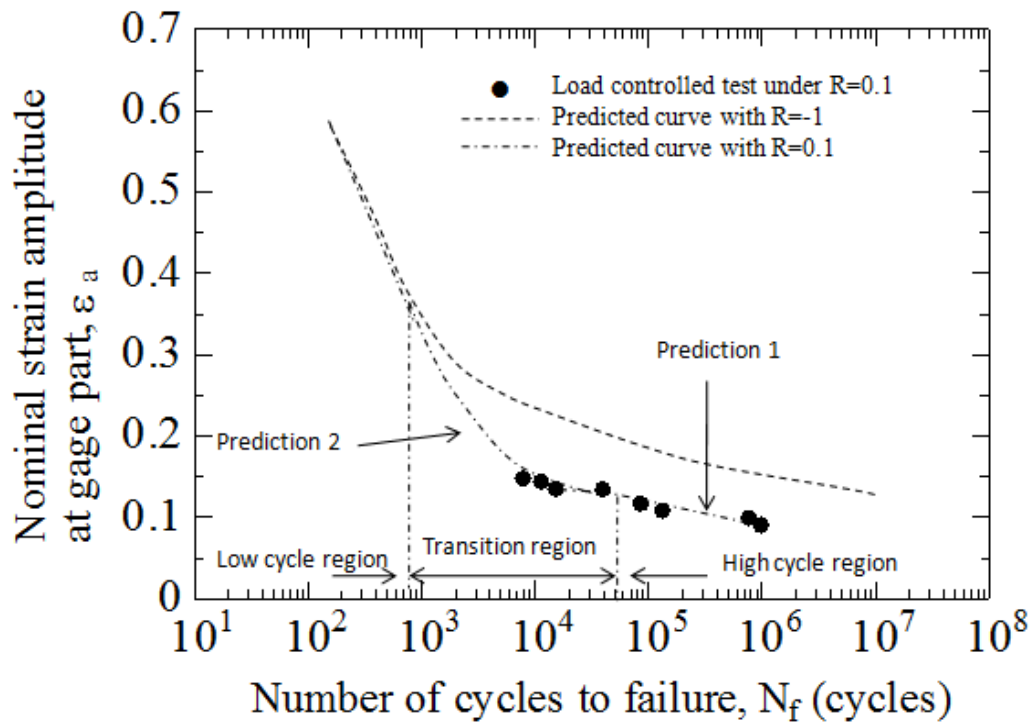


Fig. 4.26 Comparison between experimental and predicted fatigue lives for notched specimens under the remote stress ratio of 0.1 for the wide range of fatigue from low cycle to high cycle

From the foregoing results, it would be concluded as: (1) the elastic fracture mechanics approach combined with the SWT parameter is useful to predict fatigue life of the notched specimen in the high cycle fatigue regime below the critical nominal stress amplitude. At nominal stress amplitudes higher than the critical nominal stress amplitude, the predicted lives are in unsafe side. (2) The SWT parameter is useful to predict fatigue life of the notched specimen in nominal stress amplitudes higher than the critical nominal stress amplitude. However, at nominal stress amplitudes lower than the critical nominal stress amplitude, the predicted lives are in unsafe side. (3) The effect of local stress ratio

is significant at nominal stress amplitudes higher than the critical nominal stress amplitude, while it is not significant at nominal stress amplitudes lower than the critical nominal stress amplitude. The predicted lives which take into account the local stress ratio variation are in good agreement with the experimental results than those which do not take into account the local stress ratio variation.

4.5. Conclusions

The fatigue tests of A2024-T4 alloy notched specimens were carried out to investigate the effect of local stress ratio variation at the notch root on fatigue strength near the high cycle fatigue regime in the intermediate region between the high and low cycle fatigue regimes. The elastic-plastic FEA was also carried out to investigate the local stress ratio variation at the notch root. The main conclusions obtained are summarized as follows:

- (1) The S-N curve for the A2024-T4 alloy was found to be kinked when the applied nominal stress amplitude became larger than the critical nominal stress amplitude, where the local plastic deformation was formed at notch root, similar to the Ti-6Al-4V alloy.
- (2) The crack nucleated from a single site at nominal stress amplitudes lower than the critical nominal stress amplitude, while the cracks nucleated from multiple sites at nominal stress amplitudes higher than the critical nominal stress amplitude.
- (3) With increasing nominal stress amplitude, the local stress ratio at the notch root decreased even under keeping the remote applied stress ratio constant. When the plastic deformation is developed locally at notch root, the residual compressive stress would be induced due to the elastic constraint of surrounding elastic body. This will

be a main mechanism for variation of local stress ratio at the notch root.

- (4) The kinking behavior occurred when the plastic zone size increased up to the size of about 4 grains for both the titanium alloy and the aluminum alloy.
- (5) The local stress ratio at notch root decreased when the nominal stress amplitude was higher than the critical nominal stress amplitude at the kinked point. The critical nominal stress amplitudes normalized by cyclic yield stress for both two materials seemed to be almost the same under each remote stress ratio.
- (6) The significant decrease of local stress ratio with increasing nominal stress amplitude was observed in the A2024-T4 alloy with low cyclic yield stress and low cyclic hardening coefficient compared to the Ti-6Al-4V alloy with high cyclic yield stress and high cyclic hardening coefficient.
- (7) The predicted fatigue lives of the notched specimen based on the linear elastic fracture mechanics approach combined with the SWT parameter were in agreement with the experimental results in the high cycle fatigue regime lower than the critical nominal stress amplitude, where the variation of local stress ratio was not significant.
- (8) The predicted fatigue lives based on the SWT parameter which take into account the local stress ratio variation were in agreement with the experimental results at nominal stress amplitudes higher than the critical nominal stress, where the variation of local stress ratio was significant. The fatigue life prediction was improved by considering the effect of local stress ratio variation.
- (9) Unless a suitable life prediction method depending on the region higher or lower than the critical nominal stress amplitude is adopted, the prediction results would not be accurate.

References

- [1] ASTM E606-92, Standard Practice For Strain-Controlled Fatigue Testing (1998)
- [2] W. D.Pilkey, Peterson's Stress Concentration Factors^{3rd}, John Wiley & Sons New York (2007)
- [3] ASTM E468-11, Standard Practice for Presentation of Constant Amplitude Fatigue Test Results for Metallic Materials (2001)
- [4] W. J.Dixon, A. M.Mood, A Method for Obtaining and Analyzing Sensitivity Data, J Am Stat Assn 43 (1948) 109-126
- [5] S. Suresh, Fatigue of Materials 2nd, Cambridge University Press (1998)
- [6] A. J. Nachtigall, Cyclic Stress-Strain Curve Determination For D6AC Steel By ThreeMethods, Technical Report, NASA TM-73815, E-9402,Nachtigall Lewis Research Center Cleveland, Ohio United States (1977)
- [7] G. Pluvinage, Notch Effects in Fatigue and Fracture, Nato Science Series 11 (2001) 1-22
- [8] F. C.Campbell, Fatigue and Fracture-Understanding The BasicsASM International (2012)
- [9] J. C.Grosskreutz, G. G.Shaw, Mechanisms of Fatigue In 1100-0 and 2024-T4 Aluminum, Air Force Material Report, Air Force Materials Laboratory, Research and Technology Division, Air Force Systems Command, AFML-TR-65-127 (1965)
- [10] S.Khan, A.Vyshnevskyy, J. Mosler, Low Cycle Lifetime Assessment of Al2024 AlloyInt J Fatigue 32 (2010) 1270-1277
- [11] A.Merati, A Study of Nucleation and Fatigue Behavior of an Aerospace Aluminum Alloy 2024-T3, Int J Fatigue 27 (2005) 33-44

- [12] P. J. E.Forsyth, Slip-Band Damage and Extrusion, Proceedings of the royal Society of London A242 (1957) 198-202
- [13] R.Ghajar, J. K.Alizadeh, N.Naserifa, Estimation of Cyclic Strain Hardening Exponent and Cyclic Strength Coefficient of Steel By Artificial Neural Networks, ASME International Mechanical Engineering Congress and Exposition, Proceedings 12 (2008) 639-648
- [14] L. P.Borrego, L. M.Aberu, J. M.Costa, J. M.Ferreira. Analysis of Low Cycle Fatigue in AlMgSi Aluminium Alloys, Eng Fail Anal 11 (2004) 715-725
- [15] L. F. Coffin, A Study of The Effects of Cyclic Thermal Stresses on A Ductile Metal, Trans. ASME, 76 (1954) 931-950
- [16] S. S.Manson. Behavior of Materials Under Conditions of Thermal Stress, NASA Report 1170, Supersedes NASA TN 2933, (1954)
- [17] R. I.Stephens, A.Fatemi, R. R.Stephens, H. O.Fuchs, Metal Fatigue In Engineering, John Wiley & Sons New Jersey (2000)
- [18] N.Benachour, A.Hadjoui, M.Benachour, M.Benguediab, Stress Ratio and Notch Effect on Fatigue Crack Initiation and Propagation in 2024 Al Alloy, World Acad Sci Eng Technol, 5 (2011) 1384-1387

CHAPTER – 5

SUMMARY

Chapter-5

Summary

In this chapter, main points of the problems concerned, the conclusions obtained and future works are summarized. It consists of five sections: 1. Problem statement, 2. Clarification of notch fatigue behavior in the transition region, 3. Estimation of fatigue life with taking account of local stress ratio variation, 4. Notes on fatigue design, 5. Problems remained and future works.

1. Problem statement

It has been known that strain-life curves in low cycle fatigue are identical regardless of the applied remote stress ratio at high strain amplitudes and no significant stress ratio effect was observed. The stress ratio of -1 is commonly assumed in the fatigue life prediction in low cycle fatigue region as shown in Fig. 5.1(a). On the other hand, effect of stress ratio is significantly observed in high cycle fatigue region where fatigue strength decreases with increasing stress ratio as shown in Fig. 5.1(b). These common knowledge about effects of stress ratio on low cycle fatigue and high cycle fatigue behavior is successfully applied to fatigue life and strength predictions with various proposed and established models to take account of stress ratio effect. In the transition region between the low cycle fatigue region with the stress ratio of -1 even under different remote stress ratios and the high cycle fatigue region with the own remote stress ratio, the stress ratio will be changed from

the remote stress ratio to -1 and the fatigue behavior is expected to be complicated. However, there has been almost no detailed research on fatigue behavior including on variation of stress ratio in transition region. Moreover, the prediction of fatigue life in transition region has been not always reported and clarified as shown in Fig. 5.1(c). When considering the practical fatigue design, fatigue behavior of notched body will be most important and useful to be clarified in detail. Therefore, the target of the present study has been set to clarify the notch fatigue behavior in transition region between low and high cycle fatigue.

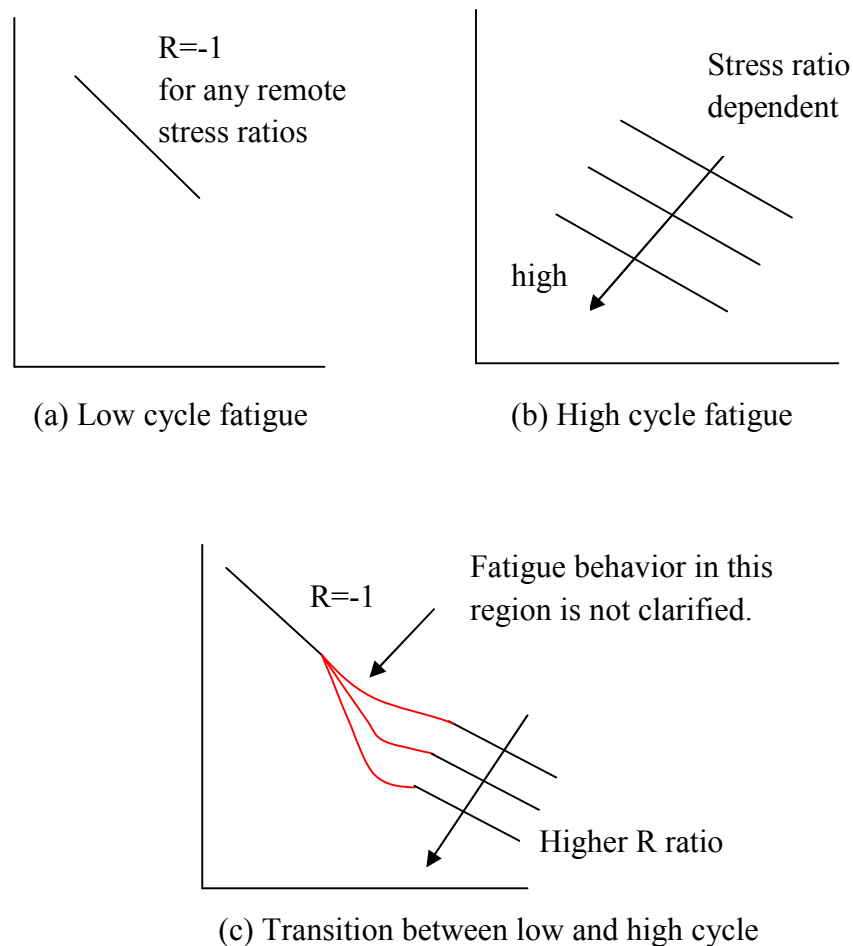


Fig. 5.1 Stress ratio effect on S-N curve in low cycle fatigue (a) and high cycle fatigue (b) as well as the intermediate uncertain fatigue behavior region between low cycle fatigue and high cycle fatigue (c)

2. Clarification of notch fatigue behavior in the transition region

The S-N curve obtained by the load-controlled high cycle fatigue test was kinked at the critical nominal stress amplitude above which the local stress ratio becomes low due to the development of plastic deformation at notch root for both Ti-6Al-4V alloy and A2024-T4 alloy. On the other hand, the S-N curve obtained by the displacement-controlled low cycle fatigue test was deflected at the low nominal strain amplitudes. From the elastic-plastic finite element analysis results, the local stress ratio at notch root in high cycle fatigue region was constant and equal to the remote stress ratio below the critical nominal stress amplitude. The local stress ratio started to decrease at the kinked point and decreased with increasing nominal stress amplitude or strain amplitude due to further development of the plastic deformation at notch root in transition region, as schematically shown in Fig. 5.2. Finally, the local stress ratio reached -1 in low cycle fatigue region. In this study, the region of local stress ratio variation is proposed to define as the transition region between low and high cycle fatigue.

Based on the variation of stress-strain distribution along the notch section during cyclic loading estimated by the elastic-plastic finite element analysis, the constraint due to reversed elastic deformation during unloading is speculated to be the main mechanism to induce the compressive stress and then vary the mean stress and local stress ratio in the transition region.

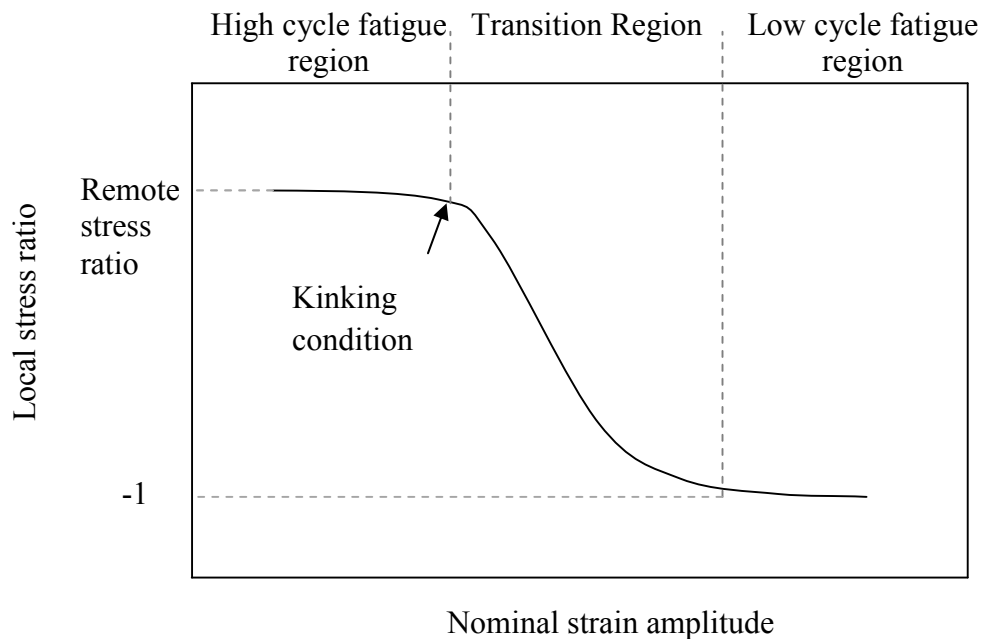


Fig. 5.2 Variation of local stress ratio at notch root

3. Fatigue life estimation with taking account of local stress ratio variation

Various fatigue life prediction models have been successfully proposed for high cycle fatigue as well as for low cycle fatigue, as Gerber, Manson-Coffin, Morrow, Glinka, SWT (Smith-Watson-Topper) models, and so on. However, the reports on fatigue life prediction in the transition region with local stress ratio variation have been hardly found. In the present study, based on the findings of local stress ratio variation at notch root, fatigue life prediction method by taking account of the local stress ratio variation at notch root based on SWT parameter combined with elastic-plastic finite element analysis under cyclic loading has been proposed. The predicted fatigue lives, which are schematically shown in Fig. 5.3, were in good agreement with the experimental fatigue lives from low cycle fatigue to high cycle fatigue including transition region. Therefore, it has been confirmed that the proposed fatigue life

prediction method with taking account of the local stress ratio variation at notch root can successfully estimate the fatigue life in transition region.

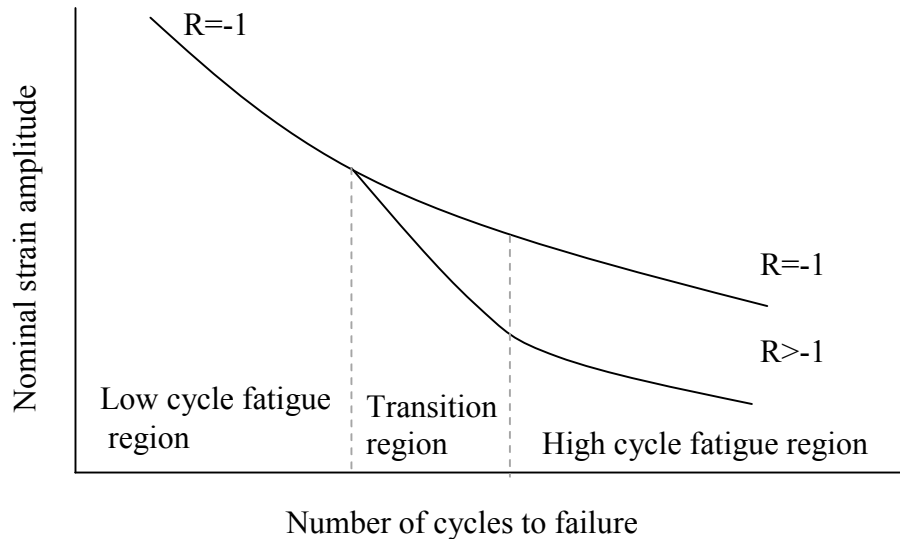


Fig. 5.3 Estimated overall S-N curves for the remote stress ratios $R = -1$ and $R > -1$ by the proposed fatigue life prediction method with taking account of local stress ratio variation

4. Note on the traditional low cycle fatigue life prediction with assumption of

$R = -1$

In low cycle fatigue region, it is common knowledge that the local stress ratio R can be assumed -1 regardless of the remote applied stress ratio. However, this assumption can not extend to the transition region since the local stress ratio is not equal to -1 anymore and decreases in the transition region, as proved by the current investigation. Since the local stress ratio in the transition region increases with decreasing nominal strain amplitude, the predicted fatigue life with the assumption of $R = -1$ would be longer than the actual fatigue life which means it gives unsafe side of

prediction. Therefore, the traditional low cycle fatigue life prediction with the assumption of $R = -1$ should not be extended into the transition region in fatigue design.

5. Problems remained and future work

In this study, notch fatigue behavior was clarified for two different materials of Ti-6Al-4V alloy and A2024-T4 alloy. It can be pointed out the problems to be solved in future as:

(1) Different composition and heat-treatment leading to different material properties which would affect the local stress ratio variation should be investigated.

(2) Various notch geometry can influence not only the localized plastic deformation behavior but also different stress state condition at notch root. Therefore, effect of notch geometry should be investigated for more detail understanding the effect of stress state and plastic zone development at notch root.

(3) The influence of tri-axial stress field on the local stress ratio variation should be considered for fatigue behavior of notched components with different thicknesses and loading modes.

(4) From the fatigue design point of view, the normalized local stress ratio variation curve is desired to be developed including effects of material properties, effect of applied remote stress ratio, effect of notch geometry, effect of size, etc. Once the normalized local stress ratio variation curve is established, it would be significantly useful for fatigue design of notched components as one of the notch fatigue design tools for fatigue life prediction.